ABSTRACT

Title of Dissertation:	A NANOCOMPOSITE HYDROGEL FOR STROMAL CELL-DERIVED FACTOR-1 ALPHA DELIVERY AND MODULATION OF MACROPHAGE PHENOTYPE FOR SKIN TISSUE REGENERATION
	Justine Ruth Yu, Doctor of Philosophy, 2021
Dissertation directed by:	Fischell Family Distinguished Professor & Department Chair John P. Fisher, Department of Bioengineering

Chronic, non-healing skin wounds arising as a sequela of underlying disease are often difficult to treat clinically, susceptible to infection, and may severely reduce a patient's quality of life. Tissue engineered constructs may be employed to aid in wound closure and skin regeneration, but no single skin substitute is currently capable of fully restoring normal skin structure and physiological function. One critical factor directing wound healing progression and the resulting functional outcome is the host inflammatory response. Circulating monocytes migrate to wound sites and differentiate into macrophages, which further polarize to pro- or anti-inflammatory phenotypes depending on microenvironmental properties including extracellular matrix composition and local cytokine gradients. In chronic wounds, polarization is predominantly pro-inflammatory, resulting in the secretion of cytokines that impede healing. Studies have identified stromal cell-derived factor-1 alpha (SDF-1α) as a

potent chemokine that recruits mesenchymal stem cells (MSCs) and macrophages, modulating their phenotype to promote the secretion of anti-inflammatory cytokines. We endeavor to fabricate a tissue engineered hydrogel-based biomaterial that can sustain the release of SDF-1α to initiate pro-healing effects at chronic wound sites. In the first aim of this project, we develop and characterize a nanocomposite hydrogel system capable of releasing SDF-1α and exerting bioactive effects on MSCs. This demonstrates its capability to controllably release the chemokine over time at physiologically relevant levels. In the second aim, we study this hydrogel's effects on macrophage migration and phenotype both *in vitro* as well as *in vivo* using wild type and diabetic murine models. We show that our material allows macrophages primarily of the anti-inflammatory phenotype to infiltrate wounded tissue, and subsequently demonstrate its ability to stimulate skin tissue formation and vascularization so as to improve the rate of healing. The findings described in this dissertation detail the successful development of a nanocomposite hydrogel delivery system for immunomodulatory and wound healing applications, which may support the future development of clinical wound dressings, skin substitutes, and other immune-informed strategies for tissue regeneration applications.

A NANOCOMPOSITE HYDROGEL FOR STROMAL CELL-DERIVED FACTOR-1 ALPHA DELIVERY AND MODULATION OF MACROPHAGE PHENOTYPE FOR SKIN TISSUE REGENERATION

by

Justine Ruth Yu

Dissertation submitted to the Faculty of the Graduate School of the
University of Maryland, College Park, in partial fulfillment
of the requirements for the degree of
Doctor of Philosophy
2021

Advisory Committee:
Professor John P. Fisher, Chair
Professor Christopher Jewell
Professor Huang-Chiao Huang
Professor Arthur J. Nam
Professor David Mosser, Dean's Representative
Professor Achsah Keegan, Medical Scientist Training Program Representative

Acknowledgements

This work was supported by the National Institute of Biomedical Imaging and Bioengineering/National Institutes of Health (NIBIB/NIH) Center for Engineering Complex Tissues (grant number P41 EB023833). The author also gratefully acknowledges support from the University of Maryland School of Medicine Medical Scientist Training Program (UMSOM MSTP) and the University of Maryland Graduate School.

The author would like to thank Dr. Huang-Chiao Huang and Barry J. Liang for assistance in liposome design and fabrication, Dr. Fu Chen for helping with nuclear magnetic resonance sample acquisition, Dr. Wen-An Chiou at the Maryland NanoCenter for assistance with scanning- and cryo-transmission electron microscopy, Dr. Wenquan Ou for assistance in mouse bone marrow isolation, Histoserv, Inc. for cryosectioning, as well as the staff of the University of Maryland Department of Laboratory Animal Resources (UMD DLAR) for their support in animal care and use.

In addition, the author would like to thank Dr. John Fisher for 4 amazing years of mentorship and support while working in the Tissue Engineering and Biomaterials Lab, as well as the committee members for their guidance and suggestions to improve this project. Grateful appreciation is extended to undergraduate mentees Miriam Janssen and Pranav Varrey for their help conducting experiments. Lastly, sincerest thanks to lab alumni and current members, friends, and family who offered cherished support throughout this project (coffee, food, or otherwise) – I couldn't have done this without you!

Table of Contents

Acknowledgements ii
Table of Contents iii
List of Tables v
List of Figures vi
Chapter 1: Introduction 1
Chapter 2: Current Applications and Strategies for Engineering Skin Tissue 5
2.1: Skin Structure and Physiology 5
2.1.1: Normal Skin Structure 5
2.1.2: Normal Skin Physiology 6
2.2: The Premise of Skin Tissue Engineering 8
2.3: Relevant Applications of Tissue Engineering in the Development of Skin Substitutes 9
2.3.1: Modeling Skin Tissue for Industrial Applications 10
2.3.2: Engineering Skin for Clinical Applications 11
2.3.3: Current Management Strategies for Acute Wounds 13
2.3.4: Current Management Strategies for Chronic Wounds 14
2.4: The Future of Skin Tissue Engineering 14
Chapter 3: The Delivery of Immunomodulatory Cues in ECM-Based Scaffolds to Guide Skin Tissue Regeneration 16
3.1: ECM-Based Scaffolds to Guide Regeneration 16
3.2: Delivery of Immunomodulatory Cues to Promote Wound Healing 19
3.2.1: Responses Stimulated by Mesenchymal Stem Cells (MSCs) 23
3.2.2: Modulation of Macrophage Polarization 26
Chapter 4: A Liposome/Gelatin Methacrylate (GelMA) Nanocomposite Hydrogel System for the Delivery of Stromal Cell-Derived Factor-1α 30
4.1: Introduction 31
4.2: Materials and Methods 35
4.2.1: GelMA Synthesis and Hydrogel Preparation 35
4.2.2: Nuclear Magnetic Resonance (NMR) Spectroscopy 35
4.2.3: Assessment of Hydrogel Degradation 36
4.2.4: Rheology 36
4.2.5: Liposome Synthesis and Protein Loading 36
4.2.6: Liposome Characterization 37
4.2.7: Characterization of SDF-1α Release 38
4.2.8: Cell Culture 39
4.2.9: Western Blotting 39
4.2.10: Statistical Methods 40
4.3: Results 40
4.3.1: Characterization of GelMA Hydrogels 40
4.3.2: Characterization of Liposomes 43
4.3.3: Release of SDF-1α from Liposomes and GelMA 46
4.3.4: Transwell Migration Assays 50
4.3.5: Western Blots to Assess for mTOR Signaling Activity 52

4.4: Discussion 54
4.5: Conclusions 60
Chapter 5: SDF-1α Delivery in Nanocomposite Hydrogels Promotes Migration and Anti-Inflammatory Responses in Macrophages 62
5.1: Introduction 63
5.2: Materials and Methods 64
5.2.1: GelMA Synthesis 64
5.2.2: LipoSDF Preparation 65
5.2.3: Cell Culture 65
5.2.4: Hydrogel Preparation and Cell Seeding 65
5.2.5: *In Vivo* Experiments 66
5.2.6: Western Blotting 67
5.2.7: Immunofluorescent Staining 68
5.2.8: Statistical Methods 68
5.3: Results 69
5.3.1: Migration of BMDMs in SDF-Containing Hydrogels 69
5.3.2: Cytokine Production by Seeded BMDMs 71
5.3.3: Treatment of Full-Thickness Skin Defects in Wild Type Mice 73
5.3.4: Western Blots to Assess Changes in Macrophage Phenotype in Wild Type Mice 75
5.3.5: Immunofluorescence to Assess for the Presence and Phenotype of Macrophages Present in Wounds of Wild Type Mice 77
5.4: Discussion 79
5.5: Conclusions 82
Chapter 6: Liposomal SDF-1α Delivery in Nanocomposite Hydrogels Promotes Skin Tissue Regeneration in Murine Diabetic Wound Models 84
6.1: Introduction 84
6.2: Materials and Methods 86
6.2.1: *In Vivo* Experiments 86
6.2.2: Planimetric Analysis 87
6.2.3: Histological and Immunofluorescent Staining 87
6.2.4: Statistical Methods 88
6.3: Results 88
6.3.1: Planimetric Analysis of Wound Closure in Diabetic Mice 88
6.3.2: Histological Examination of Regenerated Epidermis 90
6.3.3: Immunofluorescence to Assess for Vascularization in Regenerated Skin Tissue 92
6.4: Discussion 94
6.5: Conclusions 96
Chapter 7: Summary and Future Directions 98
7.1: Summary 98
7.2: Contributions 100
7.3: Future Directions 101
References 104

List of Tables

Table 2.1: Major structures, cell types, and ECM components present in each layer of normal skin tissue......8

List of Figures

Figure 2.1: Physiology of healthy human skin. Schematic representation of the major structures and layers of skin tissue that are necessary for normal skin function.7

Figure 3.1: Mesenchymal stem cells (MSCs) participate in many aspects of wound healing. They directly and indirectly promote several cellular functions by: (Clockwise from top) releasing pro-angiogenic cytokines; recruiting macrophages and producing immunomodulatory cytokines; releasing chemokines as well as factors for cell proliferation and remodeling; differentiating into fibroblasts and even skin appendage cells.....26

Figure 4.1: Strategy for SDF-1α delivery using a nanocomposite liposome/GelMA hydrogel. Schematic of the overall delivery system, which is composed of liposomal SDF-1α (lipoSDF) loaded in a UV-crosslinkable gelatin methacrylate (GelMA) hydrogel derived from Type B gelatin. Anionic liposomes are formed by mixing DSPC, DSPG, and cholesterol at a 65:10:25 molar ratio.....34

Figure 4.2: Characterization of the GelMA hydrogel. (A) Representative 1H NMR spectrums of gelatin (red) and GelMA (blue), with the boxed peaks representing protons attached to the vinyl group of methacrylate (red ⫧). (B) Degradation of GelMA hydrogels in collagenase IV shows a slower rate of degradation as GelMA content is increased (n = 3, mean ± STD). One-way ANOVAs with Tukey's post-hoc comparisons were conducted between groups at each time point. *p < 0.005 and **p < 0.001).....41

Figure 4.3: GelMA hydrogels deform elastically under shear before and after swelling. Representative rheological plots of storage (G') and loss (G") moduli of hydrogels with different GelMA content loaded with liposomes. G' > G" for all groups before and after swelling, indicating that the gels tend to deform elastically rather than flow under applied shear, and that they remain mechanically stable after swelling. This is hypothesized to occur due to the presence of highly structured hydrogel networks containing well-developed crosslinks.....42

Figure 4.4: SDF-1α loaded into liposomes does not alter particle diameter or surface charge. (A) Quantification of liposomal polydispersity index (PdI), encapsulation efficiency (EE%), and diffusion coefficients in water as measured by dynamic light scattering. (B) Cryo-TEM imaging of lipoSDF shows mostly spherical, unilamellar particles averaging around 200 nm in diameter (Scale bar: 200 nm). (C, D) Size and (E, F) zeta potential distributions of loaded and unloaded liposomes. The means between the two groups do not differ significantly (n = 3, mean ± STD. Student's T-test, p > 0.05). Each measurement was conducted with a different preparation of liposomes.....44

Figure 4.5: Liposomes remain stable in storage over time. (A) Representative size and (B) zeta potential distribution of the same batch of liposomal SDF-1α over 2 weeks at 4 ^{o}C. The distributions slightly widen and shift right respectively but in general remain narrow.....45

Figure 4.6: The release kinetics of SDF-1α can be tuned by incorporating the protein in a GelMA hydrogel. (A) Cumulative SDF-1α released from liposomes over 1 week is characterized by burst release kinetics (n = 4, mean ± STD). (B) SEM imaging of GelMA + lipoSDF shows small particles of less than 500 nm dispersed throughout the surface of a hydrogel fiber (Scale bar: 5 μm). (C) Cumulative percentage of unencapsulated SDF-1α or (E) lipoSDF released from GelMA over 1 week, normalized to the amount of initial detectable protein (n = 4, mean ± STD). One-way ANOVAs with Tukey's post-hoc comparisons were conducted between groups at each time point. (*$p < 0.0001$, **$p = 0.001$, ***$p < 0.01$). (D) Release exponent (n) and r^2 values derived from the release of unencapsulated SDF-1α from GelMA hydrogels, fit to the Korsmeyer-Peppas model. (F) Shape parameter (β) and r^2 values derived from release of lipoSDF, fit to the Weibull release model.....47

Figure 4.7: The release profiles of lipoSDF from GelMA do not fit the Korsmeyer-Peppas model of drug release. Plotted release data of (A) unencapsulated SDF-1α and (B) lipoSDF from GelMA hydrogels, with linear trend lines indicating the profile of the Korsmeyer-Peppas model for each group. (C) Release exponent (n) and r^2 values derived from the latter indicate that the data does not fit this model.....49

Figure 4.8: Liposomal encapsulation does not impair the chemotactic activity of SDF-1α and is able to induce chemotaxis for up to 1 week. (A) Representative images and (B) quantitative cell counts from Hoechst-stained MSCs in a region of interest (ROI) that have migrated through a transwell membrane in response to the respective chemotactic factor: PBS, 80 ng/mL of free or liposomal SDF-1α (Scale bar: 100 μm. n = 3, mean ± STD. One-way ANOVAs with Tukey's post-hoc comparisons, *$p < 0.01$). (C) Comparison of MSC migration in response to media conditioned over 1 week by PBS, 80 ng/mL SDF-1α, or either 5 μg/mL of free or liposomal SDF-1α in 10% GelMA. Two sets of one-way ANOVAs with Tukey's post-hoc comparisons were conducted between groups (groups being compared are denoted by either upper- or lower-case letters). Groups that do not share a letter are statistically different ($p < 0.05$).....51

Figure 4.9: SDF-1α or lipoSDF in GelMA are capable of exerting effects on key proteins of the mTOR signaling pathway over 1 week. (A) Representative Western blots of phosphorylated AKT and RPS6 compared to their respective total protein controls in MSCs exposed to PBS, 80 ng/mL free SDF-1α, or 5 μg/mL of either free or liposomal SDF-1α in GelMA. (B) Densitometry analysis of phosphorylated AKT and (C) RPS6. (n = 3, mean ± STD. Two sets of one-way ANOVAs with Tukey's post-hoc comparisons were conducted between groups. *$p < 0.05$ and **$p < 0.01$)..53

Figure 5.1: More BMDMs migrate in SDF- or lipoSDF-containing hydrogels than gels containing no chemokine. (A) Mouse BMDMs stained with CellTracker Green seeded on either GelMA, GelMA + SDF, or GelMA + lipoSDF hydrogels (n = 3/group) were imaged at 5 days post seeding in order to assess the depth of migration into the hydrogel up to 100 μm (inset). Image dimensions: 1778 x 1778 x 500 μm. Inset scale bar: 200 μm. (B) Quantification of the z-stack images above was conducted to visualize the number of cells that were able to migrate to 50 μm (solid) or 100 μm (striped) in the hydrogel (x denotes the mean). (C) The GelMA + SDF group was shown to have the greatest proportion of migrated cells at more than 100 μm deep in the gel (mean ± STD). One-way ANOVAs with Tukey's *post-hoc* comparisons were made between the groups ($^{*}p < 0.05$ and $^{**}p < 0.01$).....70

Figure 5.2: BMDMs seeded onto hydrogels containing SDF-1α or lipoSDF produce different amounts of pro- and anti-inflammatory cytokines. Cytokine expression as measured by ELISA of (A) TNF-α, (B) IL-1β, (C) IL-10, and (D) TGF-β1 (n = 3, mean ± STD. One-way ANOVAs with Tukey's *post-hoc* comparisons were conducted between groups. *p < 0.05, n.s.: not significant, N.D.: not detected). In general, the GelMA + lipoSDF group produced lower levels of pro-inflammatory, M1-associated cytokines than the other groups, and all groups produced similar levels of M2-associated cytokines, suggesting that these materials were not likely to stimulate powerful inflammatory responses when exposed to macrophages.....72

Figure 5.3: Skin regeneration in wild type mice is accelerated in SDF-containing hydrogel-treated groups. (A) Schematic diagram of the procedure, in which mice receive bilateral full-thickness dorsal defects that are splinted open to prevent contraction. (B) Representative whole-wound images at Day 0 (top) and Day 7 (bottom) show wound healing occurring after one week in each group, with greater amounts of scab tissue in the sham and more healthy skin tissue in the hydrogel-treated groups. Traces of hydrogel were left at the wound site (arrows). Scale: 1 mm/mark.....74

Figure 5.4: Western blot densitometry and representative images from wound beds of wild type mice. Approximately 20 μg of tissue from each wound (n = 6 per experimental group and 19 sham controls) was probed for total protein content of key pro-inflammatory macrophage markers (A) CD80, (B) CD86, and (C) iNOS as well as anti-inflammatory markers (D) Arg-1, (E) CD206, and (F) TGM-2 (mean ± STD. One-way ANOVAs with Tukey's *post-hoc* comparisons were conducted between groups. *p < 0.05). Overall, the experimental groups showed less expression of pro-inflammatory markers and higher expression of anti-inflammatory markers compared to sham wounds that received no treatment.....76

Figure 5.5: Both M1- and M2-associated macrophages are present in wounds from wild type mice after 7 days. (A) Representative image of a dorsal wound defect after 7 days. The wound margin can be seen clearly on the left, and the white arrows indicate regions where $F4/80^{+}$ macrophages (red) are present. Scale bar: 500 μm. (B) Representative image of wound bed tissue co-stained with DAPI (blue, cell

nuclei), F4/80 (yellow, macrophages), iNOS (green, M1 marker), and YM-1 (red, M2 marker). Scale bar: 50 μm. (C) Quantitative comparison of mean intensity in double-positive F4/80 + iNOS versus F4/80 +YM-1 macrophages shows a significant difference in hydrogel-treated groups compared to the sham (n = 6 per group unless noted, mean ± STD. One-way ANOVA with Tukey's *post-hoc* comparisons, *p < 0.05).....78

Figure 6.1: Treatment with GelMA + lipoSDF decreases wound area variability and improves closure rates in diabetic mice after 28 days. Planimetric analysis of wound closure percentage (WC%) at days 7, 14, and 28 reveal a gradual decrease in wound surface area in all groups, with the lowest WC% variability and greatest increase in median WC% in the GelMA + lipoSDF group (White dot: median, colored line: mean, n = 6 unless otherwise indicated; Kruskal-Wallis test with *p < 0.01).....89

Figure 6.2: Regenerated epidermis is histologically normal and varies in both maturity and thickness. (A) Representative hematoxylin- and eosin- (H&E-) stained wounds from each group at 28 days show formation of dermal tissue, vessels, epidermis, and keratin stratification. Scale bar: 50 μm. (B) Quantification of epidermal thickness from H&E images indicate steady epidermal regeneration over time in all groups, with the GelMA + lipoSDF group having the thickest epidermal layer overall (3 images/animal; two-way ANOVA with *p < 0.05; groups that do not share a letter are significantly different from each other).....91

Figure 6.3: CD31 staining of harvested wound tissue shows progressive angiogenesis over 28 days in diabetic mice. (A) Representative images from diabetic mouse wounds treated with GelMA + lipoSDF at days 7 (top), 14 (middle), and 28 (bottom). Increasing amounts of $CD31^+$ round structures indicate more vascular regeneration within the wound tissue. Scale bar: 500 μm. (B) Quantification of CD31 expression between groups shows the highest amount of vessel formation in the GelMA + lipoSDF group at each time point (3 images/animal, red ⧧ indicates n = 5 animals in the group; Kruskal-Wallis test with *p < 0.01).....93

Chapter 1: Introduction

As the outermost layer of the body, the skin is the first line of defense against external mechanical, biochemical, and environmental factors. During cases of extensive injury or severe dysfunction, the skin is often susceptible to infection and may be difficult to treat clinically, potentially leading to a severe reduction in a patient's quality of life.[1] Beyond its protective function, the aesthetic appearance and texture of the skin also plays an important role in an individual's self-identity, making this organ an active area of research interest across a broad range of disciplines including the biomedical, pharmaceutical, and cosmetics fields.

Strategies to replace injured skin or stimulate its growth have made great advances in recent years, but still face a variety of obstacles for regulatory approval and effective clinical integration. Despite the high levels of active scientific research and logistical progress in this field, there is currently no single skin substitute on the commercial market that is capable of fully recapitulating healthy skin structure and physiological function.[1,2] One specific barrier to this is the relative discrepancy in our current understanding of how biomaterials interact with the host immune system to influence wound healing progression and outcome. In recent years, biomaterials design has shifted from an emphasis on avoiding strong immune reactions – remaining relatively inert after implantation – to actively modulating the immune response and stimulating desired effects to ultimately improve the clinical outcome.[3] In this new paradigm, tissue engineering in particular represents a promising approach to

developing novel materials that can directly interact with immune cells, or deliver therapeutics and other signaling cues that would elicit the desired result.

The delivery of small therapeutic proteins such as growth factors and chemokines has traditionally faced obstacles in implementation as a result of their short half-lives due to rapid diffusion and susceptibility to enzymatic degradation. Nanoparticles can be used to improve local retention and control their release over a desired timespan.[4,5] In particular, liposomes have been commonly utilized to encapsulate a wide range of cargoes due to their tunable physical characteristics, allowing charged growth factors and chemokines such as stromal cell-derived factor-1 alpha (SDF-1α) to be incorporated into the hydrophilic core.[6–8]

In this dissertation, we endeavor to fabricate a tissue engineered nanocomposite hydrogel that can controllably release SDF-1α to initiate local pro-healing effects at chronic wound sites. This chemokine in particular was chosen due to its known activity in directing migration of mesenchymal stem cells and macrophages to injury sites and supporting angiogenesis.[9–11] We hypothesize that our proposed construct will recruit and polarize macrophages towards anti-inflammatory phenotypes when applied as an immunomodulatory, hydrogel-based wound dressing, and subsequently induce skin tissue formation and vascularization so as to support rapid healing. Specifically, the aims established to test this hypothesis are as follows:

1) Develop an approach to control and sustain the release of SDF-1α from gelatin methacrylate (GelMA) hydrogels, and then characterize the cellular-level responses to the released chemokine.
    a. Characterize the material properties and release kinetics of the SDF-1α delivery system to ensure that the chemokine is released at both a physiologically relevant concentration and timespan.
    b. Evaluate the ability of the released protein to induce migration and activate intracellular signaling to demonstrate preserved bioactivity after being incorporated into the delivery system.
2) Characterize specific phenotypic changes within macrophages that occur as a result of exposure to SDF-1α released through our nanocomposite delivery strategy, and assess the tissue-level responses using murine wound healing models.
    a. Assay both the cytokine profile *in vitro* and the pattern of surface marker expression in wild type mice to assess polarization of these macrophages to pro- or anti-inflammatory phenotypes.
    b. Examine the subsequent impact on wound healing *in vivo* using full-thickness skin defects in diabetic mice and quantify the resulting changes in skin tissue regeneration as determined by wound closure, epidermal regeneration, and angiogenesis.

This dissertation describes the successful development of a hydrogel-based nanocomposite delivery system to controllably release the chemokine SDF-1α. This

system represents a promising tissue engineering strategy that could potentially be applied as a wound dressing or skin substitute to recruit mesenchymal stem cells and macrophages, influencing their phenotypes to facilitate the development of a pro-healing microenvironment. Overall, the results offer encouraging support of tissue engineering approaches to deliver therapeutics that modulate the host immune system and stimulate the regeneration of healthy tissue after injury.

Chapter 2: Current Applications and Strategies for Engineering Skin Tissue[1]

The skin is responsible for several important physiological functions and has enormous clinical significance in wound healing. Tissue engineered substitutes may be used in patients suffering from skin injuries to support regeneration of the epidermis, dermis, or both. Skin substitutes are also gaining traction in the cosmetics and pharmaceutical industries as an alternative to testing in animal models. While the skin is one of the most commonly studied tissues in the tissue engineering field due to the relative simplicity of its architecture, in this review we address current challenges in fabricating multilayered, multi-component skin and provide perspectives on efforts and strategies to meet those limitations. By considering each of these key concepts while translating emerging technologies from the bench to the bedside, tissue engineering may be leveraged to create improved skin substitutes for both *in vitro* testing and clinical applications.

2.1: Skin Structure and Physiology

2.1.1: Normal Skin Structure

Mammalian skin is composed of multiple stratified layers, broadly the epidermis, dermis, and subcutaneous fat tissue (often referred to as the hypodermis).[12] The

[1] Adapted from: Yu JR, Navarro J, Coburn JC, Mahadik B, Molnar J, Holmes JH, Nam AJ, Fisher JP. Current and Future Perspectives on Skin Tissue Engineering: Key Features of Biomedical Research, Translational Assessment, and Clinical Application. *Adv Healthc Mater*. 2019;8(5):1801471. doi:10.1002/adhm.201801471

thinnest and most external layer of skin – the epidermis – is avascular and composed of a single basal layer of proliferating keratinocytes that are gradually pushed upwards and leave behind a keratin matrix.[13] This layer also contains pigment-producing melanocytes as well as antigen-presenting Langerhans cells that play a role in the host immune response.[12,14–16] The underlying dermis is rich in blood vessels, nerve endings, and various glands, and is comprised mainly of fibroblasts that synthesize type I collagen for the extracellular matrix (ECM).[12,14–18] Lastly, the hypodermis, which may also be considered part of the endocrine system, consists mostly of adipose cells that function in energy storage and thermoregulation.

2.1.2: Normal Skin Physiology

Collectively, the epidermis and dermis work to function as a barrier between the host and the external environment, protecting the body from harmful microbial, chemical, and physical factors as well as absorbing ultraviolet (UV) radiation and sequestering free radicals from the underlying tissues.[13,19] Furthermore, these tissues play a role in preventing excessive fluid loss via evaporation, maintaining homeostasis and electrolyte balance, and thermoregulation.[20] In addition to these protective functions, a variety of mechanoreceptors present in the skin allow for the ability to distinguish different sensations such as pain, temperature, and pressure.[19] Lastly, the skin functions as an important site for Vitamin D_3 synthesis (in the presence of UV light) as well as the secretion of Vitamin E from sebaceous glands.[13,21]

While the hypodermis is often dismissed in skin models as simply a system of fat storage, it also functions as a complex lipid barrier rich in stem cells, hormones, and

growth factors.[16,17,22–27] As this tissue layer supplies the nerves and blood vessels that permeate into the upper layers, the hypodermis plays a key role in re-epithelization, wound healing, and angiogenesis.[22,28–30] The structure and major components of normal human skin are summarized in **Figure 2.1** and **Table 2.1** below.

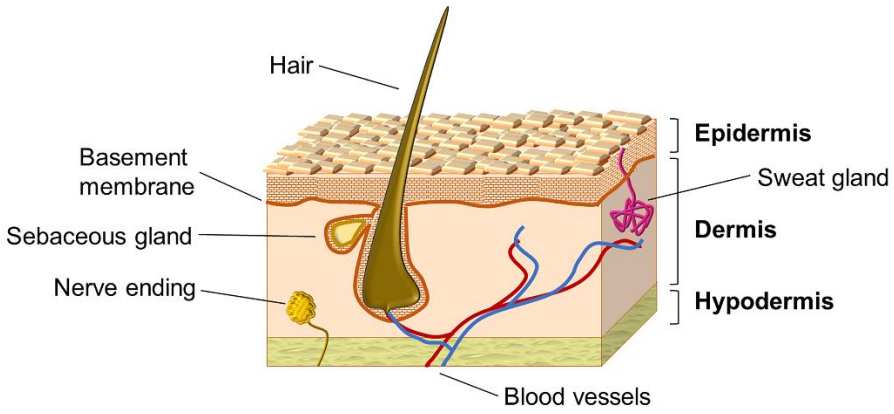

Figure 2.1: Physiology of healthy human skin. Schematic representation of the major structures and layers of skin tissue that are necessary for normal skin function.

Table 2.1: Major structures, cell types, and ECM components present in each layer of normal skin tissue.

Layer[a)]	Major structures	Major cell types	Major ECM components
Epidermis	Stratified squamous keratinized epithelium	Keratinocytes, melanocytes, Langerhans cells, Merkel cells	Keratin, type IV/VII collagen (basement membrane)
Dermis	Blood vessels, nerves, mechanoreceptors, hair follicles, sebaceous glands, sweat glands	Fibroblasts, endothelial cells, Langerhans cells, mechanoreceptor cells, smooth muscle cells, hair follicle cells	Type I collagen, elastin, proteoglycans, type IV/VII collagen (basement membrane)
Hypodermis	Blood vessels, nerves, hair follicles	Adipocytes, fibroblasts, endothelial cells, smooth muscle cells, hair follicle cells	Type I collagen, elastin

[a)] Besides multicellular structures and ECM, all skin layers also produce growth factors critical for tissue function. These include, among others, epidermal growth factor (EGF), transforming growth factor beta (TGF-β), fibroblast growth factor (FGF), vascular endothelial growth factor (VEGF), and insulin-like growth factor 1 (IGF-1).

2.2: The Premise of Skin Tissue Engineering

The tissue engineering field was originally established more than 25 years ago by Langer and Vacanti in the aim of combining engineering design principles with our understanding of biological mechanisms to replace or regenerate damaged tissue.[31] Since then, tissue engineering has been leveraged for a variety of biomedical applications including disease modeling, resource sustainability, novel clinical therapies, and has also facilitated the development of powerful technologies such as gene editing, bioreactor culture, and 3D bioprinting among many others.[32]

Central to this field is the principle that successful tissue formation involves the synergistic activity of many cell types, not just the isolated effects of any single population. Furthermore, these cells communicate with each other in a 3D system through both living and non-living components. This overarching theme of combining cells, 3D scaffolds, and environmental signals represents a promising strategy to create tissues for studying or treating diseases, but – like many other biomedical technologies – it often faces challenges in translation into clinically effective therapies. Examples of such challenges include the accurate recapitulation of tissue physiology, scalability to meet clinical needs, and financial cost.[32] These requirements are particularly important for skin tissue engineering, where there has been high demand driven by clinicians as well as the cosmetics and pharmaceutical industries for personalized, functional, and cost-effective skin substitutes. Current strategies for fabricating such constructs will be discussed in detail, accompanied by recent noteworthy examples pertinent to clinical regenerative applications and *in vitro* skin models.

2.3: Relevant Applications of Tissue Engineering in the Development of Skin Substitutes

The purpose of tissue engineered skin is to replace or model skin tissue with a construct that mimics native physiological form or function. Such a construct could be used in research and product development to examine the potential effects of various stimuli on skin without using animal models. Alternatively, tissue engineered

skin constructs could have potential application as wound dressings or skin substitutes in cases of severe skin injury, where patient survival and clinical outcome are highly dependent on restoring the skin's normal barrier function in a timely manner.[1,33,34]

2.3.1: Modeling Skin Tissue for Industrial Applications

Generally speaking, the field of tissue engineering remains in its early stages of development. It relies heavily on academic research advancement and, while startup companies are sprouting up and developing worldwide, successful clinical outcomes have not been consistently achieved and large-scale industrial production is often unattainable. However, the case of skin is unique. Advances in skin tissue engineering and modeling have been chiefly led by large commercial entities in the last several decades, particularly the cosmetics and pharmaceutical industries. Therefore, it is important to highlight their role in the advancement of this field. Skin care products, cosmetics, and other topical agents have been traditionally tested in animal models; publications assessing skin corrosion and irritation (such as the Draize rabbit skin irritation test) date back to as early as the 1940s.[35,36] These testing methods have since evolved, in large part thanks to investments into developing alternative models to *in vivo* animal and *ex vivo* human skin approaches. A critical turning point occurred in the early 2000s with the introduction of the European Union's 7th Amendment to the Cosmetics Directive. This amendment prohibited animal testing of finished products or cosmetic ingredients, introducing a marketing ban regardless of the availability of alternative non-animal tests.[35–37] Industry was thus forced to find alternatives or develop new methods.

The economic muscle behind the cosmetics industry energized efforts in developing living skin equivalents that could recapitulate part or all of the skin's natural structure. These efforts have resulted in major scientific advances in skin tissue engineering, particularly in the development of skin models, living tissue equivalents, and protocols to assess skin properties. These include, among others, reproducible, *in vitro* assays using engineered human skin constructs to assess chromosomal damage from topically applied agents,[38,39] full-thickness skin equivalents to serve as complex skin models,[40] compromised skin assays to study chemical penetration through wounded skin,[41] and skin models to study the use of LED light for acne therapy.[42] Furthermore, since 2004, the Organization for International Cooperation and Development (OECD) has developed several *in vitro* methods for testing dermal corrosivity and irritation based on commercially available products.[43] Several US and EU agencies recognize these alternate test methods as a way to reduce animal testing and increase global harmonization.[44] Overall, the innovation and R&D departments of major companies have produced substantial advancements in the use and development of skin models.

2.3.2: Engineering Skin for Clinical Applications

Perhaps an even more obvious application of skin tissue engineering is to augment or develop replacements for skin grafts used to treat patients with serious cutaneous injuries. In the clinical setting, skin grafts may be used to treat extensive tissue defects by restoring normal barrier function while stimulating wound repair responses. However, if normal tissue healing is impaired, or if there are insufficient

amounts of healthy donor tissue available, tissue engineered constructs may be necessary.[45] While some products have been shown to reduce morbidity and improve clinical outcomes after injury, no single skin substitute currently on the market has been demonstrated to fully restore normal skin structure and physiological function.[1,46]

When the skin is extensively injured, it loses its ability to prevent bacterial infection and regulate temperature or fluid transport.[15,47] The natural response to severe skin injury in adults, involving tissue granulation and re-epithelialization, is characterized by a rapid proliferation of fibroblasts that deposit randomly-oriented collagen fibers to fill the tissue defect, followed by the migration of keratinocytes and contraction of myofibroblasts that restore the barrier.[48] This collection of disorganized tissue results in a fibrotic scar, and is often accompanied by lack a of sensation and elasticity as well as flawed features – in effect, "healing" does not restore native skin function, histological structure, or aesthetics.[14,15,47,49]

Another point to consider is that other cell types normally present in the skin may be slower to regenerate, or do not grow back at all. For example, even if sebaceous glands are transplanted in skin grafts, normal secretory function typically does not occur for months.[45,50] Similarly, sensory and autonomic nerves present in neighboring areas of healthy skin may ingrow to eventually re-innervate the wound area, but the process is slow and never fully complete.[45] This leads to patches of skin that may experience abnormal sensation or sweat function. Finally – and perhaps even more

importantly to patients – the loss of melanocytes leads to changes in skin pigmentation, which can be disfiguring and difficult to treat with current cosmetic techniques.[51]

2.3.3: Current Management Strategies for Acute Wounds

Cutaneous wounds may be classified as acute or chronic, depending on the etiology. Some of the most common causes of acute skin injury include mechanical trauma, burns, or the surgical excision of skin malignancies.[1,51] When the damage is extensive, the current gold standard for treating such wounds is autologous skin grafting, which – while able to cover the tissue defect and restore barrier function using the patient's own skin tissue – suffers from the same limitations as described above in that the wound site experiences significant contraction and haphazard tissue remodeling.[14,15,52,53]Furthermore, the procedure is restricted by the availability of appropriate tissue harvest sites from the patient, as well as the fact that the donor site becomes another wound requiring management. Studies have also indicated that hypertrophic healing and keloid formation may occur unpredictably, especially among those who already have a genetic bias.[14,48]

The availability of autologous skin is also a limitation in cases where a patient's wounds exceed more than 60% of their total body surface area; in these cases the injuries cannot be adequately covered by autografts due to the lack of enough harvestable tissue.[53,54] Treatment thus requires the use of alternative startegies, most commonly cadaveric allografts.[1] These function mainly as a temporary dressing to protect and stimulate healing in the wound bed before an autograft can be placed.[1,51]

2.3.4: Current Management Strategies for Chronic Wounds

In contrast to acute skin injuries, chronic wounds develop due to a deviation from the normal wound healing process.[55] Examples include diabetic ulcers, venous leg ulcers, and pressure sores. In each of these cases, an underlying comorbidity prolongs inflammation and delays the closure of an open wound, leading to an increased risk of infection. Difficulty in healing is often further compounded by tissue ischemia or continual pressure on the site.[55,56]

Treatments for chronic wounds usually involve addressing the underlying condition, mechanically offloading the affected area, and debriding infected sites. In extreme cases, amputation may be indicated.[56] To try to prevent this, a wide range of clinical products to aid in the rate of wound closure and tissue granulation have been developed, although their use is generally limited due to unproven clinical efficacy, high cost, and extensive time required for in vitro cell expansion.[1,46] Examples of these products include biologic dressings, cultured epithelial autografts, and composite skin substitutes.[1,50]

2.4: The Future of Skin Tissue Engineering

Being able to meet or exceed the quality of current gold standard autologous skin grafts with off-the-shelf, composite, full-thickness constructs represents the “Holy Grail” of skin tissue engineering. For clinical applications, there is the added requirement of minimizing or altogether eliminating scar formation, as well as the need for broad effectiveness across a wide range of patient populations and wound types. Other qualities of the ideal skin substitute include the integration of functional

appendages into these substitutes, as well as the ability match patient-specific pigmentation. The regenerated skin not only must look like native skin but also has to function appropriately; the clinical and physiological properties of the skin layers and structures have to be just right.

So what is the route to this “Holy Grail”? The potential for accelerated and complete skin regeneration from the field of tissue engineering has greatly expanded over the last few decades, with many novel strategies and viable technologies reaching the product market. However, the current options available still remain limited in a number of ways – for instance, the tradeoff between efficacy and cost is often too high for a product to be regularly used in most healthcare settings. Further efforts to achieve an ideal skin substitute will require continued communication and collaboration among researchers, clinicians, and regulatory bodies to ensure that the final product optimally attains the wide range of objectives discussed here. In this way, skin substitutes will become more widely accepted as a viable solution for reducing the number of animals used for commercial testing, or for improving the quality of life in patients with serious skin injuries.

Chapter 3: The Delivery of Immunomodulatory Cues in ECM-Based Scaffolds to Guide Skin Tissue Regeneration[2]

Recent biomedical advances, ranging from cellular-level therapies such as mesenchymal stem cell (MSC) or growth factor delivery, to large-scale biofabrication techniques including 3D printing, have enabled the implementation of unique strategies and novel biomaterials to recapitulate the biological, architectural, and functional complexity of native skin. In this chapter, we specifically highlight some of the latest approaches to skin tissue engineering using extracellular matrix- (ECM-) based scaffolds to deliver or stimulate local immunomodulatory, pro-regenerative cues for tissue healing.

3.1: ECM-Based Scaffolds to Guide Regeneration

The reconstruction of skin in tissue engineering has for the most part been focused on the development of stratified constructs mimicking the bilayered structure of the epidermis and dermis.[57–66] Early approaches used synthetic components to minimize fluid loss and mechanical stress while maintaining structural stability at the wound site. Nylon and silicone composites proved popular and could be further coated with biomolecules and skin cells, leading to the emergence of products such as Biobrane™, Transcyte®, and Integra®.[67–70]

[2] Adapted from: Yu JR, Navarro J, Coburn JC, Mahadik B, Molnar J, Holmes JH, Nam AJ, Fisher JP. Current and Future Perspectives on Skin Tissue Engineering: Key Features of Biomedical Research, Translational Assessment, and Clinical Application. *Adv Healthc Mater*. 2019;8(5):1801471. doi:10.1002/adhm.201801471

Scaffolds using only natural materials have since gained popularity because they contain protein motifs that facilitate cell adhesion, and demonstrate better compatibility and degradation *in vivo*, particularly when incorporating biomolecules already naturally part of the skin ECM.[50] Proteins such as collagen,[60,71] gelatin,[72] plasma-based fibrin,[63,73] keratin,[74–76] chitosan,[77] and dextran[78] have been used both separately or in combination to culture fibroblasts and keratinocytes in efforts to mimic the dermis and epidermis, respectively. In general, these naturally-derived biomaterials are used to produce porous, soft substrates by a variety of methods including self-assembly,[73], chemical crosslinking,[72] freeze-drying,[74,79] electrospinning,[62,77] and knitting.[62] These constructs may also incorporate growth factors and cells of interest (generally fibroblasts, keratinocytes, or stem cells grown *in vitro*) in order to facilitate native cell ingrowth or the proliferation of seeded cells from autologous or allogeneic sources. Such growth factor- or cell-laden hydrogels are widely used to study skin properties such as immunoreactivity,[60] wound closure,[71] epithelialization,[72,73,77] angiogenesis,[72,74] or hair growth.[74,78]

ECM-based scaffolds are also commonly used *in vitro* for modeling aspects of skin physiology and transport phenomena to take advantage of characteristic properties found in protein-based materials. While these models are helpful for addressing specific properties of native skin tissue, they are generally not comprehensive in that they take a narrow approach towards a singular goal while neglecting the complexity of skin physiology as a whole. For instance, Uchino et al. developed a cell-laden 3D human skin model containing vitrified collagen that supported the culture of dendritic

cells in a layered construct.[60] In another recent publication, Sakamoto et al. used a pliable gelatin hydrogel sheet that sustained the release of basic fibroblast growth factor (FGF) and conformed to the shape of the wound.[72] This construct was shown to accelerate epithelialization, granulation tissue formation, and angiogenesis in mice. In these and other similar publications, there is thorough characterization and careful study of a specific property – in these cases, formation of either stratified or vascularized tissue – yet, in order to be successfully translated for clinical wound healing and tissue regeneration, such models must be further developed to study both these factors and more simultaneously.

As compartmentalized as these models may be however, they have justified the use protein-based scaffolds in clinical trials, which have generally reflected the positive trends observed *in vitro*. In 2016, for example, Loan et al. published a clinical cohort study on the use of keratin-based scaffolds for superficial and partial thickness burn injuries.[76] When compared to the current clinical standard of care, keratin-based products provided faster re-epithelialization rates, reduced scarring, as well as improved clinical parameters such as reducing healing time, inpatient time, outpatient appointments, and antibiotic use.

While many other commercialized clinical ECM constructs (including Dermagraft®, Apligraf®, Integra®, AlloDerm™, MatriStem™, MatriDerm®, PriMatrix®, and PELNAC™) have been marketed as dermal equivalents or degradable dressings that aid in accelerating wound closure, the cosmetic results still typically remain poor.[80]

This perhaps reflects the heavy focus of skin regeneration research on detailed cell behavior and molecular pathways. Translation from a series of cellular functions to the macroscopic processes of scarring and wound contraction is often difficult to achieve. However, as fabrication techniques and biomaterial options continue to expand, skin substitutes that are functional both at the micro- and macroscale may be expected to emerge in the near future.

3.2: Delivery of Immunomodulatory Cues to Promote Wound Healing

Another element of tissue engineering involves delivering biochemical cues to constructs to stimulate tissue regeneration. This may be promoted by drugs, cytokines, or growth factors, or mediated by the material properties of the scaffold itself.[3,81] In the physiological process of wound healing, a critical factor that dictates the outcome is the host's immune response. When the skin is injured, the body will attempt to heal the wound by engaging inflammatory and regenerative processes in an ordered sequence.[48] In the first 24 - 48 hours post-injury, neutrophils infiltrate the tissue and play a critical role in early host defense by clearing necrotic tissue and bacteria from the site. Circulating monocytes then enter the tissue and differentiate into macrophages. These macrophages may further polarize to different phenotypes – "M1" macrophages are pro-inflammatory but necessary for early host defense, while "M2" macrophages are anti-inflammatory and stimulate tissue healing via cytokines such as IL-10, TGF-β, and VEGF.[82] In chronic wounds, however, macropahge polarization is predominantly M1, resulting in the secretion of cytokines such as IL-1β and TNF-α that maintain a state of chronic inflammation and prevent M2-

mediated tissue healing from occurring.[56,83,84] Thus, the presence of underlying comorbidities may affect a wound's ultimate outcome, for instance prolonging inflammation and inducing chronic ulceration instead of closing the wound.

Major research efforts have focused on the use and release of signaling ligands or small molecule analogues to modulate the behavior of the immune system locally and over extended periods of time.[85] One such example is sphingosine-1-phosphate (S1P), whose receptors are highly expressed on monocytes and macrophages. This sphingolipid plays a major role in their proliferation, phenotype, and migration in both the central nervous system and peripheral blood.[86,87] When exposed to S1P *in vitro*, these cells preferentially adopt anti-inflammatory phenotypes and display a reduced secretion of pro-inflammatory cytokines if stimulated.[82,87] Lim, et al. used S1P in combination with the antifungal agent ciclopirox olamine, which also displays pro-angiogenic activity.[88] The group found that injection of the two agents into a polyvinyl alcohol sponge implanted in diabetic fatty rats supported endothelial migration and the formation of functional vessels. Similarly, fingolimod (also known as FTY720 and Gilenya) is a small molecule drug that acts as an agonist for several S1P receptors and has been previously shown to support endothelial cell function and stabilize microvasculature. [86,89] Past work in a muscle ischemia model using thin films of PLGA to control fingolimod release showed that the drug preferentially recruits anti-inflammatory monocytes and M2 macrophages via stromal cell derived factor-1 alpha- (SDF-1α-) mediated chemotaxis and supports local arteriogenesis.[90]

As mentioned previously, physiological wound healing is a multi-step process. While these and many other immunomodulatory strategies focus on influencing the cellular effectors of the host immune response and their downstream effects on tissue regeneration, other have aimed to directly combat sources of inflammation and the key biochemical signals that prolong this response. For instance, curcumin, a naturally occurring polyphenol found in turmeric, has gained some interest as a potential agent for stimulating wound healing. Although its full mechanism of action has not yet been elucidated, it has been previously shown to demonstrate some anti-inflammatory as well as anti-microbial potential.[85,91] Tong, et al. developed a cellulose nanocrystal film to release curcumin.[92] The group demonstrated that this system was able to inhibit bacterial growth when applied topically to streptozotocin-induced diabetic rats with full-thickness skin defects. Furthermore, the treatment resulted in a significant increase in wound closure rate compared to controls, and regrowth of skin layers as well as glands and hair follicles. Likewise, resveratrol, another natural polyphenol, has also been investigated for its anti-inflammatory and bacteriostatic properties. Berce, et al. fabricated chitosan-sodium hyaluronate-resveratrol sponges that were shown to support the formation of granulation tissue with reduced neutrophilic infiltration in mice.[93] Furthermore, the construct displayed a lack of bacterial contamination compared to the control, and supported local angiogenesis and re-epithelialization.

Beyond the delivery of factors to stimulate wound healing, another potential strategy may be to instead locally inhibit signals for inflammation and tissue damage at the

wound site. Towards this aim, Kasiewicz, et al. used lipidoid nanoparticles loaded with siRNA targeting TNF-α.[94] Transfection with these nanoparticles decreased TNF-α production by macrophages and inhibited further recruitment of inflammatory macrophages. Although this strategy was only tested in an *in vitro* co-culture model, it represents a promising method for reducing inflammation locally, especially since systemic anti-TNF-α therapy carries a risk of global immunosuppression and opportunistic infection.

Lastly, scaffold material properties may directly influence immune cell response and the resulting effects on tissue regeneration. For instance, Waters et al. investigated the *in vitro* response of macrophages cultured on oxidized keratin isolated from human hair.[95] The group found that this material induced polarization to an M2-like phenotype as characterized by both surface marker expression and cytokine production. Similarly, Sun described the use of a dextran-isocyanatoethylmethacrylate-ethylamine (DexIEME) hydrogel to stimulate skin regeneration in both porcine and mouse models.[96] This dextran-based, bioabsorbable hydrogel was also shown to promote healing at pre-existing scar sites and promote the formation of hair follicles. The author examined macrophage polarization in response to DexIEME macromers and found that this predominantly led to M2 polarization, suggesting that the material is able to modulate the behavior of macrophages to affect wound outcome.

Other scaffold factors such as topographical patterning and surface chemistry may also alter the microenvironment of immune cells to directly influence their phenotype.[97,98] Additionally, peptide motifs may be used to create immunomodulatory scaffolds, as evidenced by the self-assembling hydrogel composed of substance P and other bioactive peptides fabricated by Kim, et al. which was shown to recruit mesenchymal stem cells **(**MSCs) and facilitate wound closure in a diabetic mouse model.[99] Characterizing the immune profile of chronic wounds and determining how various biochemical and material factors may modulate it to promote wound healing represents a promising direction of research that has yet to be fully explored.

3.2.1: Responses Stimulated by Mesenchymal Stem Cells (MSCs)

Besides the direct delivery of cells or pro-regenerative factors that act to replace or stimulate the major cell populations of the skin, other therapies under development instead aim to use stem cells as "cytokine factories" to induce natural tissue regeneration. One of the most popular choices for this strategy are mesenchymal stem cells. MSCs were originally isolated and characterized from mouse bone marrow by Friedenstein et al. in 2970, and categorically defined by the International Society for Cell Therapy in 2006 as plastic adherent, CD90/CD73/CD105^{+}, CD14/CD34/CD45/CD19/HLA-DR^{-}, and capable of multilineage differentiation.[100,101] They have been shown to readily differentiate into osteoblasts, chondroblasts, and adipocytes when exposed to various stimulating factors.[100,102] Studies also indicate that MSCs have the potential to differentiate into other cell types outside of the mesodermal germ layer including endothelial cells, keratinocytes, and

skin appendage cells.[103–105] These cells are still most commonly derived from adult bone marrow,[106–110] but they can also be isolated from many other tissues in the human body such as adipose tissue,[111] umbilical cord blood,[112] or peripheral blood.[113,114] While they are perhaps most well-known for their use in cartilage and bone repair therapies, MSCs have also been extensively researched for immunomodulatory applications.[101] The diverse range of *in situ* cellular activities either induced directly by MSCs or indirectly stimulated by their pro-healing cytokines are summarized in **Figure 3.1**.

In their undifferentiated state, MSCs exhibit immune-privileged properties and have been previously leveraged for allogeneic implantation in multiple human clinical trials, as unprimed MSCs have a tendency for immune homeostasis and exhibit little immunomodulatory activity unless triggered.[115] On the other hand, MSCs can also be primed or licensed to become either pro- or anti-inflammatory based on their microenvironment.[116,117] These cells produce a wide variety of cytokines and growth factors, many with immunomodulatory functions. This has made them an interesting research topic for adjunct to tissue engineered constructs and skin regeneration cell therapies; rather than replacing the host cells, MSCs used in this way can affect or facilitate a therapy simply by their presence.[105,118–120]

Unsurprisingly, the cytokine production, immunomodulatory behavior, and differentiation potential of MSCs have long been investigated for beneficial effects on wound healing. In the mid-2000s, several groups showed that healing in various types

of cutaneous wounds (e.g. excisional, burn, radiation damage) could be accelerated and improved with application of autologous bone marrow-derived MSCs.[121–123] These pro-healing effects may even persist over significant periods of time – studies have shown that, when introduced systemically, exogenous MSCs can localize to damaged areas and maintain viability for up to 6 years after implantation in humans.[124,125] However, the responsiveness of MSCs to immune signaling is mostly localized to their microenvironment, requiring either induction of endogenous MSCs migration, or direct placement of exogenous cells at the site to maximize therapeutic benefit.[126] Many hydrogel and polymer scaffolds have been thus been developed to induce activity and maintain MSC viability to promote the production of angiogenic, immunomodulatory, matrix remodeling, or other regenerative cytokines.[127,128] In skin tissue engineering in particular, MSCs can function to promote wound healing when immobilized in hydrogels placed over the wound site or when added as an intermediary layer in split-thickness skin graft procedures.[129,130]

Consequently, the function and benefit of adding MSCs or MSC-conditioned media directly to a tissue engineered construct is an ongoing research topic. Their angiogenic, immunomodulatory, and paracrine signaling functions are also of immense interest, as well as their multipotent differentiation capabilities. However, while promising, the general efficacy of MSC-based therapies is often difficult to determine due to the phenotypic variation of cells that occurs both between donors and even within the same individual.[131,132] This perhaps contributes to the fact that according to data reported by the US National Institutes of Health

(http://www.clinicaltrials.gov), there are 1248 ongoing or completed clinical trials using MSCs as of March 2021, yet none have so far been able to successfully bring a product to market in the US. Nevertheless, as techniques for assessing MSC phenotype and understanding their capabilities become more advanced, specific and therapeutically active populations of cells may be isolated and used to develop clinically efficacious procedures.

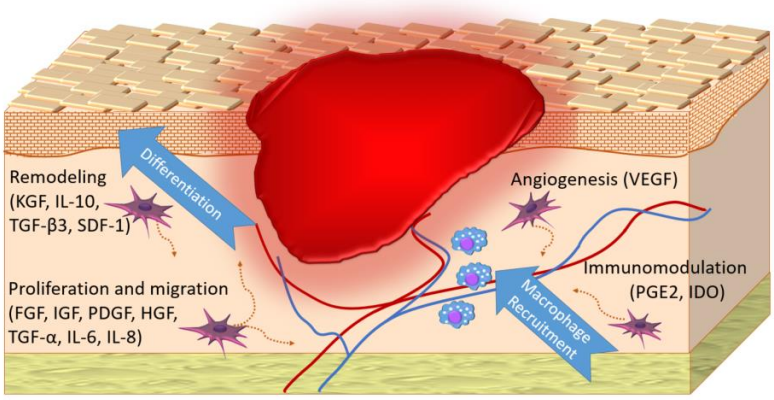

Figure 3.1: Mesenchymal stem cells (MSCs) participate in many aspects of wound healing. They directly and indirectly promote several cellular functions by: (Clockwise from top) releasing pro-angiogenic cytokines; recruiting macrophages and producing immunomodulatory cytokines; releasing chemokines as well as factors for cell proliferation and remodeling; differentiating into fibroblasts and even skin appendage cells.

3.2.2: Modulation of Macrophage Polarization

Macrophages play a crucial role in host defense by phagocytosing microbes and necrotic tissue, and by generating a foreign body response to encapsulate unknown materials. As such, they are heavily implicated in both the physiological responses to

tissue injury, as well as the pathological processes of many diseases.[83,133] Many recent biomedical developments have sought to leverage the immunomodulatory properties of this vital cell population in order to develop immune-informed technologies for applications in areas such as tissue engineering and the development of cancer therapeutics.[3]

Monocytes, macrophages, and tissue-specific phagocytic cells can be grouped together and described as the mononuclear phagocyte system (MPS).[134] These cells collectively belong to the myeloid lineage and share a common precursor found in the bone marrow.[134,135] Monocytes released into the periphery may adopt different phenotypes and function – classical $CD14^{+}/CD16^{-}$ monocytes are able to extravasate from vessels to sites of tissue injury and inflammation, while non-classical $CD14^{+}/CD16^{+}$ monocytes patrol the vasculature to maintain normal vessel function.[82,136]

Following an injury, monocytes are recruited to the affected site in response to chemokines generated by resident tissue macrophages stimulated by pathogen- or damage-associated molecular patterns (PAMPs or DAMPs), as well as infiltrating neutrophils.[137] Differentiation into macrophages is then triggered by the physical characteristics of the local microenvironment such as the cytokine milieu and the surface stiffness or topography.[3] Broadly speaking, macrophages can be described as being able to be polarized into “classically activated” M1 macrophages, and “alternatively activated” M2 macrophages, though the phenotypes are recognized to

exist along a continuum and may be easily altered given the presence or absence of various stimuli.[133,136] Canonically, these M1 macrophages are associated with inflammation and increased phagocytic and tumoricidal activity, while the M2 phenotype is related to wound healing, fibrosis, and tumor formation.[138]

In recent years, the control of macrophage polarization has become a widely studied immunomodulation strategy in order to curb inflammation and hasten wound healing. In these cases, researchers often aim to skew polarization towards the M2 and away from the M1 phenotype. Recent studies have leveraged biomaterials with specially-engineered physical properties to stimulate appropriate phenotypic changes in macrophages, ultimately allowing them to elicit a specific biological response or functional outcome.[139,140] However, much remains to be explored in taking advantage of this approach. It is widely recognized that the timing and magnitude of M1-to-M2 transition is important. Ideally, this transition should occur while macrophage numbers are at their peak within the tissue (typically within 7-10 days after a wound), and the polarization to the M2 phenotype should not be completely unopposed so as to induce undesirable effects such as fibrotic scarring or tumorigenic activity.[81,141] Furthermore, there is a need to study the interactions between macrophages, the cytokines they produce, and other cell types present within the local microenvironment including other immune cells, MSCs, and the cell types that make up the native tissue or organ.

The modulation of macrophage polarization can help elucidate complex relationships between the host immune system and tissue behavior in both healthy and diseased states. Understanding the roles and behaviors of these cells is particularly important for regenerative medicine applications where foreign materials and therapeutics are delivered to a site of injury to stimulate a pro-healing environment for the cells comprising that tissue. By studying these cells' influences on (and by) other cell types, the surrounding ECM, and implanted biomaterials, novel biomedical devices and therapies may be developed to interact with the host immune system in a synergistic and beneficial way.

Chapter 4: A Liposome/Gelatin Methacrylate (GelMA) Nanocomposite Hydrogel System for the Delivery of Stromal Cell-Derived Factor-1α[3]

Chronic, non-healing skin and soft tissue wounds are a major clinical challenge to treat, and represent a significant burden to the healthcare system as well as patient quality of life. A key aspect of this issue is the impaired recruitment of mesenchymal stem cells (MSCs), which secrete regenerative cytokines and modulate the phenotypes of other effector cells that promote healing. We have engineered a therapeutic delivery system that can controllably release the pro-healing chemokine stromal cell-derived factor-1α (SDF-1α) to induce the migration of MSCs. In order to protect the protein cargo from hydrolytic degradation and control its release, we have loaded SDF-1α in anionic liposomes (lipoSDF) and embedded them in gelatin methacrylate (GelMA) to form a nanocomposite hydrogel. In this study, we quantify the release of SDF-1α from our hydrogel system and measure the induced migration of MSCs *in vitro* via a transwell assay. Lastly, we evaluate the ability of this system to activate intracellular signaling in MSCs by using Western blots to probe for the phosphorylation of key proteins in the mTOR pathway. To our knowledge, this is the first study to report the delivery of liposomal SDF-1α using a nanocomposite approach. The results of this study expand on our current understanding of factors that can be modified to affect MSC behavior and phenotype. Furthermore, our

[3] Adapted from: Yu JR, Janssen M, Liang BJ, Huang H-C, Fisher JP. A liposome/gelatin methacrylate nanocomposite hydrogel system for delivery of stromal cell-derived factor-1α and stimulation of cell migration. *Acta Biomater*. 2020;108:67-76. doi:10.1016/j.actbio.2020.03.015

findings contribute to the development of new hydrogel-based therapeutic delivery strategies for clinical wound healing applications.

4.1: Introduction

Non-healing skin ulcers are a common complication in patients suffering from chronic conditions such as diabetes and peripheral vascular disease, or in situations where sustained pressure compromises local circulation (i.e. decubitus ulcers).[50,55] While mild to moderate cases are typically managed with non-surgical methods, severe wounds may warrant the use of tissue engineered skin substitutes to address wound defects and stimulate healing, especially if skin grafting techniques are limited by other comorbid conditions. [2,19,142] Such constructs may further incorporate exogenous proteins or small molecule drugs in order to locally accelerate wound closure and facilitate tissue regeneration. [34,143]

Chronic wounds are characterized by an inflammatory environment that impairs the recruitment of mesenchymal stem cells (MSCs), which play an important role in directing the progression of normal healing mechanisms that lead to wound closure and skin tissue regeneration.[144] These MSCs normally migrate in response to chemotactic factors secreted by cells at the wound site, where they in turn produce immunomodulatory and pro-healing cytokines.[145] Towards this end, we seek to develop a nanocomposite hydrogel to tune the release kinetics of a pro-healing chemokine such as stromal cell-derived factor-1α (SDF-1α, also known as CXCL12) over a physiologically relevant timespan. SDF-1α is a protein constitutively produced by endothelial cells, pericytes, and dermal fibroblasts, and upregulated when there is

injury.[146] This protein has been previously used in tissue regeneration and vascular remodeling applications due to its ability to stimulate cell migration and promote pro-healing behavior in anti-inflammatory subsets of monocytic immune cells.[10,11,147,148] Furthermore, SDF-1α is also known to facilitate the mobilization of MSCs from the bone marrow, which in turn secrete anti-inflammatory, pro-healing cytokines or are phagocytosed by macrophages to induce phenotypic changes (a process known as efferocytosis).[149–151] Previous studies have successfully utilized engineered hydrogel or thin film systems to deliver SDF-1α in applications such as promoting cell homing to cardiac tissue and supporting angiogenesis or myogenesis.[9–11]

However, the direct delivery of therapeutic agents is often hampered by rapid diffusion and (in the case of growth factors and chemokines) the activity of proteolytic enzymes, which are especially prevalent in chronic inflammatory environments.[152] Furthermore, hydrogel delivery systems composed of natural, extracellular matrix- (ECM-) derived materials tend be mechanically fragile and degrade quickly *in vivo*.[153] Thus a major challenge to the local delivery of proteins is the need to maintain controllable release at therapeutically effective concentrations while minimizing the loss of the protein cargo by proteolytic degradation or passive diffusion.[154,155]

Nanocomposite hydrogels are composed of nanostructures or nanoparticles that physically interact with crosslinked polymer chains in a hydrogel network.[156–158] Liposomes in particular are an attractive option for this strategy due to their

biocompatibility and tunability in protecting and delivering protein or small molecule cargos across a wide range of physical properties.[157,159] However, on their own, nanoscale substances such as liposomes and their cargo diffuse away quickly from the site of administration, effectively decreasing the therapeutic concentration at the injury site.[156,157] In order to achieve a longer rate of localized release, liposomes may be combined with a hydrogel, which serves to physically sequester the encapsulated material within the construct and aids in sustaining release at concentrations high enough to stimulate physiological activity.[156]

In this work, we develop a nanocomposite liposome/gelatin methacrylate (GelMA) hydrogel system to generate a localized, sustained release of SDF-1α capable of inducing migration and phenotypic changes in MSCs. We hypothesize that SDF-1α may be stably incorporated in anionic liposomes and further embedded in a negatively charged, Type B GelMA hydrogel (**Figure 4.1**), which contain protease-sensitive motifs but also chemical crosslinks that preserve mechanical stability.[153] As the protein is released from the liposomes, it is then sequestered within the hydrogel network via electrostatic interactions with polymer chains, which slows its diffusion into the periphery. The objectives of our work are to demonstrate that the delivery system that we have developed is capable of controllably releasing SDF-1α, that the protein is released at concentrations that effectively induce MSC migration, and that this released chemokine is bioactive and capable of exerting an effect on intracellular cell signaling pathways in MSCs.

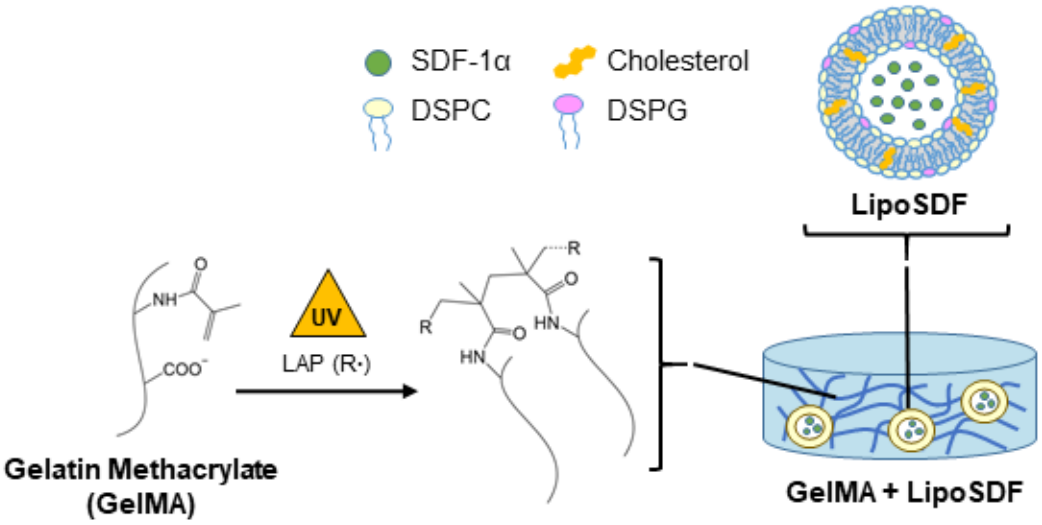

Figure 4.1: Strategy for SDF-1α delivery using a nanocomposite liposome/GelMA hydrogel. Schematic of the overall delivery system, which is composed of liposomal SDF-1α (lipoSDF) loaded in a UV-crosslinkable gelatin methacrylate (GelMA) hydrogel derived from Type B gelatin. Anionic liposomes are formed by mixing DSPC, DSPG, and cholesterol at a 65:10:25 molar ratio.

4.2: Materials and Methods

4.2.1: GelMA Synthesis and Hydrogel Preparation

We have adapted protocols previously published by our group to synthesize GelMA polymer.[160,161] Briefly, Type B gelatin (225 Bloom from bovine skin, Sigma) was dissolved in phosphate buffered saline (PBS) at 0.1 g/mL. Methacrylic anhydride (MA, Sigma) was then slowly added dropwise at a proportion of 0.6 g MA/1 g gelatin, and the solution was allowed to react for 1 hour. Afterwards, the mixture was diluted and dialyzed against deionized water for 72 hours, adjusted to a pH of 7.4, and frozen at -80 ^{o}C before lyophilization for another 72 hours. This procedure yielded a porous foam that was stored at -80 ^{o}C until use. GelMA hydrogels were formed by dissolving lyophilized GelMA in PBS with 0.1% w/v lithium phenyl-2,4,6-trimethylbenzoylphosphinate (LAP, Tocris) at 50 ^{o}C. 200 μL of the resulting mixture was then pipetted into 8 mm-diameter cylindrical molds and placed at 4 ^{o}C for 20 minutes to allow for soft gelation. Afterwards, the gels were exposed to UV light for 2 minutes in a UV box to photocrosslink.

4.2.2: Nuclear Magnetic Resonance (NMR) Spectroscopy

1H NMR (Bruker AVIII-600 MHz) was used to verify the addition of vinyl groups from the methacrylation reaction. Lyophilized GelMA polymer was dissolved in deuterium oxide (Sigma-Aldrich) at a concentration of 10 mg/mL, and samples were run at 40 ^{o}C. Data was analyzed using Bruker TopSpin3.5 software.

4.2.3: Assessment of Hydrogel Degradation

To assess the rate of enzymatic degradation, GelMA hydrogels (7.5, 10, and 15% w/v) were incubated at 37 ºC in 16 µg/mL collagenase IV (EMD Millipore) for up to 1 week. At each time point, hydrogels were collected, lyophilized, and massed. Degradation rate was determined by calculating the mass remaining at each time point using the following formula:

$$\text{Mass remaining } (\%) = (m_0 - m_t)/m_0 \times 100$$

where m_0 is the initial dry weight of undigested samples and m_t is the dry weight of digested samples at each time point.[162]

4.2.4: Rheology

GelMA was cast into cylindrical molds to form 1 mL-hydrogels for oscillatory rheological testing (ARES-G2, TA Instruments). Hydrogels were placed between a set of parallel plates and subjected to a frequency sweep between 0.1-10 rad/s with a constant strain of 0.1%. Rheological studies conducted on swollen samples were conducted after soaking the hydrogels in PBS overnight.

4.2.5: Liposome Synthesis and Protein Loading

Adapting procedures described by our group and others,[163–168] anionic liposomes were formed by dissolving ovine wool cholesterol in chloroform (10 mg/mL, Sigma) and combining it with 10 mg/mL each of 1,2-distearoyl-sn-glycero-3-phosphocholine (DSPC, Avanti Polar Lipids) and 1,2-dioctadecanoyl-sn-glycero-3-phospho-(10-rac-

glycerol) (sodium salt) (DSPG, Avanti Polar Lipids) at a molar ratio of 25:65:10. The 1 mL mixture was placed on a rotovap overnight (Büchi R-100) at 40 ^{o}C and 100 mBar to remove the chloroform and generate a thin lipid film, which was subsequently rehydrated with 1 mL SDF-1α solution in PBS (12.5 μg/mL, Peprotech). This solution was vortexed to form an emulsion and extruded 10 times through a polycarbonate filter with a pore size of 200 nm (Whatman) at 55 ^{o}C to produce liposomes of uniform size. Before use in experiments, liposomes were dialyzed against PBS at 4 ^{o}C in a Float-A-Lyzer G2 dialysis device with a 300 kD cutoff (Repligen) overnight to remove unencapsulated protein.

4.2.6: Liposome Characterization

The hydrodynamic diameter, polydispersity index (PdI), and zeta potential of fresh liposomes were measured at 25 ^{o}C by dynamic light scattering (DLS) and electrophoretic light scattering (ELS) with the NanoBrook Omni particle size and zeta potential analyzer (Brookhaven Instruments). 5 μL of the liposome suspension was diluted in 2 mL of ultrapure water for DLS or 1.5 mL of 1 mM NaCl for ELS. Measurements were then repeated for up to 2 weeks to examine particle stability at 4 ^{o}C.

Encapsulation efficiency (EE%) was determined by sampling the liposome suspension before dialysis and quantifying the amount of unencapsulated SDF-1α by enzyme-linked immunosorbent assay (ELISA, Peprotech) following the manufacturer's protocols. EE% was then indirectly calculated by the following formula:

$$EE\% = (m_i - m_d)/m_i \times 100$$

where m_i is the initial mass of SDF-1α used in film rehydration and m_d is the mass of unencapsulated SDF-1α detected by ELISA.

Cryo-transmission electron microscopy (cryo-TEM) images were obtained using the JEM-2100 LaB6 TEM (JEOL) at the Advanced Imaging and Microscopy Laboratory at the Maryland NanoCenter. Scanning electron microscopy (SEM) with ionic liquid treatment was conducted using the SU-70 Field Emission SEM (Hitachi).

4.2.7: Characterization of SDF-1α Release

To characterize protein release from liposomes, 500 μL of fresh liposomal SDF-1α (lipoSDF) suspension was added to the top chamber of a Slide-A-Lyzer MINI Dialysis device (20k MWCO, Thermo Fisher) and dialyzed against PBS for one week at 37 ^{o}C. At each time point, a 50 μL sample was taken and centrifuged at 1500 g for 30 minutes at 4 ^{o}C to separate the liposomes from the released protein. The supernatants were then transferred into separate tubes for analysis by ELISA to determine the amount of SDF-1α released.

To assess the ability of SDF-1α to be released from within the GelMA matrix over time, 5 μg/mL of SDF-1α or lipoSDF was added to GelMA solutions before crosslinking. Samples were incubated in PBS/0.1% BSA for 1 week at 37 ^{o}C in the presence of 16 μg/mL collagenase IV. At each time point, supernatants were

collected from each sample and replaced with fresh solution. The cumulative release of SDF-1α into these supernatants was then assessed by ELISA as before.

4.2.8: Cell Culture

Human bone marrow-derived MSCs (RoosterBio) were expanded in RoosterNourish media (RoosterBio) until confluency and used up to passage 8. Cells were seeded at 1 x 10^5 cells/well for transwell experiments and 2.5 x 10^5 cells/well for Western blot experiments. In both cases, MSCs were first serum-starved overnight in Dulbecco's Modified Eagle Medium (DMEM, Thermo Fisher) before seeding the following day.

4.2.9: Western Blotting

Media was conditioned over 1 week by GelMA containing 5 μg/mL of SDF-1α or lipoSDF as detailed above. MSCs were then exposed to conditioned media for 2 hours before lysis with RIPA buffer (Thermo Scientific) containing a cocktail of phosphatase and protease inhibitors (Abcam). Lysates were then mixed with Laemmli buffer (Bio-Rad) and run on a 12% SDS/PAGE electrophoresis gel before being transferred onto a nitrocellulose membrane using a Trans Blot semi-dry transfer machine (Bio-Rad). Membranes were then probed with primary rabbit antibodies against human AKT p473, RPS6 pS235/236 (1:250 dilution, Abcam), as well as total AKT and RPS6 (1/500, 1/5000, Abcam). A secondary horseradish peroxidase-conjugated goat anti-rabbit antibody (1:10,000 dilution, Abcam) was used in conjunction with enhanced chemiluminescence substrate (Bio-Rad) to visualize the protein bands.

4.2.10: Statistical Methods

Unless noted, data is presented as mean ± STD with n = 3 biological replicates per group. Depending on the comparisons being made, a Student's T-test or one-way analysis of variance (ANOVA) with Tukey's *post hoc* test was used to determine statistical differences between groups, with $p < 0.05$ considered to be significant. Statistical analyses were conducted using Minitab 18.

4.3: Results

4.3.1: Characterization of GelMA Hydrogels

The reaction of methacrylic anhydride with Type B gelatin to form GelMA was confirmed by 1H NMR spectroscopy by assessing for the presence of vinyl groups in the sample spectrums. A pair of peaks was observed between 5.5 – 6 ppm, corresponding to the protons from the vinyl group of methacrylate (**Figure 4.2 A,** blue spectrum) [169,170]. These peaks were not present in the NMR spectrum of gelatin (red spectrum).

GelMA hydrogels digested in collagenase IV solution were collected at each time point, lyophilized, and massed in order to determine their rates of degradation (**Figure 4.2 B**). This produced a content-dependent trend with slower degradation as GelMA content was increased (*$p < 0.005$, **$p < 0.001$).

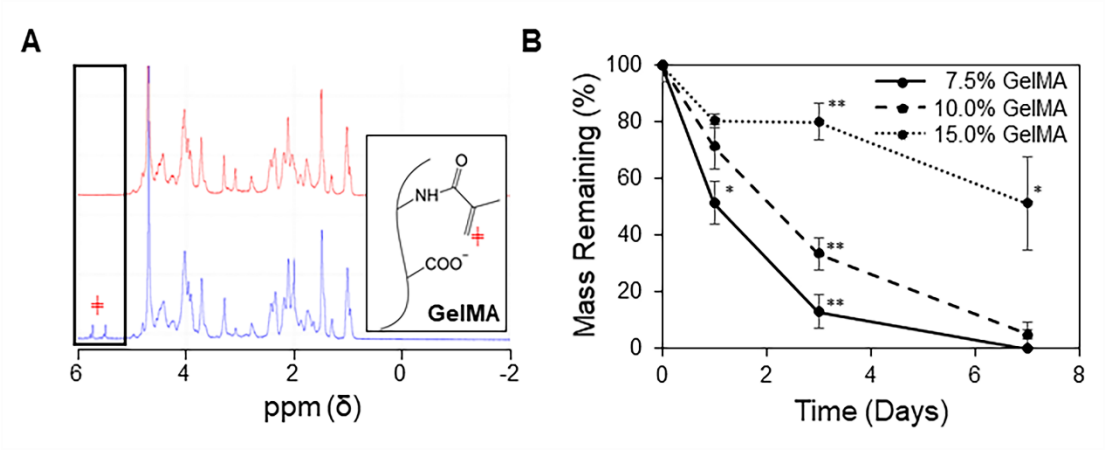

Figure 4.2: Characterization of the GelMA hydrogel. (A) Representative 1H NMR spectrums of gelatin (red) and GelMA (blue), with the boxed peaks representing protons attached to the vinyl group of methacrylate (red ╪). (B) Degradation of GelMA hydrogels in collagenase IV shows a slower rate of degradation as GelMA content is increased (n = 3, mean ± STD). One-way ANOVAs with Tukey's post-hoc comparisons were conducted between groups at each time point. *$p < 0.005$ and **$p < 0.001$).

Rheology conducted on GelMA + lipoSDF hydrogels showed that for all concentrations of GelMA used, the storage modulus (G') was greater than the loss modulus (G") across the entire frequency range **(Figure 4.3)**. This effect was observed in both newly-fabricated hydrogels and as well as gels that were allowed to swell in PBS overnight.

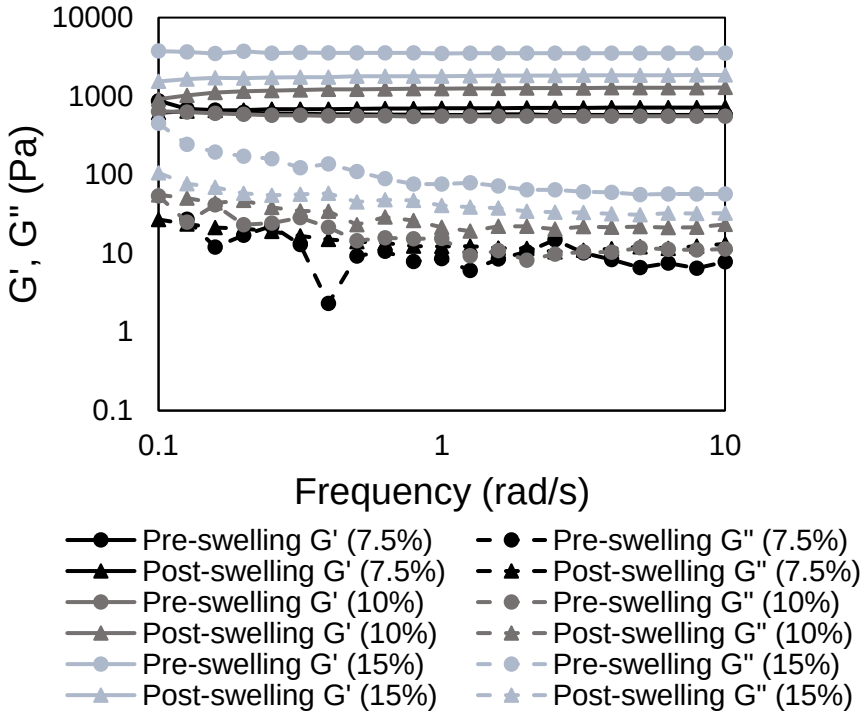

Figure 4.3: GelMA hydrogels deform elastically under shear before and after swelling. Representative rheological plots of storage (G') and loss (G") moduli of hydrogels with different GelMA content loaded with liposomes. G' > G" for all groups before and after swelling, indicating that the gels tend to deform elastically rather than flow under applied shear, and that they remain mechanically stable after swelling. This is hypothesized to occur due to the presence of highly structured hydrogel networks containing well-developed crosslinks.

4.3.2: Characterization of Liposomes

Unilamellar empty liposomes (lipo) and lipoSDF were formed with a hydrodynamic diameter of 227 ± 5 and 236 ± 3 nm, respectively, and with a narrow size distribution (PdI < 0.1) (**Figures 4.4 A, C**). The diffusion coefficients of lipo and lipoSDF particles was measured to be 2.1 and 2.0 x 10^{-8} cm^2/s respectively in water, which when compared against the diffusion coefficient of free SDF-1α protein (1 x 10^{-6} cm^2/s),[171] indicates that these larger particles are slower to diffuse in the medium.[172] In order to minimize the destabilizing electrostatic interactions between the liposomes and the negatively charged GelMA, the surface charge of the liposomes was engineered to have a slight negative charge between -48 and -41 mV, as measured by ELS (**Figure 4.4 E**). To determine the encapsulation efficiency of lipoSDF, an ELISA assay was conducted to determine the protein concentration in lipoSDF after dialysis and compared the amount that was added initially. Passive loading of SDF-1α into liposomes resulted in an encapsulation efficiency of 88 ± 6%. Lastly, the hydrodynamic diameter and zeta potential of the same batch of lipoSDF was monitored for 2 weeks to assess for particle stability (**Figure 4.5**). Narrow distributions were observed in both with minimal changes over time, suggesting that these particles remain stable over time when stored at 4 ^oC.

A

	Unloaded	Loaded
PdI	0.082 ± 0.0045	0.036 ± 0.019
EE (%)	N/A	87.8 ± 5.9
Diffusion Coefficient (cm^2/s)	2.09 ± 0.078 x 10^{-8}	2.01 ± 0.027 x 10^{-8}

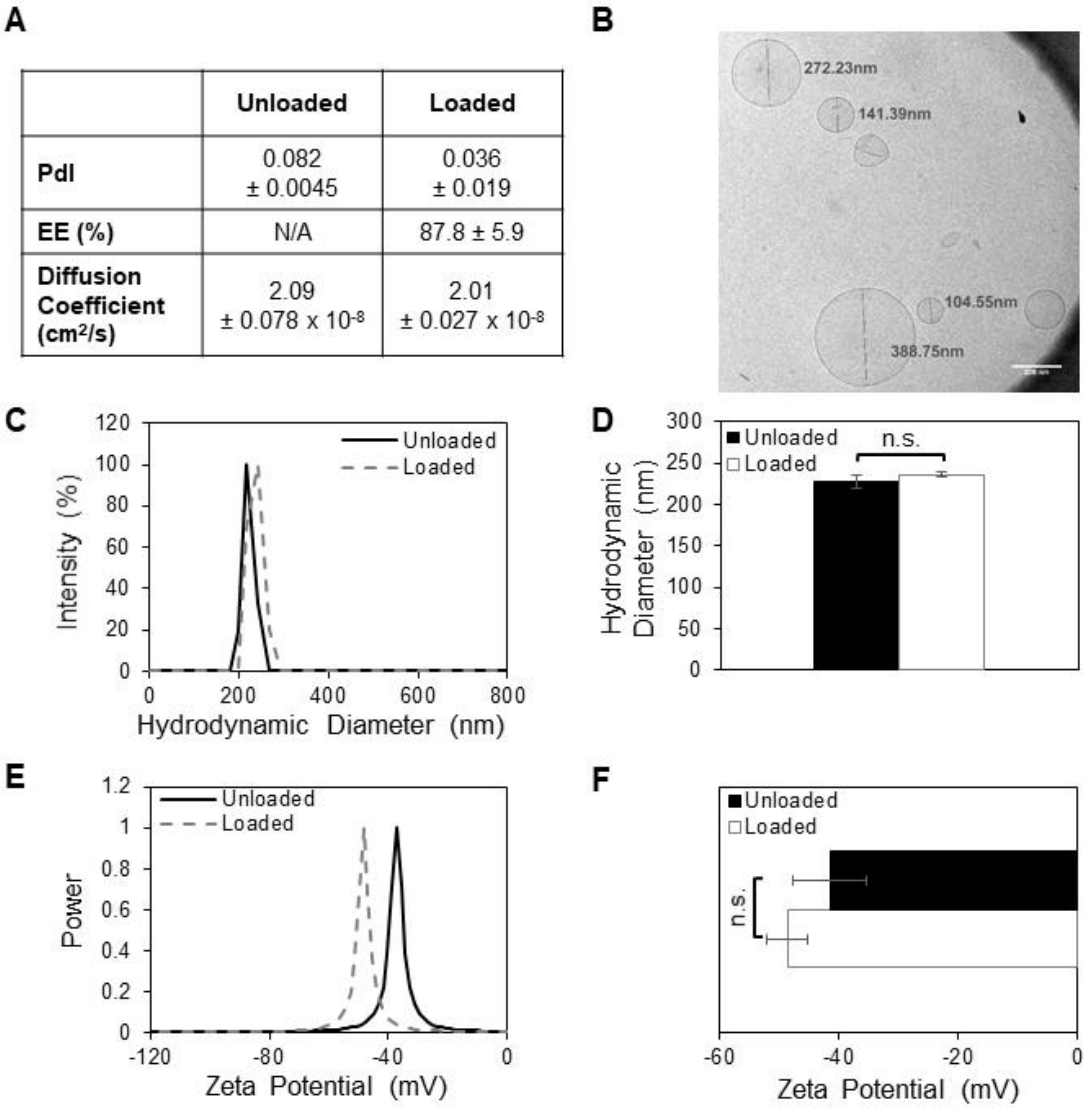

Figure 4.4: SDF-1α loaded into liposomes does not alter particle diameter or surface charge. (A) Quantification of liposomal polydispersity index (PdI), encapsulation efficiency (EE%), and diffusion coefficients in water as measured by dynamic light scattering. (B) Cryo-TEM imaging of lipoSDF shows mostly spherical, unilamellar particles averaging around 200 nm in diameter (Scale bar: 200 nm). (C, D) Size and (E, F) zeta potential distributions of loaded and unloaded liposomes. The means between the two groups do not differ significantly (n = 3, mean ± STD. Student's T-test, $p > 0.05$). Each measurement was conducted with a different preparation of liposomes.

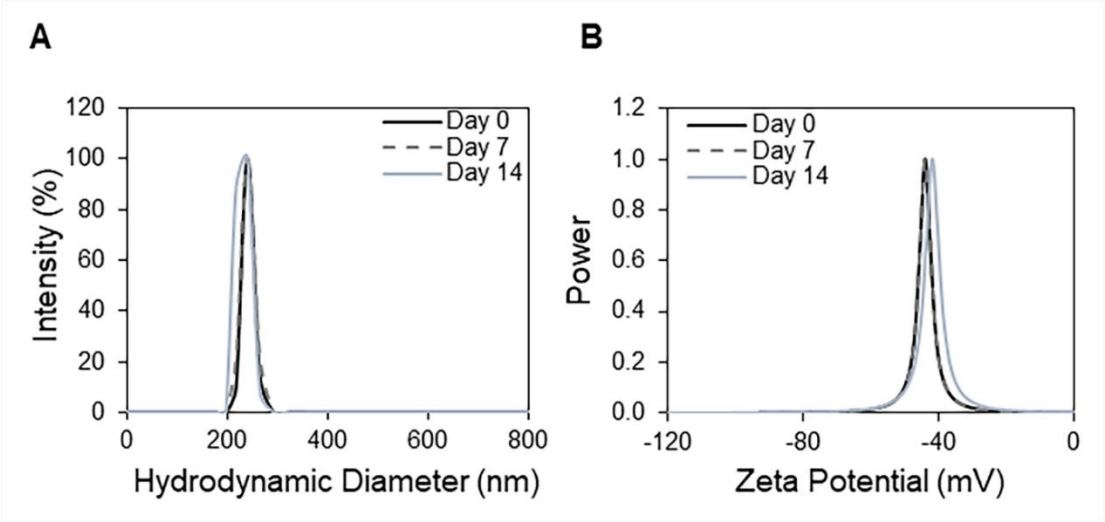

Figure 4.5: Liposomes remain stable in storage over time. (A) Representative size and (B) zeta potential distribution of the same batch of liposomal SDF-1α over 2 weeks at 4 ^{o}C. The distributions slightly widen and shift right respectively but in general remain narrow.

4.3.3: Release of SDF-1α from Liposomes and GelMA

LipoSDF was shown to follow burst release kinetics over 1 week (**Figure 4.6 A**), while hydrogel-loaded, unencapsulated SDF-1α was released more slowly and as a function of GelMA concentration (**Figure 4.6 C**). When applied to well-known models of drug release, the GelMA + SDF profiles were found to readily fit the Korsmeyer-Peppas model ($0.97 \leq r^2$, **Figures 4.6 D, 4.7 A**):

$$M_t/M_\infty = K_{KP}t^n$$

where M_t / M_∞ is the fraction of released drug at time *t*, K_{KP} is the Korsmeyer-Peppas rate constant, and *n* is the release exponent that identifies the mechanism of drug release.[173]

When GelMA hydrogels were loaded with lipoSDF, however, the release followed more exponential profiles (**Figure 4.6 E**). These release curves did not fit the Korsmeyer-Peppas model (**Figures 4.7 B, C**), but were found to fit the Weibull model of delayed release instead ($0.96 \leq r^2$, **Figure 4.6 F**):

$$M_t/M_\infty = 1 - \exp\frac{-(t-T_i)^\beta}{\alpha}$$

where M_t / M_∞ is the fraction of released drug at time *t*, T_i is the delay time before the start of release, α is the scale parameter, and β is the shape parameter.[174,175]

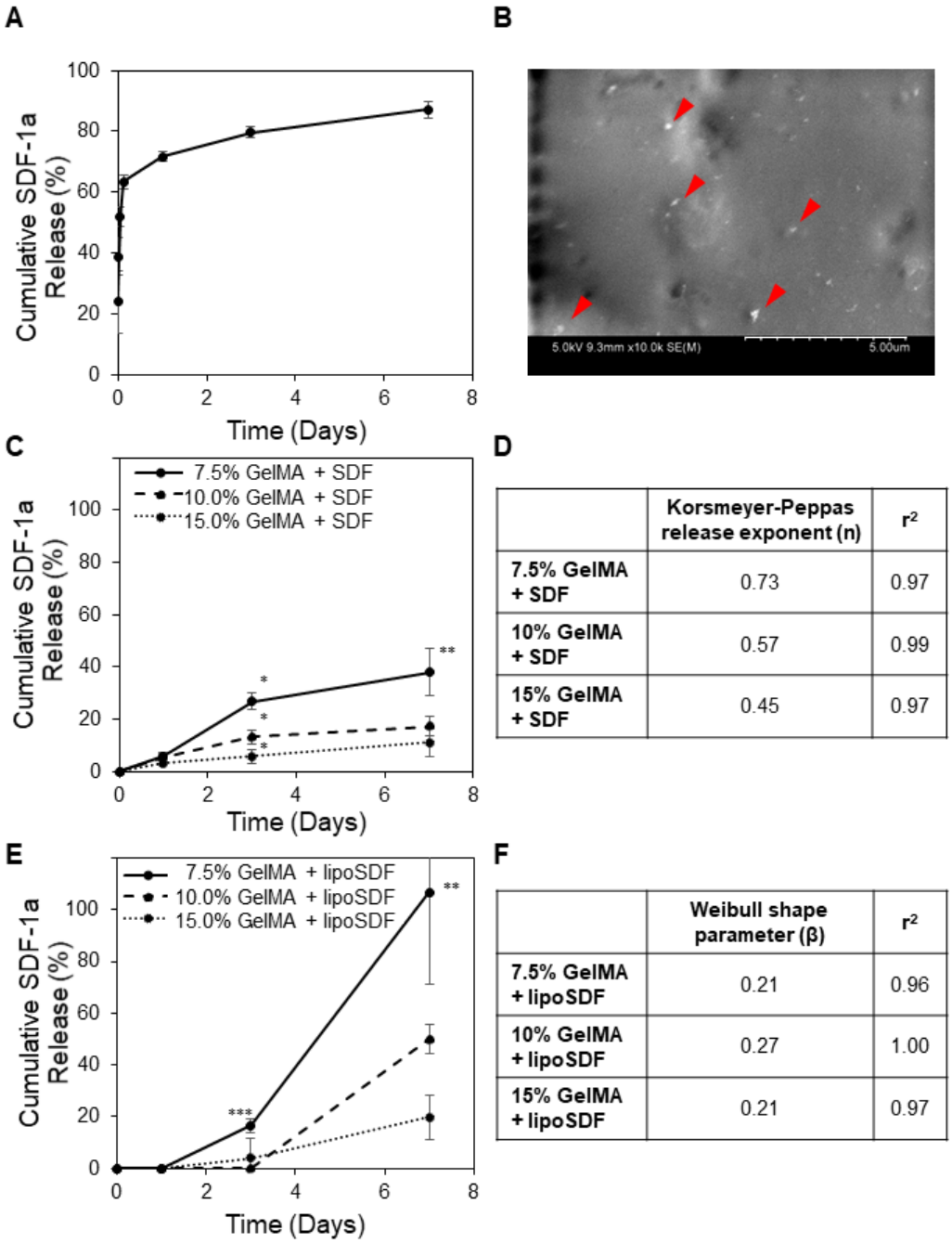

	Korsmeyer-Peppas release exponent (n)	r^2
7.5% GelMA + SDF	0.73	0.97
10% GelMA + SDF	0.57	0.99
15% GelMA + SDF	0.45	0.97

	Weibull shape parameter (β)	r^2
7.5% GelMA + lipoSDF	0.21	0.96
10% GelMA + lipoSDF	0.27	1.00
15% GelMA + lipoSDF	0.21	0.97

Figure 4.6: The release kinetics of SDF-1α can be tuned by incorporating the protein in a GelMA hydrogel. (A) Cumulative SDF-1α released from liposomes over 1 week is characterized by burst release kinetics (n = 4, mean ± STD). (B) SEM imaging of GelMA + lipoSDF shows small particles of less than 500 nm dispersed throughout the surface of a hydrogel fiber (Scale bar: 5 μm). (C) Cumulative percentage of unencapsulated SDF-1α or

(E) lipoSDF released from GelMA over 1 week, normalized to the amount of initial detectable protein (n = 4, mean ± STD). One-way ANOVAs with Tukey's post-hoc comparisons were conducted between groups at each time point. (*$p < 0.0001$, **$p = 0.001$, ***$p < 0.01$). (D) Release exponent (n) and r^2 values derived from the release of unencapsulated SDF-1α from GelMA hydrogels, fit to the Korsmeyer-Peppas model. (F) Shape parameter (β) and r^2 values derived from release of lipoSDF, fit to the Weibull release model.

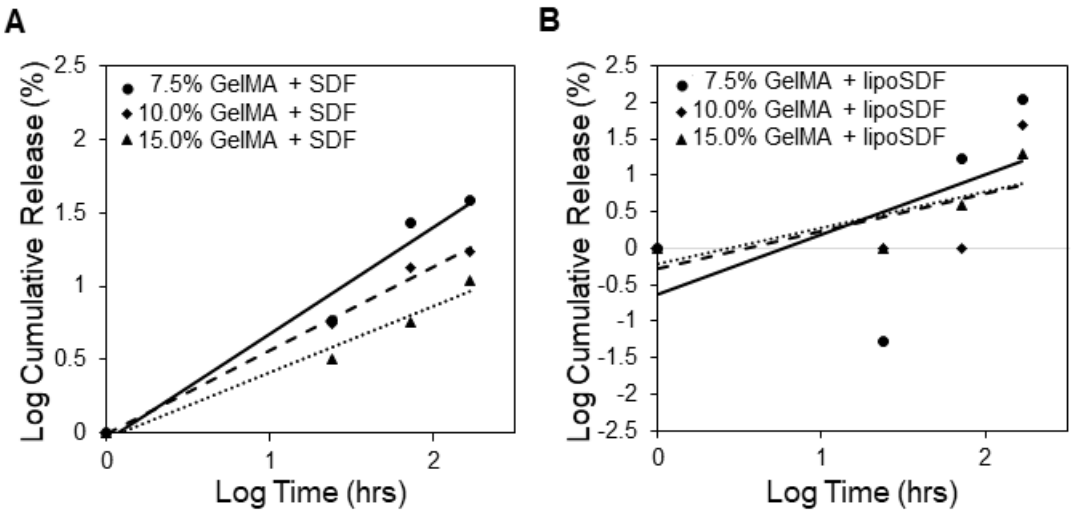

C

	Korsmeyer-Peppas release exponent (n)	r^2
7.5% + lipoSDF	0.8164	0.30
10% + lipoSDF	0.513	0.35
15% + lipoSDF	0.493	0.61

Figure 4.7: The release profiles of lipoSDF from GelMA do not fit the Korsmeyer-Peppas model of drug release. Plotted release data of (A) unencapsulated SDF-1α and (B) lipoSDF from GelMA hydrogels, with linear trend lines indicating the profile of the Korsmeyer-Peppas model for each group. (C) Release exponent (n) and r^2 values derived from the latter indicate that the data does not fit this model.

4.3.4: Transwell Migration Assays

MSCs seeded on transwells were exposed to serum-free media conditioned by 80 ng/mL of either SDF-1α or lipoSDF. Both groups were able to significantly induce more chemotaxis of MSCs compared to the negative control of DMEM supplemented only with PBS ($p < 0.01$, **Figures 4.8 A and B)**. This suggests that our lipoSDF fabrication method does not impair the ability of the chemokine to induce MSC migration.

MSC migration was assessed over 1 week in response to media conditioned by 10% GelMA + SDF or 10% GelMA + lipoSDF. At each time point, conditioned media was collected to stimulate MSCs for 2 hours before they were stained and counted. Increased migration was observed at Days 3 and 7 in the GelMA + lipoSDF group, while no such trend was observed with GelMA + SDF ($p < 0.05$, **Figure 4.8 C**).

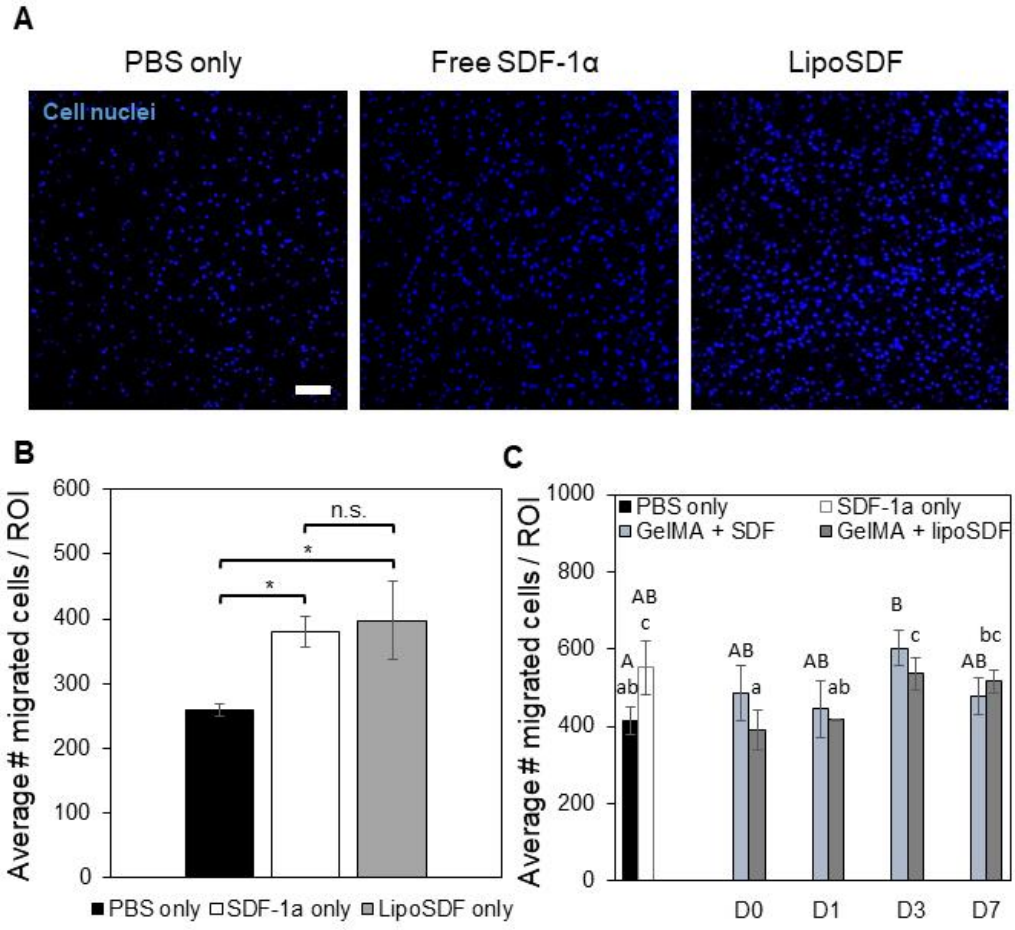

Figure 4.8: Liposomal encapsulation does not impair the chemotactic activity of SDF-1α and is able to induce chemotaxis for up to 1 week. (A) Representative images and (B) quantitative cell counts from Hoechst-stained MSCs in a region of interest (ROI) that have migrated through a transwell membrane in response to the respective chemotactic factor: PBS, 80 ng/mL of free or liposomal SDF-1α (Scale bar: 100 μm. n = 3, mean ± STD. One-way ANOVAs with Tukey's post-hoc comparisons, *$p < 0.01$). (C) Comparison of MSC migration in response to media conditioned over 1 week by PBS, 80 ng/mL SDF-1α, or either 5 μg/mL of free or liposomal SDF-1α in 10% GelMA. Two sets of one-way ANOVAs with Tukey's post-hoc comparisons were conducted between groups (groups being compared are denoted by either upper- or lower-case letters). Groups that do not share a letter are statistically different ($p < 0.05$).

4.3.5: Western Blots to Assess for mTOR Signaling Activity

Western blots for phosphorylated (phospho-) AKT and RPS6 demonstrated that our GelMA + SDF and GelMA + lipoSDF constructs are capable of exerting effects on the phosphorylation status of key signaling proteins from the mammalian target of rapamycin (mTOR) pathway (**Figure 4.9 A**). Densitometry analysis indicated that for AKT, the trends of mean intensity of the GelMA + lipoSDF group were lower (means < 1) than the negative PBS-treated control on all days, while the GelMA + SDF group did not show this effect (**Figure 4.9 B)**. For RPS6, both groups showed decreasing levels of protein over time (means < 0.91 by Day 7) below both the negative PBS control and the positive control of soluble SDF-1α (**Figure 4.9 C**).

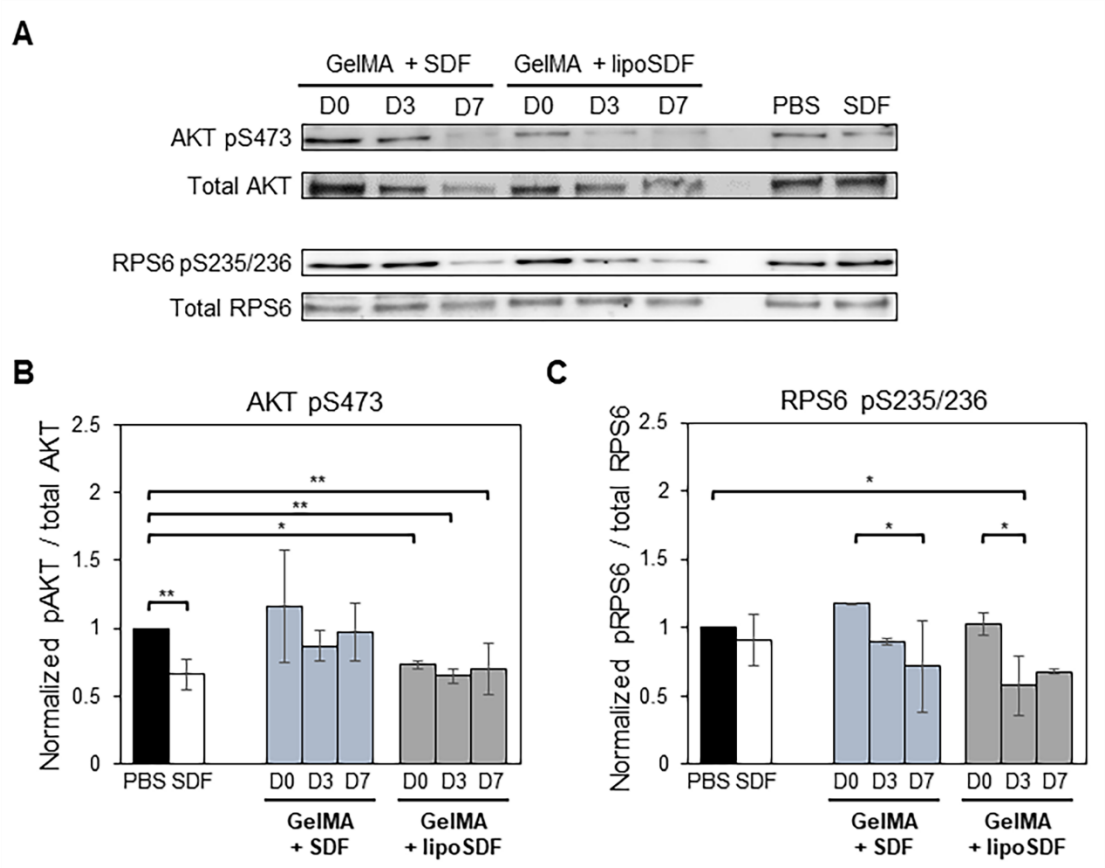

Figure 4.9: SDF-1α or lipoSDF in GelMA are capable of exerting effects on key proteins of the mTOR signaling pathway over 1 week. (A) Representative Western blots of phosphorylated AKT and RPS6 compared to their respective total protein controls in MSCs exposed to PBS, 80 ng/mL free SDF-1α, or 5 μg/mL of either free or liposomal SDF-1α in GelMA. (B) Densitometry analysis of phosphorylated AKT and (C) RPS6. (n = 3, mean ± STD. Two sets of one-way ANOVAs with Tukey's post-hoc comparisons were conducted between groups. *$p < 0.05$ and **$p < 0.01$)

4.4: Discussion

In this work, we have developed a nanocomposite hydrogel delivery system capable of releasing the chemokine SDF-1α in liposomal form and demonstrated that this system can affect cell signaling processes and induce chemotaxis in MSCs for up to 1 week. Similar nanocomposite constructs have previously been leveraged to control the delivery of therapeutic proteins such as PlGF, MCP-1, and EGF.[175,176] The use of liposomes for these applications is particularly attractive due to the high hydrophilicity of charged proteins such SDF-1α, which are thought to interact minimally with the hydrophobic membrane and allow for more efficient incorporation into the aqueous core.[6–8,177] For our work, we opted to use an anionic liposome formulation to minimize any electrostatic attraction between the liposomes and the negatively charged GelMA that could cause the hydrogel fibers to insert in the lipid bilayer and destabilize the particles.[178] We chose to use this strategy in particular because proteins such as SDF-1α are susceptible to enzymatic degradation, and this method provides an additional method of locally concentrating the protein and isolating it from nearby proteases compared to direct adsorption to a hydrogel.[5,6]

As SDF-1α is a chemokine, one of the most important indicators of its activity is its ability to induce chemotaxis in nearby cells. In our study, we assessed the bioactivity of our released SDF-1α by measuring its ability to chemoattract MSCs. Furthermore, we studied the released protein's ability to exert effects on the mTOR pathway. This requires the presence of intact, unencapsulated protein that can bind to the cells' surface receptor CXCR4 and activate downstream signaling factors. By encapsulating

SDF-1α within liposomes and further embedding them within GelMA hydrogels, we are able to deliver protein with preserved bioactivity for up to 1 week.

Our studies have demonstrated that our SDF-1α-loaded liposomes are monodisperse in solution and retain tight size and charge distributions even after 2 weeks at 4 ^{o}C (**Figures 4.4 and 4.5**). These findings suggest that our liposomes have a prolonged shelf-life, can be stably loaded in hydrogels, and will retain their therapeutic efficacy even after being stored for at least 2 weeks.

The use of GelMA in this application represents an innovative strategy to control the release of a liposomal encapsulated therapeutic protein. GelMA hydrogels contain matrix metalloproteinase- (MMP-) sensitive motifs that render them susceptible to enzymatic degradation (**Figure 4.2 B**), but this rate is modifiable by changing the number of crosslinks between methacrylate groups.[179] In our rheological studies, we found that, for all concentrations of GelMA used, the G' of our GelMA + lipoSDF hydrogels was always greater than the G", indicating that our hydrogels tend to deform elastically rather than flow when shear is applied (**Figure 4.3**). We hypothesize that this is due to the highly structured nature of the hydrogel, which is extensively crosslinked throughout the network.[180] This helps to preserve some of the structure and mechanical properties of the hydrogel constructs as they naturally degrade over time, which is especially critical in the context of dressings for wound healing applications.[34,50] This effect was also observed after the hydrogels were fully

swollen, which suggests that they can maintain mechanical stability in an aqueous environment.

One other application of GelMA is to tune the release kinetics of our protein of interest. Much like native skin ECM, which is mainly composed of type I collagen, GelMA derived from alkaline-processed, Type B gelatin (itself a denatured form of collagen) carries a net negative charge at physiological pH.[181] Proteins such as SDF-1α, which contains a large number of basic amino acid residues such as lysine and hydroxylysine that contributing to its positive charge, will form electrostatic interactions with these hydrogel fibers.[182] This will slow its diffusion out of negatively charged gels and allow it to retain a relatively high local concentration that is physiologically relevant to nearby cells, including those that may eventually migrate into the gel itself.[8,183] We have shown that we are able to tune the release kinetics by encapsulating SDF-1α in liposomes and embedding them in a GelMA hydrogel; by using this method we are able to achieve faster and higher amounts of protein release in a time-delayed manner compared to using unencapsulated SDF-1α instead. Electrostatic interactions between Type B-derived GelMA and SDF-1α would account for the attenuated burst release pattern in **Figure 4.6 C** showing decreased amounts of SDF-1α release compared to that from loaded liposomes only (**Figure 4.6 A**). Conversely, the use of anionic liposomes would prevent excessive electrostatic interactions between the lipid membranes and the GelMA fibers, which might otherwise destabilize the particles to cause earlier cargo release. The kinetics in **Figure 4.6 E** reflect this decreased release in the first 1-3 days, with higher amounts

of release in the subsequent days as the GelMA hydrogels degrade and protein is released from the nanoparticles. Furthermore, lipoSDF has a diffusion coefficient 2 orders of magnitude lower than free SDF-1α, leading to slower diffusion in aqueous environments. This may also play a role in the low release from GelMA + lipoSDF in the first 1-3 days. In comparison, the direct charge-charge interactions between the negatively charged Type B-derived GelMA and the positively charged SDF-1α causes the protein to remain complexed to the GelMA fibers and release slowly from the hydrogel over the entire time course.

We found that the release profiles of the GelMA + SDF groups could be modeled by the Korsmeyer-Peppas equation for diffusion-controlled drug release (**Figure 4.6 D**). The calculated release exponent (n) for the 10% and 15% GelMA groups was about 0.5, indicating that these systems obey classic Fickian diffusion schemes, while the 7.5% GelMA group had an exponent that suggested anomalous, non-Fickian transport characterized by both time-dependent solute diffusion and swelling of the polymer matrix ($0.45 < n < 0.89$ and $n \neq 0.5$).[173,174] Furthermore, we saw that only the GelMA + SDF, but not the GelMA + lipoSDF groups fit this model (**Figure 4.7**). Instead, the latter groups were more readily modeled as a delayed release system using the Weibull equation, whose shape parameter (β) can be used to describe the shape of the release profile (**Figure 4.6 F**).[175] For all GelMA + lipoSDF groups, $\beta < 1$, indicating that release from the system first occurs with a steep slope before following a more exponential shape.[174] We believe that this phenomenon occurs due to a small degree of leakage or burst release that results from some liposomes releasing their cargo at

early time points.[5] This might result in SDF-1α being sequestered within the gel through charge-charge interactions that prevents diffusion away from the site until the GelMA hydrogel is degraded.[9,11] Alternatively, SDF-1α may be complexed with the negatively charged DSPG lipids on the liposome surface, causing any liposomes outside the gel to be detected by our antibody-based detection assays.

As our modeling attempts indicate that SDF-1α could diffuse from our system in a manner describable by Fick's laws, and our studies have demonstrated their ability to release the cargo protein while degrading slowly over 1 week, the 10% GelMA groups were selected for use in subsequent experiments. In our transwell studies, we first confirmed that liposomal encapsulation of the protein does not negatively impact its ability to chemoattract MSCs (**Figures 4.8 A and B**). Media conditioned by either GelMA + SDF or GelMA + lipoSDF were then collected at days 0, 1, 3, and 7 to assess for the continued ability of the system to release chemokine capable of inducing cell migration. In the GelMA + lipoSDF group, we saw an increase in cell migration over time (**Figure 4.8 C**), reflecting the exponential profile of protein release suggested by our modeling data. This exponential trend of release followed what we had observed from our release studies, suggesting that lipoSDF is a more tunable method of SDF-1α release that can predictably induce the migration of MSCs for up to 1 week. Conversely, no such trend was predicted by our models for the GelMA + SDF group and did not correlate with what was observed experimentally in our migration studies.

We also found that our nanocomposite hydrogel delivery system is capable of affecting the phosphorylation status of key proteins from the mTOR pathway, which is known to be stimulated by SDF-1α through the protein's cognate receptor CXCR4.[184–186] While there are many highly complex signal transduction pathways that influence the behavior and function of cells, we opted to study the mTOR pathway in particular due to its role in stimulating cell metabolism, migration, and the production of pro-healing proteins.[187,188] Furthermore, mTOR signaling is associated with the regulation of glucose metabolism and is differentially regulated among pro- and anti-inflammatory subsets of immune cells due to their different metabolic demands.[137,189]

For our work, we chose to study the levels of phosphorylated AKT, which is the biologically active form of the protein that activates mTOR.[190] We also chose to probe for levels of phosphorylated RPS6, which is further downstream of mTOR and is implicated in protein synthesis.[187] In our Western blot experiments, we saw that GelMA + lipoSDF, but not GelMA + SDF, reached similar levels of phospho-AKT as the positive (free SDF-1α) control across all days (**Figure 4.9 B**). Curiously, the levels of phospho-AKT for the free SDF-1α control were lower than that of the negative PBS control. This may be due to feedback inhibition of phospho-AKT by mTOR as signaling reaches equilibrium.[185,187] Alternatively, exposure to the released SDF-1α may have caused the cells to adopt a lower bioenergetic state with decreased mTOR activity, a phenomenon that has been previously observed in anti-inflammatory macrophages subtypes.[189] We also hypothesize that the variations

between experiments may be due to nonspecific charge-charge interactions between GelMA and SDF-1α that may interfere with diffusion and binding of the protein to its receptor.[10,11] Similarly, the levels of phospho-RPS6 appeared to decrease slightly upon stimulation with free SDF-1α. In both our groups, we saw decreasing levels of phospho-RPS6 with time (**Figure 4.9 C**), suggesting that the amount of released protein present at each time point was still capable of inducing mTOR signaling activity within MSCs at or beyond the capability of the positive control.

Overall, our studies indicate that our nanocomposite delivery system is capable of releasing and maintaining local concentrations of bioactive SDF-1α at levels capable of stimulating MSC recruitment *in vitro*. We were able to observe these effects for up to 1 week, which is a physiologically relevant *in vivo* timespan for the migration of MSCs and other local immunomodulatory cell types such as macrophages.[48,126] The results of this work represent a promising approach that expands on current strategies for the controlled delivery of therapeutic proteins, with important implications in biomedical research and development, as well as in clinical settings.

4.5: Conclusions

The healing progression and ultimate outcome of a wound are highly dependent on the activity of immunomodulatory cell populations such as MSCs. Chronic wounds in particular are characterized by persistent inflammation preventing the progression of normal healing mechanisms that lead to wound closure and skin tissue regeneration.[84,191] This inflammatory microenvironment impairs the recruitment of

MSCs that normally secrete immunomodulatory and pro-healing cytokines which play an important role in tissue repair.[144,145] In our work, we have demonstrated that we are able to fabricate a nanocomposite liposome-hydrogel system capable of stably encapsulating and tuning the release of the chemokine SDF-1α over time. We further show that this system is able to affect intracellular mTOR signaling as well as induce chemotaxis in MSCs. To our knowledge, this is the first study to report the delivery of liposomal SDF-1α using a nanocomposite strategy. We believe that this work could be in turn extended to the delivery of other therapeutic proteins or applied to clinical applications including wound healing, immunomodulation, and tissue regeneration.

Chapter 5: SDF-1α Delivery in Nanocomposite Hydrogels Promotes Migration and Anti-Inflammatory Responses in Macrophages

In recent years, biomaterials developed to stimulate wound healing have shifted from a paradigm of "immuno-inert" to "immunomodulatory" to leverage the ability of the host immune cells to produce a microenvironment more conducive to healing. In particular, macrophages present in a wound can be stimulated to adopt either pro- or anti-inflammatory phenotypes. We have previously developed a nanocomposite hydrogel system capable of delivering stromal cell-derived factor-1 alpha (SDF-1α), and characterized its effect on migration and its bioactivity in mesenchymal stem cells. In this work, we extend our investigation to the migration of bone marrow-derived macrophages (BMDMs) into nanocomposite gelatin methacrylate (GelMA) hydrogels *in vitro*, and assay their cytokine profile to determine if they are polarized to pro- or anti-inflammatory phenotypes. Using this strategy, we further study the potential of this delivery system to promote the recruitment and polarization of macrophages *in vivo* using a full-thickness skin defect model in wild type mice. Our results demonstrate the ability of this delivery system to promote migration of BMDMs within GelMA in response to released chemokine, and also show that these biomaterials do not stimulate high levels of pro-inflammatory cytokine production upon contact with BMDMs. This is additionally supported in our animal work, where we demonstrate that our hydrogels are capable of recruiting macrophages of a primarily anti-inflammatory phenotype, potentially improving wound healing responses if used as a wound dressing or skin substitute.

5.1: Introduction

Wound healing is an extremely complex process that is dependent on a variety of different cell types, each playing a critical role. In the case of skin injury, the development of granulation tissue followed by mature dermis, along with wound closure and keratin stratification, all result from temporal- and spatial-dependent cues dictated by the local cytokine microenvironment.[48] This in turn is heavily influenced by the phenotype of infiltrated immune cells including macrophages.[192]

Hydrogel-based wound dressings and skin substitutes are commonly used in tissue engineering strategies to establish a template for tissue regeneration as cells migrate into a defect and proliferate.[55] In particular, hydrogels derived from extracellular matrix (ECM) components are attractive due to the presence of native protein motifs that facilitate cell adhesion and growth.[50,144] Such gels can be further engineered to improve their mechanical properties and also to deliver therapeutic drugs or proteins that encourage tissue regeneration.[144]

We have previously developed a nanocomposite hydrogel system composed of gelatin methacrylate (GelMA) containing liposomally-encapsulated stromal cell-derived factor-1 alpha (SDF-1α),[193] a chemokine that plays a role in stem and immune cell chemotaxis, wound healing, and angiogenesis.[152,194] In our current work, we seek to study the effects of this construct containing GelMA and liposomal SDF-1α (GelMA + lipoSDF) on the migratory ability and phenotype of macrophages. We

hypothesize that GelMA hydrogels containing chemokine such as SDF-1α or lipoSDF will promote migration into the hydrogel itself, where they will be stimulated to adopt a more anti-inflammatory phenotype instead of a pro-inflammatory one (subsequently referred to here as "M2" and "M1" respectively). When applied to an *in vivo* model of wound healing in wild type mice, we expect these findings to translate as an increased expression of M2-associated proteins in the wound bed tissue with a corresponding decrease in M1-associated proteins. Our results demonstrate that seeded bone marrow-derived macrophages (BMDMs) are able to migrate and penetrate into our hydrogels, and that these materials do not incite a strong inflammatory response in these cells *in vitro*. The predominance of M2 macrophages present in the wound sites of wild type mice also offer strong support for use of this strategy in living systems, especially in conditions where influence over the local microenvironment's cytokine milieu would be critical to the regenerative outcome and to restoring the tissue's physiological function.

5.2: Materials and Methods

5.2.1: GelMA Synthesis

Following our previously-published protocol,[193] GelMA polymer was synthesized by the addition of methacrylic anhydride (MA, Sigma) to Type B gelatin (225 Bloom from bovine skin, Sigma) dissolved in phosphate buffered saline (PBS). After reacting for 1 hour, the mixture was diluted in PBS and dialyzed against deionized water for 72 hours, adjusted to a pH of 7.4, and frozen at -80 ^{o}C before lyophilization.

The resulting GelMA foam was stored at room temperature and protected from moisture until further use.

5.2.2: LipoSDF Preparation

LipoSDF was fabricated through roto-evaporation of a 25:65:10 molar ratio solution of ovine wool cholesterol (Sigma), 1,2-distearoyl-sn-glycero-3-phosphocholine (DSPC, Avanti Polar Lipids) and 1,2-dioctadecanoyl-sn-glycero-3-phospho-(10-rac-glycerol) (sodium salt) (DSPG, Avanti Polar Lipids) in chloroform. This generated a thin lipid film that was subsequently rehydrated in an aqueous 12.5 μg/mL recombinant murine SDF-1α solution (Peprotech) and extruded 10 times through a 200-nm polycarbonate filter (Whatman). Liposomes were then dialyzed against PBS overnight at 4 ^{o}C in a Float-A-Lyzer G2 dialysis device with a 300 kD cutoff (Repligen) to remove the unencapsulated protein.

5.2.3: Cell Culture

Bone marrow was extracted from the long bones of C57BL/6 mice between 8-14 weeks old through centrifugation.[195] Bone marrow-derived macrophages (BMDM) were generated by culturing bone marrow cells in Roswell Park Memorial Institute media (RPMI, ATCC) with 10% heat-inactivated fetal bovine serum (FBS, Gibco) and 25 ng/mL murine M-CSF (Peprotech) for 6 days with partial media replenishment every 2 days.

5.2.4: Hydrogel Preparation and Cell Seeding

GelMA + SDF and GelMA + lipoSDF hydrogels were prepared by dissolving GelMA polymer at a 10% w/v concentration in PBS with 0.1% w/v lithium phenyl-2,4,6-

trimethylbenzoylphosphinate (LAP, Tocris) at 50 ºC. 5 μg/mL of either soluble SDF-1α or lipoSDF was added to the mixture, and 500 μL of the solution was pipetted into the bottom a 12-well plate. Plates were then placed at 4 °C for 20 min to allow for soft gelation before exposure to ultraviolet (UV) light for 2 min in a UV box for photocrosslinking. 1 mL of complete cell culture media was added to the hydrogels to allow for swelling for 1 hour before cell seeding.

BMDMs were stained with CellTracker™ Green CMFDA Dye (ThermoFisher) according to the manufacturer's guidelines and seeded on the hydrogels at 100,000/gel. After 5 days, z-stacks of the gels were acquired by fluorescence microscopy and the infiltrated cells counted using Nikon NIS-Elements software for 3D analysis.

5.2.5: *In Vivo* Experiments

All animal experiments were conducted with approval from the Institutional Animal Care and Use Committee (IACUC) at the University of Maryland, College Park. Female wild type C57BL/6 (Charles River) mice between 6-10 weeks old (n = 6/group) were used according to a previously defined protocol to generate dorsal full-thickness skin defects.[196] While under isoflurane anesthesia, bilateral skin defects were made at the dorsum of each mouse using a 4-mm circular biopsy punch. The skin plugs were then removed with sterile forceps and the appropriate experimental treatments administered (roughly 40 μL). The wounds were then splinted with circular silicone discs to prevent skin contraction and secured to the surrounding skin with cyanoacrylate glue and non-absorbable nylon sutures. The wounds and discs

were covered using Tegaderm surgical film dressing to serve as a protective layer. Animals then received subcutaneous injections of flunixin meglumine analgesic (2.5 mg/kg) and were allowed to recover from anesthesia under supplemental heat. Prophylactic trimethoprim/sulfamethoxazole antibiotic (95 mg/kg) was also orally administered for 3 days in hydrogel formulation starting the day prior to procedures.

Mice were euthanized after 7 days via carbon dioxide exposure and the wound beds excised for studies. The harvested tissue was halved down the center, with one half mounted and frozen in optimal cutting temperature compound (OCT, Tissue-Tek) for cryosectioning and the other half snap-frozen in liquid nitrogen and stored at -80 ^{o}C for Western blotting.

5.2.6: Western Blotting

Tissue samples were manually ground into a fine powder in liquid nitrogen using a mortar and pestle before being suspended in 1 mL of RIPA buffer with protease inhibitor (Thermo Scientific) and sonicated in an ultrasonic water bath for 5 minutes. Lysates were then centrifuged at 14,000 g for 15 minutes and the supernatants kept for analysis. A bicinchoninic acid assay (BCA, Thermo Scientific) was conducted to determine the protein concentration of each sample. 20 μg of each sample was diluted with 2x Laemmli buffer (Bio-Rad) and loaded into a 12% SDS/PAGE electrophoresis gel. After transfer to a nitrocellulose membrane and blocking in 5% nonfat dry milk, primary rabbit antibodies against mouse CD80, CD86, iNOS, Arg-1, CD206, TGM-2, and β-actin were added (at 1:1000, 1:300, 1:500, 1:1000, 1:1000, 1:2000 and 1:1000 dilution respectively). Goat anti-rabbit horseradish peroxidase-conjugated antibody

(1:10,000 dilution, Abcam) was applied as a secondary to the blot, which was then developed using an enhanced chemiluminescence substrate (Bio-Rad). When needed, blots were stripped in Restore Western blot stripping buffer (ThermoFisher Scientific) at room temperature for 30 minutes, re-blocked, and re-probed using different primary antibodies. Protein bands were visualized using a Western blot imager and densitometry analysis was conducted using AlphaView software.

5.2.7: Immunofluorescent Staining

Samples were first fixed in 10% formalin to preserve their structure and cryosectioned at a thickness of 10 µm. Sections were then permeabilized in PBS/0.1% Triton-X 100 and blocked with PBS/1% bovine serum albumin. Primary anti-mouse antibodies were applied and incubated overnight at 4 ^{o}C. Specifically, F4/80 (Invitrogen MA516624), iNOS (Abcam ab49999), and YM-1 (Stem Cell Technologies 60130) were used at concentrations of 1:100, 1:2000, 1:100 respectively. Secondary antibodies were used at respective concentrations of 1:1000, 1:1000, and 1:500 for TRITC goat anti-rat (Invitrogen), FITC goat anti-mouse (Invitrogen) and AlexaFluor633 goat anti-rabbit (Invitrogen). Samples were then mounted and counter-stained in Vectashield mounting medium + DAPI (Vectorlabs). Images was acquired using a fluorescence microscope with ImageJ used for quantitative analysis.

5.2.8: Statistical Methods

Unless otherwise specified, n = 3 biological replicates were used per group for the *in vitro* studies, and n = 6 animals were used per group for the *in vivo* work. Minitab 19

was used to conduct a one-way analysis of variance (ANOVA) followed by a Tukey's *post-hoc* test. Statistical significance was defined as $p < 0.05$, and data is presented as mean ± standard deviation.

5.3: Results

5.3.1: Migration of BMDMs in SDF-Containing Hydrogels

The depth of migration by BMDMs seeded onto GelMA hydrogels was assessed 5 days after seeding by fluorescence microscopy (**Figure 5.1 A**). The number of cells that were able to migrate to a depth of 50 µm was compared to those that migrated to 100 µm in the z-direction (**Figure 5.1 A inset**). Within each hydrogel type, some cells were observed to migrate to 50 µm, with a smaller number able to migrate even further to 100 µm (**Figure 5.1 B**). A slightly greater number of cells were seen to migrate into hydrogels contining either SDF or lipoSDF than hydrogels containing no chemokine. Among BMDMs observed to migrate 50 µm into the hydrogel, a greater proportion of cells seeded onto GelMA + SDF or GelMA + lipoSDF gels were observed to have migrated even deeper, with the SDF-containing group showing the greatest proportion of cells that migrated 100 µm or more (**$p < 0.01$, **Figure 5.1 C**).

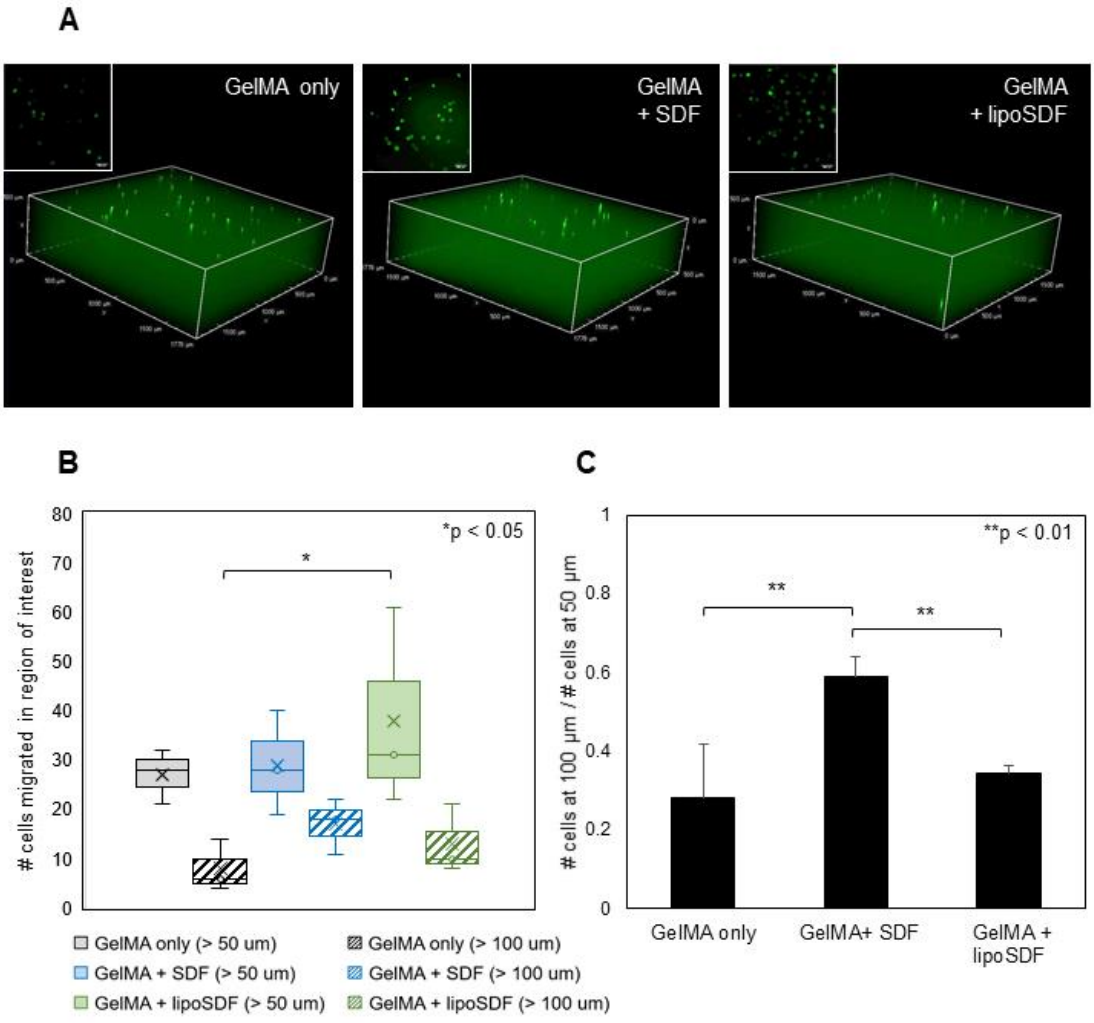

Figure 5.1: More BMDMs migrate in SDF- or lipoSDF-containing hydrogels than gels containing no chemokine. (A) Mouse BMDMs stained with CellTracker Green seeded on either GelMA, GelMA + SDF, or GelMA + lipoSDF hydrogels (n = 3/group) were imaged at 5 days post seeding in order to assess the depth of migration into the hydrogel up to 100 µm (inset). Image dimensions: 1778 x 1778 x 500 µm. Inset scale bar: 200 µm. (B) Quantification of the z-stack images above was conducted to visualize the number of cells that were able to migrate to 50 µm (solid) or 100 µm (striped) in the hydrogel (x denotes the mean). (C) The GelMA + SDF group was shown to have the greatest proportion of migrated cells at more than 100 µm deep in the gel (mean ± STD). One-way ANOVAs with Tukey's *post-hoc* comparisons were made between the groups ($^{*}p < 0.05$ and $^{**}p < 0.01$).

5.3.2: Cytokine Production by Seeded BMDMs

Cell culture supernatants were collected from the BMDMs seeded onto GelMA, GelMA + SDF, and GelMA + lipoSDF hydrogels after 48 hours. ELISA was conducted to assess for the presence of pro- and anti-inflammatory cytokines. Specifically, TNF-α and IL-1β were measured as markers of M1 macrophage activity, while IL-10 and TGF-β1 were assayed as M2 markers.

BMDMs seeded on GelMA + lipoSDF hydrogels produced significantly less TNF-α than either the GelMA only or GelMA + SDF groups ($*p < 0.05$, **Figure 5.2 A**). For IL-1β, there was lower (but not significant) expression of the protein in the GelMA + lipoSDF group compared to the other groups ($p > 0.05$, **Figure 5.2 B**). Interestingly, there was little to no IL-10 was detected in any of the groups (**Figure 5.2 C**), and there was no significant difference in TGF-β1 production (**Figure 5.2 D**). These findings will be examined in greater detail in the Discussion section, but taken together they would suggest that the BMDMs adopted a M2-leaning phenotype when exposed to GelMA, and were not induced to shift to M1-like polarization by the addition of free or liposomal SDF-1α.

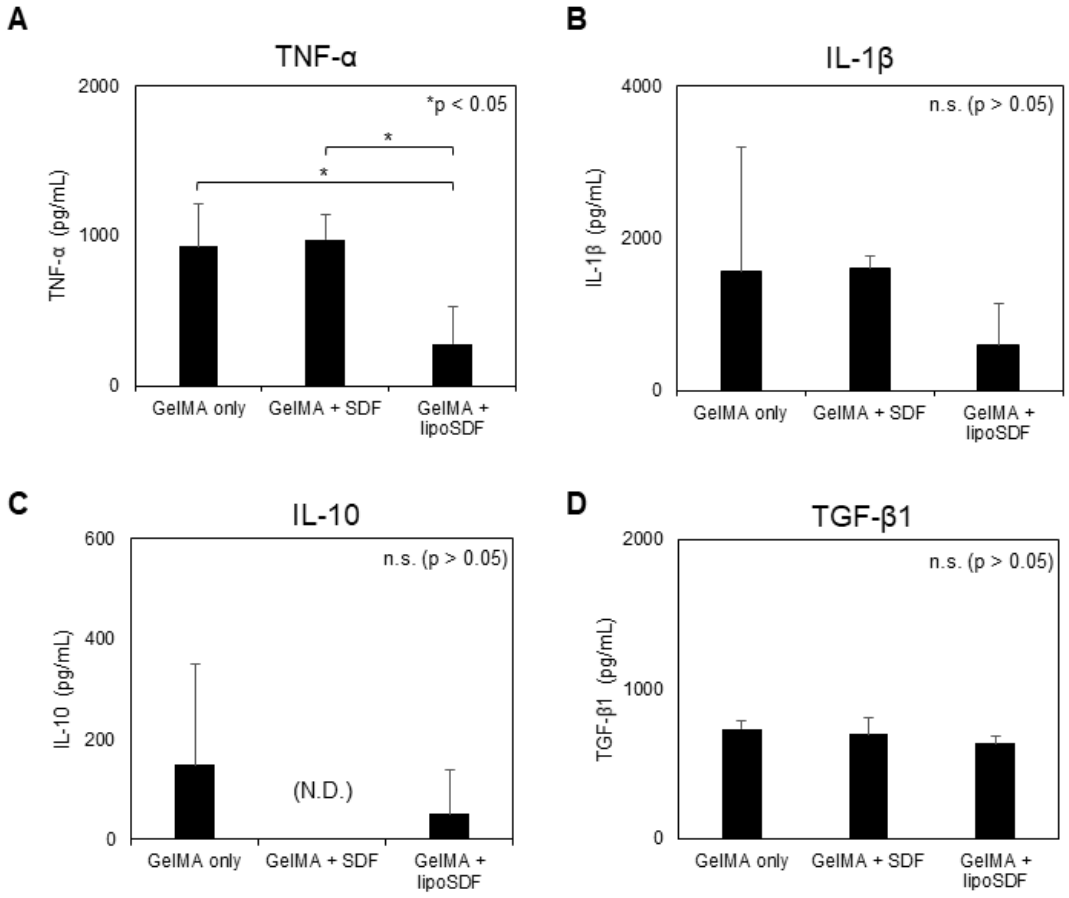

Figure 5.2: BMDMs seeded onto hydrogels containing SDF-1α or lipoSDF produce different amounts of pro- and anti-inflammatory cytokines. Cytokine expression as measured by ELISA of (A) TNF-α, (B) IL-1β, (C) IL-10, and (D) TGF-β1 (n = 3, mean ± STD. One-way ANOVAs with Tukey's *post-hoc* comparisons were conducted between groups. *p < 0.05, n.s.: not significant, N.D.: not detected). In general, the GelMA + lipoSDF group produced lower levels of pro-inflammatory, M1-associated cytokines than the other groups, and all groups produced similar levels of M2-associated cytokines, suggesting that these materials were not likely to stimulate powerful inflammatory responses when exposed to macrophages.

5.3.3: Treatment of Full-Thickness Skin Defects in Wild Type Mice

Wild type C57BL/6 mice (n = 6/group) received bilateral full-thickness skin defects on the dorsum, with one wound receiving an experimental treatment and one serving as a sham. (**Fig. 5.3 A**) Wounds were splinted open to prevent healing by contraction and to ensure that subsequent skin regeneration would occur from the bottom of the wound bed. Gross images taken one week after the procedure showed that all groups had begun to generate granulation tissue to fill the defect site, with the sham group exhibiting the most dried scab tissue while the hydrogel-treated groups appeared well-hydrated with some healthy skin tissue beginning to form at the wound edges (**Fig. 5.3 B**). Remnants of hydrogel were also found at some wound sites in the hydrogel-treated groups (**Fig. 5.3 B arrows**).

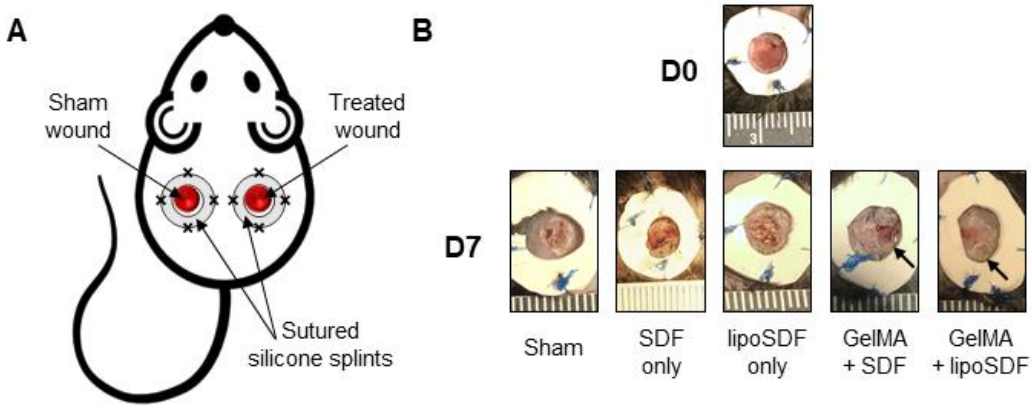

Figure 5.3: Skin regeneration in wild type mice is accelerated in SDF-containing hydrogel-treated groups. (A) Schematic diagram of the procedure, in which mice receive bilateral full-thickness dorsal defects that are splinted open to prevent contraction. (B) Representative whole-wound images at Day 0 (top) and Day 7 (bottom) show wound healing occurring after one week in each group, with greater amounts of scab tissue in the sham and more healthy skin tissue in the hydrogel-treated groups. Traces of hydrogel were left at the wound site (arrows). Scale: 1 mm/mark.

5.3.4: Western Blots to Assess Changes in Macrophage Phenotype in Wild Type Mice

Tissues harvested from the wounds beds of wild type mice were assayed through Western blotting in order to determine the total protein content of key markers of macrophage polarization. These consisted of iNOS, CD80, and CD86 as pro-inflammatory markers (**Figs. 5.4 A-C**) and Arg-1, CD206, and TGM-2 as anti-inflammatory markers (**Figs. 5.4 D-F**). In general, the experimental groups tended to express relatively lower levels of classically M1 markers and higher levels of M2 markers when compared to the sham control that received no treatment ($*p < 0.05$).

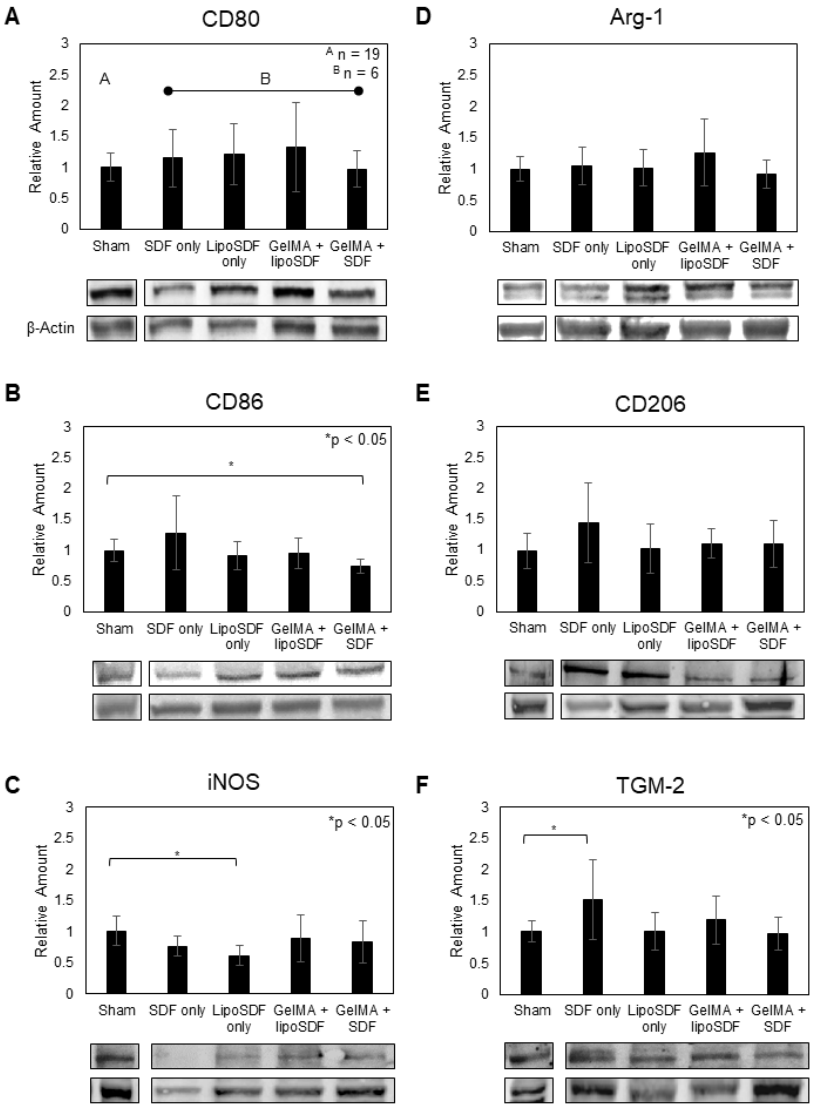

Figure 5.4: Western blot densitometry and representative images from wound beds of wild type mice. Approximately 20 µg of tissue from each wound (n = 6 per experimental group and 19 sham controls) was probed for total protein content of key pro-inflammatory macrophage markers (A) CD80, (B) CD86, and (C) iNOS as well as anti-inflammatory markers (D) Arg-1, (E) CD206, and (F) TGM-2 (mean ± STD. One-way ANOVAs with Tukey's *post-hoc* comparisons were conducted between groups. *p < 0.05). Overall, the experimental groups showed less expression of pro-inflammatory markers and higher expression of anti-inflammatory markers compared to sham wounds that received no treatment.

5.3.5: Immunofluorescence to Assess for the Presence and Phenotype of Macrophages Present in Wounds of Wild Type Mice

Tissue sections were also obtained from the wound beds of wild type mice 7 days post-wounding and immunostained for the presence of macrophages, as defined as the expression of the F4/80 marker. As demonstrated in **Figure 5.5 A**, $F4/80^+$ macrophages were found broadly distributed at and below the surface of the wound bed tissue (white arrows). Samples were additionally co-stained with iNOS and YM-1 (also known as chitinase-like protein 3/Chil3) as markers of the M1 and M2 phenotypes, respectively.[197] The mean fluorescence intensities of double-positive F4/80 + iNOS and F4/80 + YM-1 macrophages were compared in each section at both wound margins and at the center (**Figure 5.5 B**; 3 fields per section, n = 6 animals per group unless otherwise indicated). Comparing the sham and experimental groups, it was found that wounds treated with SDF or lipoSDF in hydrogels expressed a higher ratio of $YM\text{-}1^+$ to $iNOS^+$ macrophages compared to administering the proteins without hydrogel, and that this ratio was significantly higher when compared to the sham control ($*p < 0.05$, **Figure 5.5 C**).

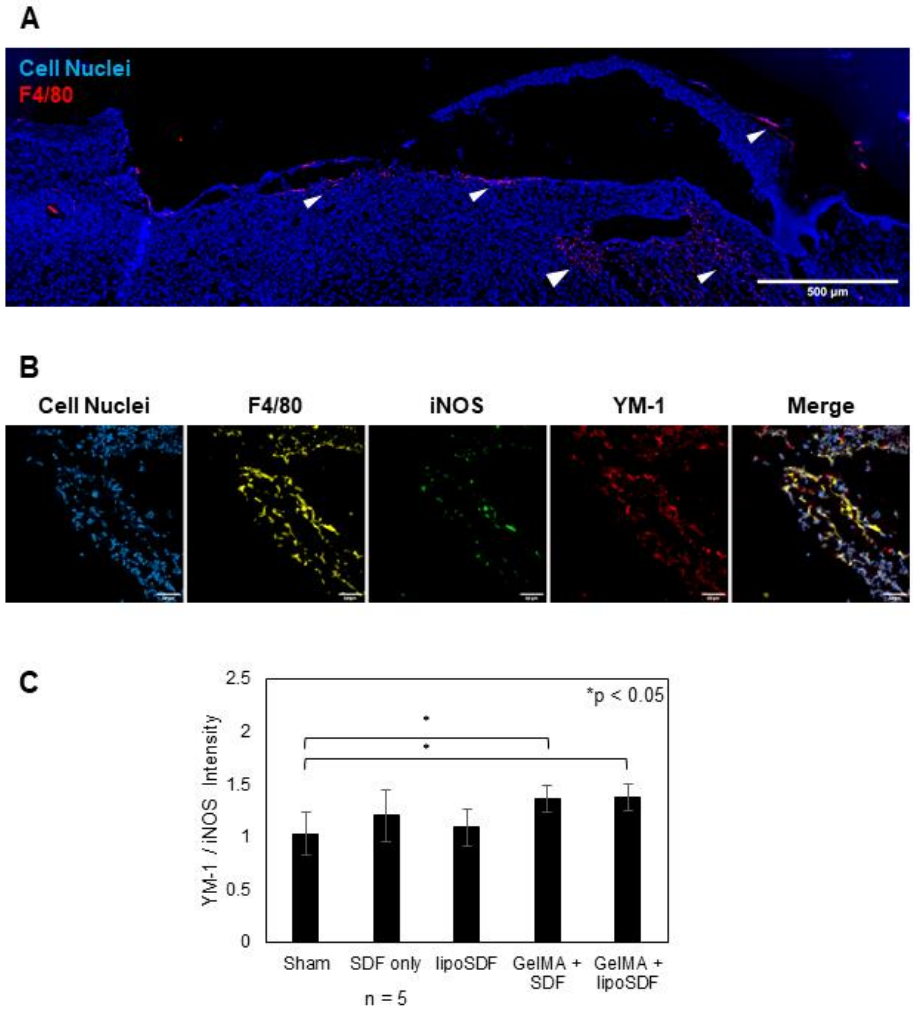

Figure 5.5: Both M1- and M2-associated macrophages are present in wounds from wild type mice after 7 days. (A) Representative image of a dorsal wound defect after 7 days. The wound margin can be seen clearly on the left, and the white arrows indicate regions where F4/80^{+} macrophages (red) are present. Scale bar: 500 µm. (B) Representative image of wound bed tissue co-stained with DAPI (blue, cell nuclei), F4/80 (yellow, macrophages), iNOS (green, M1 marker), and YM-1 (red, M2 marker). Scale bar: 50 µm. (C) Quantitative comparison of mean intensity in double-positive F4/80 + iNOS versus F4/80 +YM-1 macrophages shows a significant difference in hydrogel-treated groups compared to the sham (n = 6 per group unless noted, mean ± STD. One-way ANOVA with Tukey's *post-hoc* comparisons, *p < 0.05).

5.4: Discussion

In these *in vitro* experiments, BMDMs that were seeded onto hydrogels containing SDF-1α or lipoSDF were seen to exhibit a slightly greater migratory effect after 5 days when compared to hydrogels containing no chemokine (**Figures 5.1 A and B**). Among BMDMs observed to migrate at least 50 μm into the hydrogel, a greater proportion of cells seeded onto GelMA + SDF gels were observed to have migrated even deeper than 100 μm (**Figure 5.1 C**). This suggests that chemokine-containing hydrogels are capable of inducing cell migration directly into gels, even if the protein is liposomally encapsulated.

Supernatants from these migrating macrophages were also taken for ELISA of known pro-inflammatory (TNF-α, IL-1β) and anti-inflammatory (IL-10, TGF-β) cytokines (**Figure 5.2**). Among the groups, the GelMA + lipoSDF group expressed the significantly lowest amount of TNF-α ($p < 0.05$). Overall, all groups appeared to produce less TNF-α compared to typical reported literature values of BMDMs stimulated by lipopolysaccharides (LPS), which are known to be highly inflammatory factors (typically producing TNF-α at concentrations greater than 1000 pg/mL).[148,198–200] This pattern was also reflected among our experimental groups (but not significant) when IL-1β was measured. As a whole, these trends suggest that these cells are not driven to adopt a M1-like polarization state by the addition of free or liposomal SDF-1α in GelMA hydrogels.

On the other hand, low to negligible levels of IL-10 were observed in all groups, which is an expected response of M2-polarized macrophages in the absence of any highly pro-inflammatory stimuli (such as LPS).[189,201] This may indicate that the BMDMs adopted a more M2-like phenotype when exposed to GelMA and SDF-1α. Alternatively, the low levels of detectable IL-10 may be attributed to its pattern of transient expression and relatively short half-life, which would impede detection of the protein 48 hours after cell seeding.[202,203] Lastly, analysis of TGF-β1 concentrations showed that this cytokine was produced by all groups at similar levels, but higher than typical literature-reported values for BMDMs.[204,205] This further supports the hypothesis that the seeded BMDMs adopted a more anti-inflammatory state in the presence of GelMA, and were not induced to shift to an inflammatory phenotype by the addition of either free or liposomal SDF-1α.

Our *in vivo* studies with wild type mice indicated that after 7 days, dorsal full-thickness skin defects receiving a treatment containing SDF or lipoSDF tended to contract and fill with more regenerated tissue compared to the untreated sham (**Figure 5.3 B**). There was also less visible scab tissue overlying the defect in all groups receiving a treatment. These effects were even more prominent in the GelMA + SDF and GelMA + lipoSDF groups. We hypothesized that this might be caused by a prolonged release of SDF-1α over the study period, which would in turn recruit more macrophages of a pro-healing phenotype and accelerate wound healing. As a result, we sought to identify the presence and characterize the phenotype of macrophages present within this wound tissue.

Wounds receiving a treatment containing SDF-1α or lipoSDF were found to generally express lower levels of M1-associated, pro-inflammatory protein markers and higher M2-associated, anti-inflammatory markers when probed by Western blot of tissue lysates (**Figure 5.4**). In particular, the trends were most noticeable between the sham wounds and those treated with GelMA + SDF (significantly lower CD86 expression), lipoSDF (significantly lower iNOS expression), and SDF (significantly higher TGM-2 expression). While other groups did not indicate a statistically significant difference in protein expression levels (defined as $p < 0.05$), there were similar patterns of expression between M1 markers and the M2 markers as a whole. The most noticeable exception to this was the CD80 expression, where experimentally treated wounds tended to have slightly higher expression compared to the sham. This could possibly be explained by the known pattern of differential expression of CD80 compared to its costimulatory receptor CD86, which is a trend that has previously been described in both human and murine systems.[206,207]

While the results from the Western blot experiments appear to support our overall hypothesis, we recognize that this method evaluates the total protein marker content present in the tissue lysate, irrespective of cellular origin. It is possible that these proteins, expressed by and canonically associated with macrophages, were also produced other immune cells, fibroblasts, or keratinocytes present in the wound bed and surrounding tissue.[135,207] To augment this study, we further confirmed our results by immunofluorescence, as we were also interested in the overall tissue structure and

spatial distribution of macrophages within the wound area. Specifically, we conducted immunostaining for F4/80, a pan-macrophage marker, and looked for co-localization of this protein with M1- and M2-associated markers iNOS and YM-1. In all groups, we were able to identify the diffuse presence of infiltrated macrophages in the wound bed tissue after 7 days (**Figure 5.5 A**), which were co-localized with iNOS and/or YM-1 expression (**Figure 5.5 B**). Quantitative comparison of mean fluorescence intensity in double-positive F4/80 + YM-1 versus F4/80 + iNOS cells revealed that groups treated with SDF or lipoSDF in GelMA hydrogels produced a higher ratio of $YM\text{-}1^+$ macrophages to $iNOS^+$ ones compared to sham controls ($p < 0.05$, **Figure 5.5 C**). This supports our findings from the Western blot experiments and strongly endorses our theory that increased M2 macrophage presence contributes to the improved wound healing as was observed in **Figure 5.3 B**.

5.5: Conclusions

In this work, we study the chemotactic effects of SDF-1α and lipoSDF on mouse macrophages seeded on nanocomposite hydrogel surfaces and also characterize the resulting changes in expression of key cytokines implicated in inflammation and wound healing. We demonstrate that the presence of these chemotactic factors in GelMA is capable of inducing BMDM migration into these hydrogels, and that these materials do not stimulate strong inflammatory responses when exposed to macrophages. We further apply this SDF-1α delivery system to treat full-thickness skin defects in a wild type mouse model, where we show that it is capable of recruiting and polarizing macrophages to the M2 state. Macroscopically, we observed

increased wound bed infill and reduced scabbing at the wound sites, which could be attributed to increased expression of M2-associated proteins within the wound bed as well as a corresponding decrease in M1-associated proteins. These findings taken together represent an important step of investigation in developing immunomodulatory biomaterials that can influence macrophage phenotype and promote healing as hydrogel-based wound dressings.

Chapter 6: Liposomal SDF-1α Delivery in Nanocomposite Hydrogels Promotes Skin Tissue Regeneration in Murine Diabetic Wound Models

Skin regeneration in chronic wounds is known to be delayed due to a persistent state of inflammation typically induced by an underlying condition such as diabetes. In this work, we seek to therapeutically release a pro-healing chemokine using a nanocomposite hydrogel to promote skin tissue regeneration and wound closure. We employ our previously developed nanocomposite hydrogel system to release stromal cell-derived factor-1 alpha (SDF-1α) or liposomal SDF-1α (lipoSDF) in dorsal full-thickness skin wounds of diabetic mice. We demonstrate a decreased amount of open wound surface area in diabetic mice after 28 days, accompanied by histological observations of epidermal stratification and dermal angiogenesis. These findings support the use of our biomaterial as a potential wound dressing or skin substitute that could have clinical implications for stimulating wound closure, skin regeneration, and revascularization of chronic wounds.

6.1: Introduction

The infiltration and differentiation of immunomodulatory cell types including macrophages into tissue has been extensively shown to contribute to positive outcomes in wound healing.[208] Specifically, macrophages are able to polarize into distinct phenotypes based on the status of the local microenvironment and further produce cytokines that either promote inflammation (the "M1" phenotype) or reduce it in order to support wound healing (the "M2" phenotype).[84,133,209] While these

classifications are frequently used in the biomedical community and are generally helpful in classifying distinct macrophage phenotypes, the explicit surface marker and cytokine profiles of these macrophage categories are not formally defined and are known to exist on a continuous, dynamic spectrum.[210] For the purposes of this discussion, however, we will refer to "M1" macrophages as the pro-inflammatory phenotype classically activated by inflammatory stimuli such as lipopolysaccharide (LPS), and "M2" macrophages as the wound healing-associated, pro-healing phenotype.

In our previous work, we developed a nanocomposite hydrogel system capable of releasing stromal cell-derived factor-1 alpha (SDF-1α) protein in its bioactive form or encapsulated in liposomes.[193] We confirmed that the release can be sustained over at least 1 week and capable of exerting migratory and phenotypic changes in mouse bone marrow-derived macrophages (BMDMs) and mesenchymal stem cells (MSCs). *In vivo* work in wild type C57BL/6 mice demonstrated that macrophages predominantly of the M2 phenotype were recruited to wound sites where gelatin methacrylate (GelMA) hydrogels containing SDF-1α or lipoSDF were placed, and that the overall expression of M2-associated proteins was improved with a corresponding reduction in M1-associated proteins. We seek to further analyze the regenerative effects of these hydrogels *in vivo* in diabetic murine models and hypothesize that our delivery system will be able to accelerate wound closure and vascularized skin regeneration in the context of a disease where wound healing is known to be impaired.[211]

6.2: Materials and Methods

6.2.1: *In Vivo* Experiments

All animal experiments were conducted with approval from the Institutional Animal Care and Use Committee (IACUC) at the University of Maryland, College Park. Female diabetic B6.BKS(D) Lepr^{db}/J (Jackson Laboratory) mice between 6-8 weeks old (n = 6/group) underwent procedures as described in the previous chapter to evaluate the wound healing potential of the nanocomposite hydrogels. Briefly, animals were anesthetized under isoflurane and bilateral full-thickness dorsal skin defects were introduced with a 4-mm circular biopsy punch. Treatments were then administered, and the wounds splinted with circular silicone rings. Animals were bandaged with Tegaderm dressing and then received subcutaneous injections of flunixin meglumine analgesic (2.5 mg/kg) and 1 mL of warm saline. Analgesic and warm saline injections were continued twice daily up to 2 days post-operatively, and supplemental heat was provided up to 7 days post-operatively. Prophylactic trimethoprim/sulfamethoxazole antibiotic (95 mg/kg) was also administered for 3 days in oral hydrogel formulation starting the day prior to procedures.

Mice were euthanized after 7, 14, or 28 days by carbon dioxide inhalation, and the wound beds excised along with the surrounding skin. The tissue was bisected at the center of the wound, submerged in optimal cutting temperature compound (OCT, Tissue-Tek), and stored at -80 ^{o}C prior to cryosectioning.

6.2.2: Planimetric Analysis

Wound images were taken immediately after the induction and splinting of the dorsal wounds in each animal, as well as immediately after euthanization and prior to tissue harvesting at each time point. The surface area of each wound was measured in ImageJ in order to determine the amount of wound closure (WC%) over time, as defined by the following formula:

$$WC\% = \frac{Original\ Wound\ Area - Remaining\ Wound\ Area}{Original\ Wound\ Area} \times 100$$

6.2.3: Histological and Immunofluorescent Staining

Cryosections were taken at 10 μm thickness in the plane perpendicular to the dorsal surface, transferred onto glass slides, and stored at -80 ^{o}C. Prior to staining, the sections were fixed in ice-cold 4% paraformaldehyde (PFA). Hematoxylin and eosin (H&E) staining was completed according to manufacturer protocols. For immunostaining, samples were permeabilized in phosphate-buffered saline (PBS)/0.1% Triton-X 100 and blocked with PBS/1% bovine serum albumin/0.3 M glycine. Primary rabbit anti-mouse CD31 antibody (Abcam) was applied at a 1:100 dilution overnight and followed with a secondary FITC-conjugated donkey anti-rabbit antibody (Abcam) at 1:1000 before mounting with Vectashield + DAPI (VectorLabs). Images was taken using a color/fluorescence microscope (Nikon) and ImageJ was used for quantitative analysis. For measurement of fluorescence, relative fluorescence levels (expressed as arbitrary units a.u.) were acquired by baseline comparison

against a negative control of unwounded mouse skin stained without primary antibody.

6.2.4: Statistical Methods

Unless otherwise stated, n = 6 animals were used per group and Minitab 19 was used to conduct statistical analyses. For all studies, the Anderson-Darling test was used to determine if the data distributions of each group were normal; if so, one- or two-way analysis of variance (ANOVA) with Tukey's *post-hoc* test was conducted. Otherwise, a Kruskal-Wallis non-parametric analysis (comparing medians of individual samples) was performed instead and followed by a Dunn's test for individual comparisons.[152,212] P-values of less than 0.05 were considered to indicate statistical significance between groups. Values are presented as either mean ± standard deviation (STD) or median ± STD depending on the test used.

6.3: Results

6.3.1: Planimetric Analysis of Wound Closure in Diabetic Mice

Bilateral skin defects were introduced and treated in diabetic B6.BKS(D) $Lepr^{db}$/J mice as described before with wild type mice, with tissue harvesting occurring at days 7, 14, and 28. For each animal, whole-wound images were taken immediately after the procedure and were compared to images taken after euthanization on the day of tissue harvesting. Planimetric analysis of the remaining wound area was conducted in order to determine the amount of wound closure over time.[213,214] Comparisons of median values revealed a steady trend of WC% over time in all groups, with the sham

wounds exhibiting the highest range of variability in remaining wound area by day 28 (**Figure 6.1**). In the SDF-only, lipoSDF-only, and GelMA + SDF groups, a moderate increase in median WC% was observed over the study period, with a greater range in variability in the SDF-only and GelMA + SDF groups after 28 days. Conversely, in animals treated with GelMA + lipoSDF, a more drastic increase in median WC% was seen over time, along with the least variability between individual animals and greatest WC% compared to the sham by day 28 (*p < 0.01).

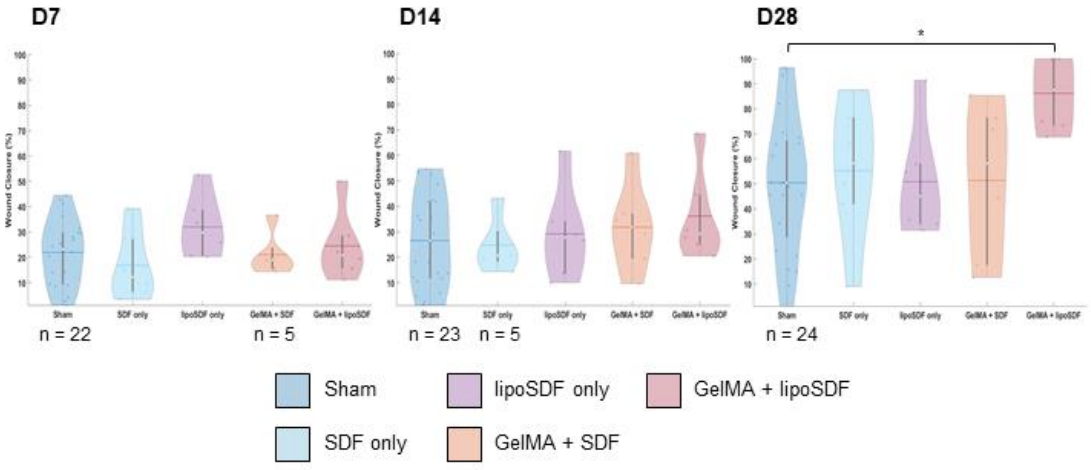

Figure 6.1: Treatment with GelMA + lipoSDF decreases wound area variability and improves closure rates in diabetic mice after 28 days. Planimetric analysis of wound closure percentage (WC%) at days 7, 14, and 28 reveal a gradual decrease in wound surface area in all groups, with the lowest WC% variability and greatest increase in median WC% in the GelMA + lipoSDF group (White dot: median, colored line: mean, n = 6 unless otherwise indicated; Kruskal-Wallis test with *p < 0.01).

6.3.2: Histological Examination of Regenerated Epidermis

Hematoxylin and eosin (H&E) staining was conducted in order to visualize the presence of the different components of normal skin tissue. As shown in **Figure 6.2 A**, all groups were able to form stratified skin tissue by 28 days, as indicated by the presence of dermal tissue, blood vessels, an uninterrupted layer of epidermis, and keratin at the dorsal surface. Of particular interest, the GelMA + lipoSDF group had the most mature-looking skin tissue comparable to the structure of stratified squamous keratinized epithelium canonically associated with healthy mammalian skin.[215] Specifically, a continuous and well-organized layer of keratinocyte nuclei was observed at the base of the epithelium which gradually flattened and faded to result in a flaky layer of dead keratin at the surface. Quantification of the H&E images (**Figure 6.2 B**, 3 images per animal taken at the wound center and both margins) was also performed and followed by a two-way ANOVA to assess for statistical significance between experimental groups and between time points. The interaction between these two factors was found to not be significant but instead contributed independently from each other to increase epidermal regeneration over time (groups not sharing letters are statistically different from each other, $p < 0.01$. Lack-of-fit p-value > 0.05). Pairwise comparisons across all groups showed the thickest epidermal layer was present at 14 and 28 days in the GelMA + lipoSDF group ($^*p < 0.05$).

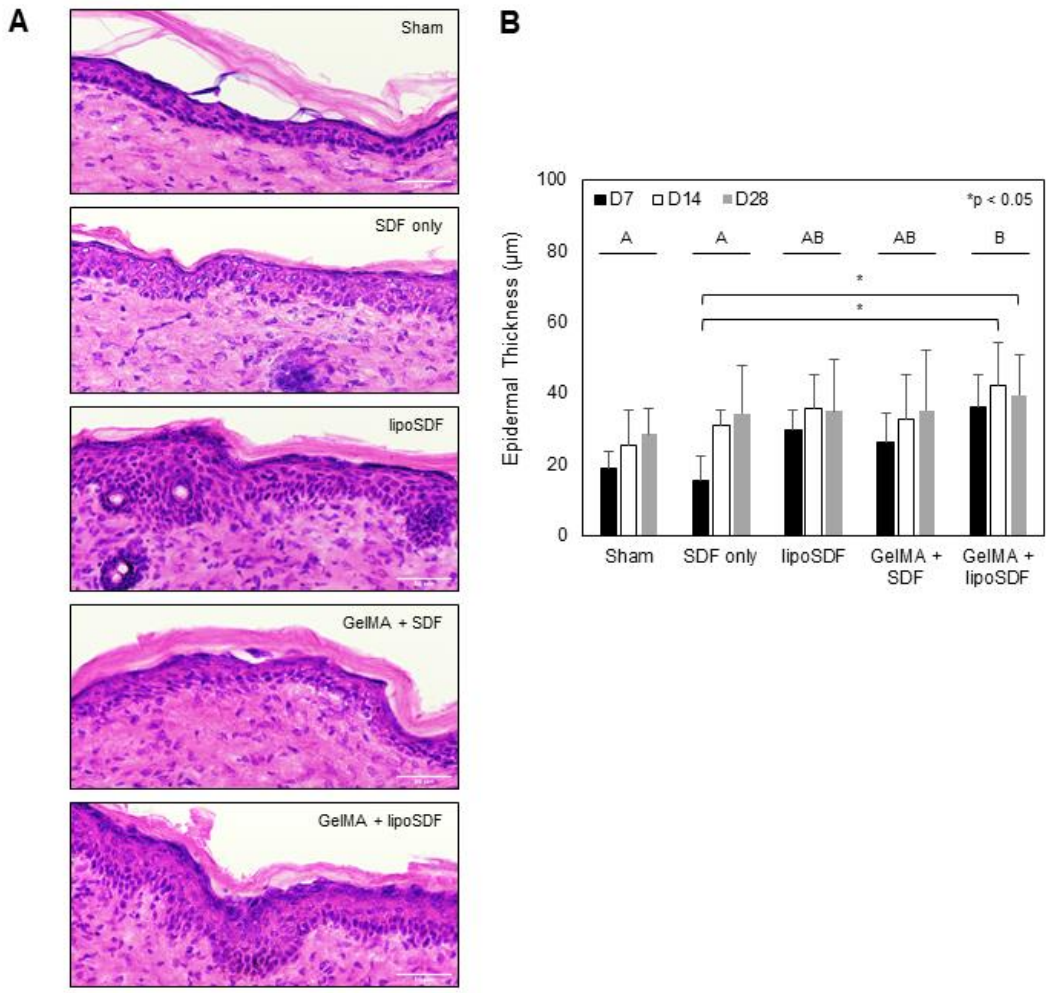

Figure 6.2: Regenerated epidermis is histologically normal and varies in both maturity and thickness. (A) Representative hematoxylin- and eosin- (H&E-) stained wounds from each group at 28 days show formation of dermal tissue, vessels, epidermis, and keratin stratification. Scale bar: 50 µm. (B) Quantification of epidermal thickness from H&E images indicate steady epidermal regeneration over time in all groups, with the GelMA + lipoSDF group having the thickest epidermal layer overall (3 images/animal; two-way ANOVA with *$p < 0.05$; groups that do not share a letter are significantly different from each other).

6.3.3: Immunofluorescence to Assess for Vascularization in Regenerated Skin Tissue

Tissue sections were stained for CD31 (also known as PECAM-1) to assess for the presence of endothelial cells comprising the lumens of blood vessels in the tissue. Increasing amounts of $CD31^+$ circular structures were observed at the margins and center of the wound beds over time, which also tended to become larger and more circular as typically seen in mature vessels (**Figure 6.3 A**). Quantification of CD31 positivity was performed as a series of Kruskal-Wallis non-parametric analyses for each time point, as preliminary analysis determined non-normal data distributions and possible interactions between time and treatment over the course of the experiment (lack-of-fit p-value < 0.05). The results showed statistically significant higher amounts of CD31 present in wounds treated with GelMA + lipoSDF compared to the sham at every time point (**Figure 6.3 B**). At days 7 and 14, higher amounts of CD31 were also found in the lipoSDF group compared to the sham ($^*p < 0.01$).

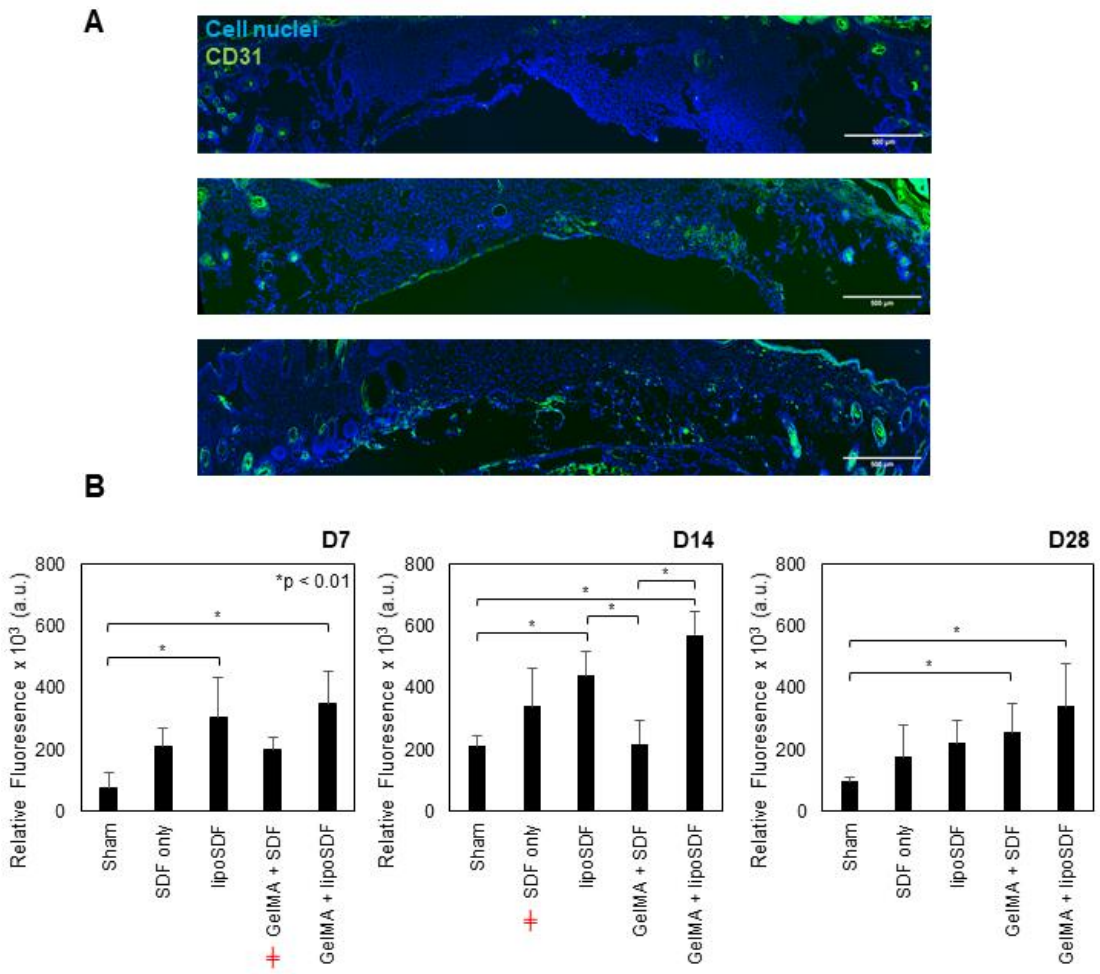

Figure 6.3: CD31 staining of harvested wound tissue shows progressive angiogenesis over 28 days in diabetic mice. (A) Representative images from diabetic mouse wounds treated with GelMA + lipoSDF at days 7 (top), 14 (middle), and 28 (bottom). Increasing amounts of $CD31^+$ round structures indicate more vascular regeneration within the wound tissue. Scale bar: 500 μm. (B) Quantification of CD31 expression between groups shows the highest amount of vessel formation in the GelMA + lipoSDF group at each time point (3 images/animal, red ⫩ indicates n = 5 animals in the group; Kruskal-Wallis test with *p < 0.01).

6.4: Discussion

We expanded our *in vivo* wound healing study to diabetic mice, as delayed healing is a characteristic of this disease in both humans and animal models and typically characterized by prolonged inflammation and a predominance of M1 macrophages.[85,211,216] Planimetric analysis of the healing sites was conducted to calculate wound closure percentage (WC%) for up to 28 days. The results (**Figure 6.1**) indicated that in all groups, the median WC% increased over time, but very few individual wounds healed completely; this confirms the observation of delayed diabetic wound healing described in literature. In the sham group, a wide distribution in WC% was noted, with some defects closing almost completely by the end of the study and some not closing at all. In comparison, the distributions in most of the experimentally treated groups were narrower and demonstrated a higher median WC% over time. Particularly, the GelMA + lipoSDF group was observed to have the highest increase in WC% at 28 days ($p < 0.01$), and had the smallest variation in WC% distribution out of all groups. These results could potentially be attributed to the material's ability to influence recruited macrophage phenotype and promote their polarization to a pro-healing state, leading to an overall increased potential for wound closure compared to untreated sham wounds. Our observations from this experiment support our hypothesis that the use of GelMA hydrogel to deliver SDF-1α can accelerate wound closure, especially if the protein is encapsulated and delivered as a liposomal formulation.

These findings were further supported by H&E histology of the wound bed tissue, which visually confirmed the presence of healthy, regenerating skin (**Figure 6.2 A**). In all cases, the wounds from each group were characterized by granulated and scab tissue containing high amounts of infiltrated immune cells (likely macrophages and granulocytes) in the early time points, which gradually transitioned to the conventional structure of healthy skin consisting of vascularized dermal connective tissue underlying clearly delineated layers of epidermis and keratin. The time scale of our observations corresponds to that typically reported in literature for healthy humans, where basic epithelialization occurs by roughly 8 days and barrier function is established starting around 3-4 weeks.[217] In particular, the GelMA + lipoSDF group seemed to produce the most mature-looking skin epithelium at 28 days that mirrored the structure of normal stratified squamous keratinized epithelium. This was exemplified by the presence of a well-organized layer of basal keratinocytes whose nuclei gradually flattened as they approach the surface, as well as an attached layer of keratin from dead keratinocytes. Quantification and analysis of these H&E images (**Figure 6.2 B**) suggested that epithelialization occurred with time and experimental treatment as separate independent factors (as determined via two-way ANOVA), though these factors may interact outside the tested parameters measured in this study. Overall, the GelMA + lipoSDF group was deemed to be statistically different from both the sham and SDF-only groups ($p < 0.01$), and the epidermal thickness measured in this group at days 14 and 28 was statistically higher ($p < 0.05$).

Lastly, we assessed for vascularization in the regenerating skin tissue by staining for $CD31^+$ endothelial cells and histologically observing the formation of blood vessels over time. As shown in **Figure 6.3 A**, increasing amounts of $CD31^+$, round, vessel-like structures could be found in the tissue over time, becoming progressively circular and thick-walled similar to mature vessels by day 28.[215] Quantification of CD31 levels in the sections indicated that, statistically, the GelMA + lipoSDF group tended to express the highest amounts of this glycoprotein at each time point ($p < 0.01$), although by day 28 most groups had demonstrated some increase in CD31 expression over the sham (**Figure 6.3 B**). Taken together with the H&E data where larger increases in measured epidermal thickness were observed between days 7 and 14, it might be possible to theorize that the chemokine is released and reaches its maximal activity by day 14 (especially if liposomes are used), leading to induction of keratinocyte homing as well as stimulation of angiogenesis. This is supported by the fact that epidermal keratinocytes and endothelial cells are known to also express the receptor CXCR4 to bind to SDF-1α, and that this receptor/ligand interaction is known to contribute to the activation of tip cells critical for vessel sprouting.[218,219] These earlier effects would potentially set an important foundation for further skin regeneration and wound closure at 28 days and beyond.

6.5: Conclusions

In this work, we demonstrate that our nanocomposite hydrogel is capable of promoting vascularized skin tissue regeneration in diabetic mice with dorsal full-thickness wounds. We show that when we use these GelMA hydrogels containing

SDF-1α – particularly encapsulated in liposomal form – to treat the wounds, there was an increased amount of wound closure over 28 days as measured by a reduction in wound surface area compared to the original wound. Furthermore, these findings were complemented by significantly increased amounts of epidermal regeneration and vascularization. Particularly in the GelMA + lipoSDF group, the regenerated tissue was noted to be histologically the most mature-looking and similar to healthy mouse skin. Taken together, this nanocomposite hydrogel system represents a promising strategy to deliver SDF-1α to stimulate the formation of skin tissue in chronic wounds where healing is typically delayed due to an inflammatory microenvironment. This tissue engineering-based approach could potentially be further expanded upon to be applied clinically as a wound dressing or skin substitute to accelerate wound closure and promote multi-component regeneration of skin.

Chapter 7: Summary and Future Directions

7.1: Summary

In this dissertation, we develop a novel nanocomposite hydrogel delivery system capable of releasing stromal cell-derived factor-1 alpha (SDF-1α) and demonstrate its potential as an immunomodulatory biomaterial that can influence cell behaviors such as migration and polarization in mesenchymal stem cells (MSCs) and macrophages. We further demonstrate that this system is able to stimulate wound healing and skin tissue regeneration using both wild type and diabetic mice.

The first aim of this work was to encapsulate SDF-1α protein within liposome nanoparticles (lipoSDF) and characterize their physical properties and release kinetics. We then demonstrate that bioactivity of SDF-1α is retained even after liposomal encapsulation, and that the protein released from gelatin methacrylate (GelMA) hydrogels is able to stimulate responses within MSCs. These findings set an important foundation for this project by describing the physical transport phenomena and biochemical effects that would affect cells in contact with our biomaterial.

In Chapter 5, we further expand on the previous findings by examining the effects of our SDF-1α release system on the activity and phenotype of bone marrow-derived macrophages (BMDMs). Our findings indicated that our hydrogels containing either SDF-1α or lipoSDF could induce BMDM migration directly into the hydrogel when seeded on the gel surface, and that these BMDMs produced cytokines that were not

associated with a highly inflammatory phenotype. This is particularly important, as the rates of wound healing and skin tissue regeneration are typically impaired in inflammatory microenvironments that are highly influenced by the presence of M1 macrophages.[55,84]

Lastly, we make use of *in vivo* murine models to confirm our previous findings and test our nanocomposite system's ability to recruit and polarize macrophages at 7 days post-wounding. We show that macrophages were able to infiltrate wound sites in wild type mice and that observable differences between the amounts of M1 and M2 macrophages present could be attained by releasing SDF-1α or lipoSDF from GelMA hydrogels placed at the wound sites. Furthermore, we examine the amount of wound closure and skin tissue regeneration at up to 28 days in diabetic animals. Our findings show that our biomaterial is capable of stimulating epidermal stratification and wound closure, as well as the regeneration of blood vessels in the dermis. These results suggest that positive effects on skin wound healing in living systems – both healthy and diabetic – can be induced through nanocomposite hydrogel-based delivery of SDF-1α.

In conclusion, the findings described within this dissertation demonstrate a novel application of tissue engineering principles to leverage synergistic activities of biomaterials, bioactive factors, and host cells to stimulate skin tissue regeneration after a wound. This nanocomposite system could potentially also be used to deliver other pro-healing factors to sites where the temporospatial control of release is critical

to shaping the outcome of the regenerating tissue. Furthermore, the ability to recruit macrophages and alter their phenotype to control inflammation lends this system as a potentially useful tool in developing immunomodulatory biomaterials that can stimulate native wound healing responses and improve clinical outcomes in patients with chronic, non-healing wounds.

7.2: Contributions

The work presented in this dissertation has resulted in two first-author publications, along with another first-author manuscript currently in preparation for submission. Furthermore, aspects of this research are included in an additional published work as well as two others in preparation. This dissertation research was in part supported by the National Institute of Biomedical Imaging and Bioengineering/National Institutes of Health (NIBIB/NIH) Center for Engineering Complex Tissues (grant number P41 EB023833) as well as the University of Maryland Graduate School (via the Summer Research Fellowship and the Ann G. Wylie Fellowship). Research support was also received from the University of Maryland School of Medicine Medical Scientist Training Program (UMSOM MSTP). The results of this work represent an important contribution to understanding of the role of macrophages and MSCs in directing wound healing, and further expand on the existing body of knowledge regarding the mechanisms of interaction between biomaterials and the host immune system. Lastly, this project represents a highly relevant research project for a physician-scientist-in-training to develop analytical research skills and technical knowledge that will be beneficial in both research and clinical settings.

7.3: Future Directions

The body of this work focuses on developing a strategy to controllably release the chemokine SDF-1α to stimulate activity in local MSCs and macrophages, and explores its potential as a hydrogel-based dressing that may be applied to chronic, non-healing wounds to accelerate wound healing. Future work may be directed towards studies to determine the safety and efficacy of such strategies that induce immunomodulation and stimulate tissue regeneration in the skin. This would be especially important in order to gain approval from regulatory agencies for use in humans.

Further testing and validation would also be needed to prepare this technology for clinical translation, either for wound healing or for other pathologies. In particular, the role of age- and sex-related differences could be investigated, as it is known that vascularity is further impaired in chronic wounds of elderly diabetic individuals and often associated with poorer outcomes.[220] Establishing improved vascularized skin regeneration in this group would be especially valuable for demonstrating the efficacy of this potential wound care product, and address some of the current clinical challenges associated with treating this patient population.

Additional experiments could also be conducted to assess the adaptive immune responses to our biomaterials and determine how they influence wound healing. Specifically, changes in B- and T-cell populations could be studied to characterize

both the short- and long-term effects on these immune cells' phenotypes. This research could open up more avenues for exploration of immunogenicity associated with implantation of ECM-based scaffolds, especially the role of T-regulatory and T-helper cells in influencing fibrosis and inflammation.[221] Lastly, studies on the role of lipids in wound healing could further contribute to our understanding of how immune responses – particularly innate and complement-mediated mechanisms – are locally initiated and perpetuated in injured skin, or how lipid-based materials may interact with skin cells and ECM to facilitate the transport of released compounds.[5,222] By comprehensively investigating the roles of both the innate and adaptive immune responses influenced by our nanocomposite delivery strategy, we would be able to further elucidate the synergies between SDF-1α, macrophages, MSCs, and the various immune mechanisms that facilitate the regeneration of healthy, multi-component skin tissue.

Results from this research will likely be highly relevant to human health as it describes a novel strategy to deliver chemokines and growth factors in order to alter the phenotypes of immunomodulatory cell populations. This strategy falls in line with the recent trend of developing biomaterials that interact with the host immune system in a meaningful and positive way, in contrast to staying inert after implantation. Besides SDF-1α, it may be feasible to deliver other therapeutic agents capable of modulating the immune system to produce an environment more conducive to multicomponent tissue regeneration, which has particular significance for clinical

applications where it is necessary (or aesthetically desirable) to restore both the form and function of a particular tissue after injury.

References

1. Chua AWC, Khoo YC, Tan BK, Tan KC, Foo CL, Chong SJ. Skin tissue engineering advances in severe burns: review and therapeutic applications. *Burn Trauma*. 2016;4(1):3. doi:10.1186/s41038-016-0027-y

2. Debels H, Hamdi M, Abberton K, Morrison W. Dermal Matrices and Bioengineered Skin Substitutes. *Plast Reconstr Surg Glob Open*. 2015;3(1):63-72. doi:10.1097/GOX.0000000000000219

3. Sridharan R, Cameron AR, Kelly DJ, Kearney CJ, O'Brien FJ. Biomaterial based modulation of macrophage polarization: a review and suggested design principles. *Mater Today*. 2015;18(6):313-325. doi:10.1016/j.mattod.2015.01.019

4. Wang J, Chin D, Poon C, et al. Oral delivery of metformin by chitosan nanoparticles for polycystic kidney disease. *J Control Release*. 2020;329:1198-1209. doi:10.1016/j.jconrel.2020.10.047

5. Gainza G, Villullas S, Pedraz JL, Hernandez RM, Igartua M. Advances in drug delivery systems (DDSs) to release growth factors for wound healing and skin regeneration. *Nanomedicine Nanotechnology, Biol Med*. 2015;11(6):1551-1573. doi:10.1016/J.NANO.2015.03.002

6. Olekson MAP, Faulknor R, Bandekar A, Sempkowski M, Hsia HC, Berthiaume F. SDF-1 liposomes promote sustained cell proliferation in mouse diabetic wounds. *Wound Repair Regen*. 2015;23(5):711-723. doi:10.1111/wrr.12334

7. Ternullo S, Basnet P, Holsæter AM, Flaten GE, de Weerd L, Škalko-Basnet N. Deformable liposomes for skin therapy with human epidermal growth factor: The effect of liposomal surface charge. *Eur J Pharm Sci*. 2018;125:163-171. doi:10.1016/j.ejps.2018.10.005

8. Nam M, Lee J, Lee KY, Kim J. Sequential Targeted Delivery of Liposomes to Ischemic Tissues by Controlling Blood Vessel Permeability. *ACS Biomater Sci Eng*. 2018;4(2):532-538. doi:10.1021/acsbiomaterials.7b00815

9. Prokoph S, Chavakis E, Levental KR, et al. Sustained delivery of SDF-1α from heparin-based hydrogels to attract circulating pro-angiogenic cells. *Biomaterials*. 2012;33(19):4792-4800. doi:10.1016/J.BIOMATERIALS.2012.03.039

10. Dalonneau F, Liu XQ, Sadir R, et al. The effect of delivering the chemokine SDF-1α in a matrix-bound manner on myogenesis. *Biomaterials*. 2014;35(15):4525-4535. doi:10.1016/j.biomaterials.2014.02.008

11. Purcell BP, Elser JA, Mu A, Margulies KB, Burdick JA. Synergistic effects of SDF-1α chemokine and hyaluronic acid release from degradable hydrogels on directing bone marrow derived cell homing to the myocardium. *Biomaterials*. 2012;33:7849-7857. doi:10.1016/j.biomaterials.2012.07.005

12. McLafferty E, Hendry C, Farley A. The integumentary system: anatomy, physiology and function of skin. *Nurs Stand*. 2012;27(3):35-42. doi:10.7748/ns2012.09.27.3.35.c9299

13. Menon GK. New insights into skin structure: scratching the surface. *Adv Drug Deliv Rev*. 2002;54:S3-S17. doi:10.1016/S0169-409X(02)00121-7

14. Böttcher-Haberzeth S, Biedermann T, Reichmann E. Tissue engineering of skin. *Burns*. 2010;36(4):450-460. doi:10.1016/j.burns.2009.08.016

15. Markeson D, Pleat JM, Sharpe JR, Harris AL, Seifalian AM, Watt SM. Scarring, stem cells, scaffolds and skin repair. *J Tissue Eng Regen Med*. 2015;9(6):649-668. doi:10.1002/term.1841

16. Kolarsick PAJ, Kolarsick MA, Goodwin C. Anatomy and Physiology of the Skin. *J Dermatol Nurses Assoc*. 2011;3(4):203-213. doi:10.1097/JDN.0b013e3182274a98

17. Zhang Z, Michniak-Kohn BB. Tissue engineered human skin equivalents. *Pharmaceutics*. 2012;4(1):26-41. doi:10.3390/pharmaceutics4010026

18. Konig A, Bruckner-Tuderman L. Epithelial-mesenchymal interactions enhance expression of collagen VII in vitro. *J Invest Dermatol*. 1991;96(6):803-808. doi:10.1111/1523-1747.ep12474424

19. Seyhan T. Split-Thickness Skin Graft. In: Spear M, ed. *Skin Grafts – Indications, Applications and Current Research*. InTech; 2011:3-17. doi:10.5772/23658

20. Thornton J, Gosman A. Skin Grafts and Skin Substitutes and Principles of Flaps. *Sel Readings Plast Surg*. 2004;10(1):1-53. Accessed August 16, 2017. http://plasticsurgery.stanford.edu/content/dam/sm/plasticsurgery/documents/education/microsurgery/FlapsSelectedReadings.pdf

21. Nair R, Maseeh A. Vitamin D: The sunshine vitamin. *J Pharmacol Pharmacother*. 2012;3(2):118-126. doi:10.4103/0976-500X.95506

22. Kang JH, Gimble JM, Kaplan DL. In Vitro 3D Model for Human Vascularized Adipose Tissue. *Tissue Eng Part A*. 2009;15(8):2227-2236. doi:10.1089/ten.tea.2008.0469

23. Wong R, Geyer S, Weninger W, Guimberteau JC, Wong JK. The dynamic anatomy and patterning of skin. *Exp Dermatol*. 2016;25(2):92-98.

doi:10.1111/exd.12832

24. Shibata S, Tada Y, Asano Y, et al. Adiponectin Regulates Cutaneous Wound Healing by Promoting Keratinocyte Proliferation and Migration via the ERK Signaling Pathway. *J Immunol*. 2012;189(6):3231-3241. doi:10.4049/jimmunol.1101739

25. Salathia NS, Shi J, Zhang J, Glynne RJ. An in vivo screen of secreted proteins identifies adiponectin as a regulator of murine cutaneous wound healing. *J Invest Dermatol*. 2013;133(3):812-821. doi:10.1038/jid.2012.374

26. Jin CE, Xiao L, Ge ZH, Zhan XB, Zhou HX. Role of adiponectin in adipose tissue wound healing. *Genet Mol Res*. 2015;14(3):8883-8891. doi:10.4238/2015.August.3.11

27. Hebert TL, Wu X, Yu G, et al. Culture effects of epidermal growth factor (EGF) and basic fibroblast growth factor (bFGF) on cryopreserved human adipose-derived stromal/stem cell proliferation and adipogenesis. *J Tissue Eng Regen Med*. 2009;3(7):553-561. doi:10.1002/term.198

28. Makino T, Jinnin M, Muchemwa FC, et al. Basic fibroblast growth factor stimulates the proliferation of human dermal fibroblasts via the ERK1/2 and JNK pathways. *Br J Dermatol*. 2010;162(4):717-723. doi:10.1111/j.1365-2133.2009.09581.x

29. Rivera-Gonzalez G, Shook B, Horsley V. Adipocytes in skin health and disease. *Cold Spring Harb Perspect Med*. 2014;4(3):1-18. doi:10.1101/cshperspect.a015271

30. Hamuy R, Kinoshita N, Yoshimoto H, et al. One-stage, simultaneous skin grafting with artificial dermis and basic fibroblast growth factor successfully improves elasticity with maturation of scar formation. *Wound Repair Regen*. 2013;21(1):141-154. doi:10.1111/j.1524-475X.2012.00864.x

31. Langer R, Vacanti J. Tissue engineering. *Science (80-)*. 1993;260(5110):920-926. doi:10.1126/science.8493529

32. Khademhosseini A, Langer R. A decade of progress in tissue engineering. *Nat Protoc*. 2016;11(10):1775-1781. doi:10.1038/nprot.2016.123

33. Darwish A. Indications of Skin Graft. In: *Skin Grafts - Indications, Applications and Current Research*. ; 2011:35-42. doi:10.5772/21916

34. Madaghiele M, Sannino A, Ambrosio L, Demitri C. Polymeric hydrogels for burn wound care: Advanced skin wound dressings and regenerative templates. *Burn Trauma*. 2014;2(4):153. doi:10.4103/2321-3868.143616

35. Robinson MK, Cohen C, de Fraissinette A d. B, Ponec M, Whittle E, Fentem

JH. Non-animal testing strategies for assessment of the skin corrosion and skin irritation potential of ingredients and finished products. *Food Chem Toxicol*. 2002;40(5):573-592. doi:10.1016/S0278-6915(02)00005-4

36. Holmes AM, Charlton A, Derby B, Ewart L, Scott A, Shu W. Rising to the challenge: applying biofabrication approaches for better drug and chemical product development. *Biofabrication*. 2017;9(3). doi:10.1088/1758-5090/aa7bbd

37. Almeida A, Sarmento B, Rodrigues F. Insights on in vitro models for safety and toxicity assessment of cosmetic ingredients. *Int J Pharm*. 2017;519(1-2):178-185. doi:10.1016/j.ijpharm.2017.01.024

38. Curren RD, Mun GC, Gibson DP, Aardema MJ. Development of a method for assessing micronucleus induction in a 3D human skin model (EpiDerm TM). *Mutat Res*. 2006;607:192-204. doi:10.1016/j.mrgentox.2006.04.016

39. Mun GC, Aardema MJ, Hu T, et al. Further development of the EpiDerm^{TM} 3D reconstructed human skin micronucleus (RSMN) assay. *Mutat Res - Genet Toxicol Environ Mutagen*. 2009;673(2):92-99. doi:10.1016/j.mrgentox.2008.12.004

40. Bellas E, Seiberg M, Garlick J, Kaplan DL. In vitro 3D Full-Thickness Skin-Equivalent Tissue Model Using Silk and Collagen Biomaterials. *Macromol Biosci*. 2012;12(12):1627-1636. doi:10.1002/mabi.201200262

41. Davies DJ, Heylings JR, Gayes H, McCarthy TJ, Mack MC. Further development of an in vitro model for studying the penetration of chemicals through compromised skin. *Toxicol Vitr*. 2017;38(1):101-107. doi:10.1016/j.tiv.2016.10.004

42. Li WH, Fassih A, Binner C, Parsa R, Southall MD. Low-level red LED light inhibits hyperkeratinization and inflammation induced by unsaturated fatty acid in an in vitro model mimicking acne. *Lasers Surg Med*. 2018;50(2):158-165. doi:10.1002/lsm.22747

43. National Toxicology Program - U.S. Department of Health and Human Services. Alternative Methods Accepted by US Agencies. Accessed November 12, 2018. https://ntp.niehs.nih.gov/pubhealth/evalatm/accept-methods/

44. WSSD Global Partnership for Capacity Building to Implement the Globally Harmonized System of Classification and Labelling of Chemicals (GHS). The GHS and the Global Partnership: a success story from Rio to Rio. Achievements, lessons learned and future directions. In: ; 2012. Accessed November 12, 2018. http://www.oecd.org/chemicalsafety/risk-management/50500627.pdf

45. Seyhan T. 1. Split-Thickness Skin Grafts. In: *Skin Grafts - Indications, Applications and Current Research*. ; 2011:3-17. Accessed January 4, 2018. http://cdn.intechweb.org/pdfs/18924.pdf

46. Debels H, Hamdi M, Abberton K, Morrison W. Dermal matrices and bioengineered skin substitutes: A critical review of current options. *Plast Reconstr Surg - Glob Open*. 2015;3(1). doi:10.1097/GOX.0000000000000219

47. Peck M, Molnar J, Swart D. A global plan for burn prevention and care. *Bull World Health Organ*. 2009;87(10):802-803. doi:10.2471/BLT.08.059733

48. Gurtner G, Werner S, Barrandon Y, Longaker M. Wound repair and regeneration. *Nature*. 2008;453(7193):314-321. doi:10.1038/nature07039

49. Hu MS, Maan ZN, Wu J-C, et al. Tissue engineering and regenerative repair in wound healing. *Ann Biomed Eng*. 2014;42(7):1494-1507. doi:10.1007/s10439-014-1010-z

50. Turner NJ, Badylak SF. The Use of Biologic Scaffolds in the Treatment of Chronic Nonhealing Wounds. *Adv wound care*. 2015;4(8):490-500. doi:10.1089/wound.2014.0604

51. Thornton J, Gosman A. Skin Grafts and Skin Substitutes and Principles of Flaps. *Sel Readings Plast Surg*. 2004;10(1). Accessed August 16, 2017. http://plasticsurgery.stanford.edu/content/dam/sm/plasticsurgery/documents/education/microsurgery/FlapsSelectedReadings.pdf

52. World Health Organization (WHO). *Burn Prevention: Success Stories, Lessons Learned*.; 2011.

53. Orgill DP, Ogawa R. Current methods of burn reconstruction. *Plast Reconstr Surg*. 2013;131(5):827e-36e. doi:10.1097/PRS.0b013e31828e2138

54. Loss M, Wedler V, K??nzi W, Meuli-Simmen C, Meyer VE. Artificial skin, split-thickness autograft and cultured autologous keratinocytes combined to treat a severe burn injury of 93% of TBSA. *Burns*. 2000;26(7):644-652. doi:10.1016/S0305-4179(00)00045-0

55. Han G, Ceilley R. Chronic Wound Healing: A Review of Current Management and Treatments. *Adv Ther*. 2017;34(3):599-610. doi:10.1007/s12325-017-0478-y

56. Nunan R, Harding KG, Martin P. Clinical challenges of chronic wounds: searching for an optimal animal model to recapitulate their complexity. *Dis Model Mech*. 2014;7(11):1205-1213. doi:10.1242/dmm.016782

57. Brohem CA, Da Silva Cardeal LB, Tiago M, Soengas MS, De Moraes Barros SB, Maria-Engler SS. Artificial skin in perspective: Concepts and applications.

Pigment Cell Melanoma Res. 2011;24(1):35-50. doi:10.1111/j.1755-148X.2010.00786.x

58. Schneider RKM, Neuss S, Stainforth R, et al. Three-dimensional epidermis-like growth of human mesenchymal stem cells on dermal equivalents: Contribution to tissue organization by adaptation of myofibroblastic phenotype and function. *Differentiation*. 2008;76(2):156-167. doi:10.1111/j.1432-0436.2007.00204.x

59. Lee W, Debasitis JC, Lee VK, et al. Multi-layered culture of human skin fibroblasts and keratinocytes through three-dimensional freeform fabrication. *Biomaterials*. 2009;30(8):1587-1595. doi:10.1016/j.biomaterials.2008.12.009

60. Uchino T, Takezawa T, Ikarashi Y. Reconstruction of three-dimensional human skin model composed of dendritic cells, keratinocytes and fibroblasts utilizing a handy scaffold of collagen vitrigel membrane. *Toxicol Vitr*. 2009;23(2):333-337. doi:10.1016/j.tiv.2008.12.003

61. Lee V, Singh G, Trasatti JP, et al. Design and fabrication of human skin by three-dimensional bioprinting. *Tissue Eng Part C Methods*. 2014;20(6):473-484. doi:10.1089/ten.TEC.2013.0335

62. Hartmann-Fritsch F, Biedermann T, Braziulis E, et al. Collagen hydrogels strengthened by biodegradable meshes are a basis for dermo-epidermal skin grafts intended to reconstitute human skin in a one-step surgical intervention. *J Tissue Eng Regen Med*. 2016;10(1):81-91. doi:10.1002/term.1665

63. Cubo N, Garcia M, Cañizo JF, et al. 3D bioprinting of functional human skin: production and in vivo analysis. *Biofabrication*. 2016;9(1):015006. doi:10.1088/1758-5090/9/1/015006

64. Wills JW, Hondow N, Thomas AD, et al. Genetic toxicity assessment of engineered nanoparticles using a 3D in vitro skin model (EpiDerm^{TM}). *Part Fibre Toxicol*. 2016;13(1):50. doi:10.1186/s12989-016-0161-5

65. Téot L, Otman S, Trial C, Brancati A. The use of noncellularized artificial dermis in the prevention of scar contracture and hypertrophy. *Wound Repair Regen*. 2011;19(SUPPL. 1):49-58. doi:10.1111/j.1524-475X.2011.00712.x

66. Ali N, Hosseini M, Vainio S, Taieb A, Cario-Andre M, Rezvani HR. Skin equivalents: Skin from reconstructions as models to study skin development and diseases. *Br J Dermatol*. 2015;173(2):391-403. doi:10.1111/bjd.13886

67. Freyman TM, Yannas I V., Gibson LJ. Cellular materials as porous scaffolds for tissue engineering. *Prog Mater Sci*. 2001;46(3-4):273-282. doi:10.1016/S0079-6425(00)00018-9

68. Metcalfe AD, Ferguson MWJ. Tissue engineering of replacement skin: the crossroads of biomaterials, wound healing, embryonic development, stem cells and regeneration. *J R Soc Interface*. 2007;4(14):413-437. doi:10.1098/rsif.2006.0179

69. Choi J, Lee EH, Park SW, Chang H. Regulation of transforming growth factor B1, Platelet-derived growth factor, And basic fibroblast growth factor by silicone gel sheeting in early-stage scarring. *Arch Plast Surg*. 2015;42(1):20-27. doi:10.5999/aps.2015.42.1.20

70. Jones I, Currie L, Martin R. A guide to biological skin substitutes. *Br J Plast Surg*. 2002;55(3):185-193. doi:10.1054/hips.2002.3800

71. Wang HM, Chou YT, Wen ZH, Wang ZR, Chen CH, Ho ML. Novel Biodegradable Porous Scaffold Applied to Skin Regeneration. *PLoS One*. 2013;8(6):2-12. doi:10.1371/journal.pone.0056330

72. Sakamoto M, Morimoto N, Ogino S, Jinno C, Taira T, Suzuki S. Efficacy of gelatin gel sheets in sustaining the release of basic fibroblast growth factor for murine skin defects. *J Surg Res*. 2016;201(2):378-387. doi:10.1016/j.jss.2015.11.045

73. Llames SG, Del Rio M, Larcher F, et al. Human plasma as a dermal scaffold for the generation of a completely autologous bioengineered skin. *Transplantation*. 2004;77(3):350-355. doi:10.1097/01.TP.0000112381.80964.85

74. Xu S, Sang L, Zhang Y, Wang X, Li X. Biological evaluation of human hair keratin scaffolds for skin wound repair and regeneration. *Mater Sci Eng C*. 2013;33(2):648-655. doi:10.1016/j.msec.2012.10.011

75. Poranki D, Whitener W, Howse S, et al. Evaluation of skin regeneration after burns in vivo and rescue of cells after thermal stress in vitro following treatment with a keratin biomaterial. *J Biomater Appl*. 2014;29(1):26-35. doi:10.1177/0885328213513310

76. Loan F, Cassidy S, Marsh C, Simcock J. Keratin-based products for effective wound care management in superficial and partial thickness burns injuries. *Burns*. 2016;42(3):541-547. doi:10.1016/j.burns.2015.10.024

77. Sarkar SD, Farrugia BL, Dargaville TR, Dhara S. Chitosan-collagen scaffolds with nano/microfibrous architecture for skin tissue engineering. *J Biomed Mater Res - Part A*. 2013;101(12):3482-3492. doi:10.1002/jbm.a.34660

78. Sun G, Zhang X, Shen Y-I, et al. Dextran hydrogel scaffolds enhance angiogenic responses and promote complete skin regeneration during burn wound healing. *Proc Natl Acad Sci*. 2011;108(52):20976-20981.

doi:10.1073/pnas.1115973108

79. Coburn JC, Brody S, Billiar KL, Pandit A. Biaxial mechanical evaluation of cholecyst-derived extracellular matrix: A weakly anisotropic potential tissue engineered biomaterial. Published online 2007. doi:10.1002/jbm.a.30943

80. Webber MJ, Khan OF, Sydlik SA, Tang BC, Langer R. A Perspective on the Clinical Translation of Scaffolds for Tissue Engineering. *Ann Biomed Eng*. 2015;43(3):641-656. doi:10.1007/s10439-014-1104-7

81. Ogle ME, Segar CE, Sridhar S, Botchwey EA. Monocytes and macrophages in tissue repair: Implications for immunoregenerative biomaterial design. *Exp Biol Med*. 2016;241(10):1084-1097. doi:10.1177/1535370216650293

82. Olingy CE, San Emeterio CL, Ogle ME, et al. Non-classical monocytes are biased progenitors of wound healing macrophages during soft tissue injury. *Sci Rep*. 2017;7(1):447. doi:10.1038/s41598-017-00477-1

83. Rodero MP, Khosrotehrani K. Skin wound healing modulation by macrophages. *Int J Clin Exp Pathol*. 2010;3(7):643-653. doi:IJCEP1007002

84. Hesketh M, Sahin KB, West ZE, Murray RZ. Macrophage phenotypes regulate scar formation and chronic wound healing. *Int J Mol Sci*. 2017;18(7). doi:10.3390/ijms18071545

85. Rosique RG, Rosique MJ, Farina Junior JA. Curbing Inflammation in Skin Wound Healing: A Review. *Int J Inflam*. 2015;2015:1-9. doi:10.1155/2015/316235

86. Chun J, Hartung HP. Mechanism of action of oral fingolimod (FTY720) in multiple sclerosis. *Clin Neuropharmacol*. 2010;33(2):91-101. doi:10.1097/WNF.0b013e3181cbf825

87. Di Dario M, Colombo E, Govi C, et al. Myeloid cells as target of fingolimod action in multiple sclerosis. *Neurology*. 2015;2(6):e157. doi:10.1212/NXI.0000000000000157

88. Lim NSJ, Sham A, Chee SML, Chan C, Raghunath M. Combination of ciclopirox olamine and sphingosine-1-phosphate as granulation enhancer in diabetic wounds. *Wound Repair Regen*. 2016;24(5):795-809. doi:10.1111/wrr.12463

89. Rezaie Shirmard L, Bahari Javan N, Khoshayand MR, Kebriaee-zadeh A, Dinarvand R, Dorkoosh FA. Nanoparticulate fingolimod delivery system based on biodegradable poly (3-hydroxybutyrate-co-3-hydroxyvalerate) (PHBV): design, optimization, characterization and in-vitro evaluation. *Pharm Dev Technol*. 2017;22(7):860-870. doi:10.3109/10837450.2015.1108982

90. Awojoodu AO, Ogle ME, Sefcik LS, et al. Sphingosine 1-phosphate receptor 3 regulates recruitment of anti-inflammatory monocytes to microvessels during implant arteriogenesis. *Proc Natl Acad Sci*. 2013;110(34):13785-13790. doi:10.1073/pnas.1221309110

91. Basnet P, Skalko-Basnet N. Curcumin: An anti-inflammatory molecule from a curry spice on the path to cancer treatment. *Molecules*. 2011;16(6):4567-4598. doi:10.3390/molecules16064567

92. Tong WY, bin Abdullah AYK, binti Rozman NAS, et al. Antimicrobial wound dressing film utilizing cellulose nanocrystal as drug delivery system for curcumin. *Cellulose*. 2018;25(1):631-638. doi:10.1007/s10570-017-1562-9

93. Berce C, Muresan M-S, Soritau O, et al. Cutaneous wound healing using polymeric surgical dressings based on chitosan, sodium hyaluronate and resveratrol. A preclinical experimental study. *Colloids Surfaces B Biointerfaces*. 2018;163:155-166. doi:10.1016/J.COLSURFB.2017.12.041

94. Kasiewicz LN, Whitehead KA. Silencing TNFα with lipidoid nanoparticles downregulates both TNFα and MCP-1 in an in vitro co-culture model of diabetic foot ulcers. *Acta Biomater*. 2016;32:120-128. doi:10.1016/J.ACTBIO.2015.12.023

95. Waters M, VandeVord P, Van Dyke M. Keratin biomaterials augment anti-inflammatory macrophage phenotype in vitro. *Acta Biomater*. 2018;66:213-223. doi:10.1016/j.actbio.2017.10.042

96. Sun G. Pro-Regenerative Hydrogel Restores Scarless Skin during Cutaneous Wound Healing. *Advanced Healthcare Materials*. http://doi.wiley.com/10.1002/adhm.201700659. Published December 1, 2017. Accessed January 2, 2019.

97. Sridharan R, Cameron AR, Kelly DJ, Kearney CJ, O'Brien FJ. Biomaterial based modulation of macrophage polarization: A review and suggested design principles. *Mater Today*. 2015;18(6):313-325. doi:10.1016/j.mattod.2015.01.019

98. Hotchkiss KM, Reddy GB, Hyzy SL, Schwartz Z, Boyan BD, Olivares-Navarrete R. Titanium surface characteristics, including topography and wettability, alter macrophage activation. *Acta Biomater*. 2016;31:425-434. doi:10.1016/j.actbio.2015.12.003

99. Kim JE, Lee JH, Kim SH, Jung Y. Skin Regeneration with Self-Assembled Peptide Hydrogels Conjugated with Substance P in a Diabetic Rat Model. *Tissue Eng Part A*. 2018;24(1-2):21-33. doi:10.1089/ten.TEA.2016.0517

100. Friedenstein AJ, Chailakhjan RK, Lalykina KS. The development of fibroblast

colonies in monolayer cultures of guinea-pig bone marrow and spleen cells. *Cell Tissue Kinet*. 1970;3(4):393-403. http://www.ncbi.nlm.nih.gov/pubmed/5523063

101. Dominici M, Le Blanc K, Mueller I, et al. Minimal criteria for defining multipotent mesenchymal stromal cells. The International Society for Cellular Therapy position statement. *Cytotherapy*. 2006;8(4):315-317. doi:10.1080/14653240600855905

102. Muraglia A, Cancedda R, Quarto R. Clonal mesenchymal progenitors from human bone marrow differentiate in vitro according to a hierarchical model. *J Cell Sci*. 2000;113(7):1161-1166. doi:10.1006/excr.1999.4592

103. Kim EY, Lee KB, Yu J, et al. Neuronal cell differentiation of mesenchymal stem cells originating from canine amniotic fluid. *Hum Cell*. 2014;27(2):51-58. doi:10.1007/s13577-013-0080-9

104. Singaravelu K, Padanilam BJ. In vitro differentiation of MSC into cells with a renal tubular epithelial-like phenotype. *Ren Fail*. 2009;31(6):492-502. doi:10.1080/08860220902928981

105. Sasaki M, Abe R, Fujita Y, Ando S, Inokuma D, Shimizu H. Mesenchymal Stem Cells Are Recruited into Wounded Skin and Contribute to Wound Repair by Transdifferentiation into Multiple Skin Cell Type. *J Immunol*. 2008;180(4):2581-2587. doi:10.4049/jimmunol.180.4.2581

106. Pers YM, Ruiz M, Noël D, Jorgensen C. Mesenchymal stem cells for the management of inflammation in osteoarthritis: State of the art and perspectives. *Osteoarthr Cartil*. 2015;23(11):2027-2035. doi:10.1016/j.joca.2015.07.004

107. Le Blanc K, Davies LC. Mesenchymal stromal cells and the innate immune response. *Immunol Lett*. 2015;168:140-146. doi:10.1016/j.imlet.2015.05.004

108. Amann EM, Rojewski MT, Rodi S, et al. Systemic recovery and therapeutic effects of transplanted allogenic and xenogenic mesenchymal stromal cells in a rat blunt chest trauma model. *Cytotherapy*. 2018;20(2):218-231. doi:10.1016/j.jcyt.2017.11.005

109. Rodriguez-Menocal L, Shareef S, Salgado M, Shabbir A, Van Badiavas E. Role of whole bone marrow, whole bone marrow cultured cells, and mesenchymal stem cells in chronic wound healing. *Stem Cell Res Ther*. 2015;6(1):24. doi:10.1186/s13287-015-0001-9

110. Sargent A, Miller RH. MSC Therapeutics in Chronic Inflammation. *Curr Stem Cell Reports*. 2016;2(2):168-173. doi:10.1007/s40778-016-0044-6

111. Gaur M, Dobke M, Lunyak V, Gaur M, Dobke M, Lunyak V V. Mesenchymal Stem Cells from Adipose Tissue in Clinical Applications for Dermatological Indications and Skin Aging. *Int J Mol Sci*. 2017;18(1):208. doi:10.3390/ijms18010208

112. Madrigal M, Rao KS, Riordan NH. A review of therapeutic effects of mesenchymal stem cell secretions and induction of secretory modification by different culture methods. *J Transl Med*. 2014;12(1):260. doi:10.1186/s12967-014-0260-8

113. Mansilla E, Marín GH, Drago H, et al. Bloodstream Cells Phenotypically Identical to Human Mesenchymal Bone Marrow Stem Cells Circulate in Large Amounts Under the Influence of Acute Large Skin Damage: New Evidence for Their Use in Regenerative Medicine. *Transplant Proc*. 2006;38(3):967-969. doi:10.1016/j.transproceed.2006.02.053

114. Fu WL, Zhou CY, Yu JK. A new source of mesenchymal stem cells for articular cartilage repair: MSCs derived from mobilized peripheral blood share similar biological characteristics in vitro and chondrogenesis in vivo as MSCs from bone marrow in a rabbit model. *Am J Sports Med*. 2014;42(3):592-601. doi:10.1177/0363546513512778

115. Squillaro T, Peluso G, Galderisi U. Clinical Trials With Mesenchymal Stem Cells: An Update. *Cell Transplant*. 2016;25(5):829-848. doi:10.3727/096368915X689622

116. Waterman RS, Tomchuck SL, Henkle SL, Betancourt AM. A new mesenchymal stem cell (MSC) paradigm: Polarization into a pro-inflammatory MSC1 or an immunosuppressive MSC2 phenotype. *PLoS One*. 2010;5(4). doi:10.1371/journal.pone.0010088

117. Bernardo ME, Fibbe WE. Mesenchymal stromal cells: Sensors and switchers of inflammation. *Cell Stem Cell*. 2013;13(4):392-402. doi:10.1016/j.stem.2013.09.006

118. Conget P, Rodriguez F, Kramer S, et al. Replenishment of type VII collagen and re-epithelialization of chronically ulcerated skin after intradermal administration of allogeneic mesenchymal stromal cells in two patients with recessive dystrophic epidermolysis bullosa. *Cytotherapy*. 2010;12(3):429-431. doi:10.3109/14653241003587637

119. Cerqueira MT, Marques AP, Reis RL. Using Stem Cells in Skin Regeneration: Possibilities and Reality. *Stem Cells Dev*. 2012;21(8):1201-1214. doi:10.1089/scd.2011.0539

120. Dong HK, Keon HY, Kyung SC, et al. Gene expression profile of cytokine and growth factor during differentiation of bone marrow-derived mesenchymal

stem cell. *Cytokine*. 2005;31(2):119-126. doi:10.1016/j.cyto.2005.04.004

121. Li H, Fu X, Ouyang Y, Cai C, Wang J, Sun T. Adult bone-marrow-derived mesenchymal stem cells contribute to wound healing of skin appendages. *Cell Tissue Res*. 2006;326(3):725-736. doi:10.1007/s00441-006-0270-9

122. Chen L, Tredget EE, Wu PYG, Wu Y, Wu Y. Paracrine factors of mesenchymal stem cells recruit macrophages and endothelial lineage cells and enhance wound healing. *PLoS One*. 2008;3(4). doi:10.1371/journal.pone.0001886

123. Fu X, Li H. Mesenchymal stem cells and skin wound repair and regeneration: Possibilities and questions. *Cell Tissue Res*. 2009;335(2):317-321. doi:10.1007/s00441-008-0724-3

124. Eggenhofer E, Luk F, Dahlke MH, Hoogduijn MJ. The life and fate of mesenchymal stem cells. *Front Immunol*. 2014;5(MAY):1-6. doi:10.3389/fimmu.2014.00148

125. Hoogduijn MJ, Crop MJ, Peeters AMA, et al. Donor-derived mesenchymal stem cells remain present and functional in the transplanted human heart. *Am J Transplant*. 2009;9(1):222-230. doi:10.1111/j.1600-6143.2008.02450.x

126. Lee DE, Ayoub N, Agrawal DK. Mesenchymal stem cells and cutaneous wound healing: novel methods to increase cell delivery and therapeutic efficacy. *Stem Cell Res Ther*. 2016;7:37. doi:10.1186/s13287-016-0303-6

127. Rustad KC, Wong VW, Sorkin M, et al. Enhancement of mesenchymal stem cell angiogenic capacity and stemness by a biomimetic hydrogel scaffold. *Biomaterials*. 2012;33(1):80-90. doi:10.1016/j.biomaterials.2011.09.041

128. Lee DE, Ayoub N, Agrawal DK. Mesenchymal stem cells and cutaneous wound healing: Novel methods to increase cell delivery and therapeutic efficacy. *Stem Cell Res Ther*. 2016;7(1). doi:10.1186/s13287-016-0303-6

129. Eke G, Mangir N, Hasirci N, MacNeil S, Hasirci V. Development of a UV crosslinked biodegradable hydrogel containing adipose derived stem cells to promote vascularization for skin wounds and tissue engineering. *Biomaterials*. 2017;129:188-198. doi:10.1016/j.biomaterials.2017.03.021

130. Chen L, Xing Q, Zhai Q, et al. Pre-vascularization enhances therapeutic effects of human mesenchymal stem cell sheets in full thickness skin wound repair. *Theranostics*. 2017;7(1):117-131. doi:10.7150/thno.17031

131. Samsonraj RM, Rai B, Sathiyanathan P, et al. Establishing criteria for human mesenchymal stem cell potency. *Stem Cells*. 2015;33(6):1878-1891. doi:10.1002/stem.1982

132. Trounson A, McDonald C. Stem Cell Therapies in Clinical Trials: Progress and Challenges. *Cell Stem Cell*. 2015;17(1):11-22. doi:10.1016/j.stem.2015.06.007

133. Mosser DM, Edwards JP. Exploring the full spectrum of macrophage activation. *Nat Rev Immunol*. 2008;8(12):958-969. doi:10.1038/nri2448

134. van Furth R, Cohn ZA, Hirsch JG, Humphrey JH, Spector WG, Langevoort HL. The mononuclear phagocyte system: a new classification of macrophages, monocytes, and their precursor cells. *Bull World Health Organ*. 1972;46(6):845-852.

135. Hume DA. Differentiation and heterogeneity in the mononuclear phagocyte system. *Mucosal Immunol*. Published online 2008. doi:10.1038/mi.2008.36

136. Scatena M, Eaton K V., Jackson MF, Lund SA, Giachelli CM. Macrophages: The Bad, the Ugly, and the Good in the Inflammatory Response to Biomaterials. In: *The Immune Response to Implanted Materials and Devices*. Springer International Publishing; 2017:37-62. doi:10.1007/978-3-319-45433-7_3

137. Lech M, Anders HJ. Macrophages and fibrosis: How resident and infiltrating mononuclear phagocytes orchestrate all phases of tissue injury and repair. *Biochim Biophys Acta - Mol Basis Dis*. 2013;1832(7):989-997. doi:10.1016/j.bbadis.2012.12.001

138. Rey-Giraud F, Hafner M, Ries CH. In vitro generation of monocyte-derived macrophages under serum-free conditions improves their tumor promoting functions. *PLoS One*. 2012;7(8). doi:10.1371/journal.pone.0042656

139. Im G-I. Biomaterials in orthopaedics: the past and future with immune modulation. *Biomater Res*. 2020;24(1):7. doi:10.1186/s40824-020-0185-7

140. Chu C, Liu L, Rung S, et al. Modulation of foreign body reaction and macrophage phenotypes concerning microenvironment. *J Biomed Mater Res - Part A*. 2020;108(1):127-135. doi:10.1002/jbm.a.36798

141. Spiller KL, Nassiri S, Witherel CE, et al. Sequential delivery of immunomodulatory cytokines to facilitate the M1-to-M2 transition of macrophages and enhance vascularization of bone scaffolds. *Biomaterials*. 2015;37:194-207. doi:10.1016/j.biomaterials.2014.10.017

142. Rose JF, Giovinco N, Mills JL, Najafi B, Pappalardo J, Armstrong DG. Split-thickness skin grafting the high-risk diabetic foot. *J Vasc Surg*. 2014;59(6):1657-1663. doi:10.1016/j.jvs.2013.12.046

143. Burdick JA, Mauck RL. *Biomaterials for Tissue Engineering Applications: A*

Review of the Past and Future Trends.; 2011. doi:10.1007/978-3-7091-0385-2

144. Yu JR, Navarro J, Coburn JC, et al. Current and Future Perspectives on Skin Tissue Engineering: Key Features of Biomedical Research, Translational Assessment, and Clinical Application. *Adv Healthc Mater*. 2019;8(5):1801471. doi:10.1002/adhm.201801471

145. Xu F, Zhang C, Graves DT. Abnormal cell responses and role of TNF- α in impaired diabetic wound healing. *Biomed Res Int*. 2013;2013:754802. doi:10.1155/2013/754802

146. Hocking AM. The Role of Chemokines in Mesenchymal Stem Cell Homing to Wounds. *Adv wound care*. 2015;4(11):623-630. doi:10.1089/wound.2014.0579

147. Krieger JR, Ogle ME, McFaline-Figueroa J, Segar CE, Temenoff JS, Botchwey EA. Spatially localized recruitment of anti-inflammatory monocytes by SDF-1α-releasing hydrogels enhances microvascular network remodeling. *Biomaterials*. 2016;77:280-290. doi:10.1016/j.biomaterials.2015.10.045

148. Kim YH, Tabata Y. Recruitment of mesenchymal stem cells and macrophages by dual release of stromal cell-derived factor-1 and a macrophage recruitment agent enhances wound closure. *J Biomed Mater Res - Part A*. 2016;104(4):942-956. doi:10.1002/jbm.a.35635

149. Hu C, Yong X, Li C, et al. CXCL12/CXCR4 axis promotes mesenchymal stem cell mobilization to burn wounds and contributes to wound repair. *J Surg Res*. Published online 2013. doi:10.1016/j.jss.2013.01.019

150. Braza F, Dirou S, Forest V, et al. Mesenchymal Stem Cells Induce Suppressive Macrophages Through Phagocytosis in a Mouse Model of Asthma. *Stem Cells*. 2016;34(7):1836-1845. doi:10.1002/stem.2344

151. de Witte SFH, Luk F, Sierra Parraga JM, et al. Immunomodulation By Therapeutic Mesenchymal Stromal Cells (MSC) Is Triggered Through Phagocytosis of MSC By Monocytic Cells. *Stem Cells*. 2018;36(4):602-615. doi:10.1002/stem.2779

152. Segers VFM, Tokunou T, Higgins LJ, MacGillivray C, Gannon J, Lee RT. Local Delivery of Protease-Resistant Stromal Cell Derived Factor-1 for Stem Cell Recruitment After Myocardial Infarction. *Circulation*. 2007;116(15):1683-1692. doi:10.1161/CIRCULATIONAHA.107.718718

153. Zhao X, Lang Q, Yildirimer L, et al. Photocrosslinkable Gelatin Hydrogel for Epidermal Tissue Engineering. *Adv Healthc Mater*. 2016;5(1):108-118. doi:10.1002/adhm.201500005

154. Wang Z, Wang Z, Lu WW, Zhen W, Yang D, Peng S. Novel biomaterial

strategies for controlled growth factor delivery for biomedical applications. *NPG Asia Mater*. 2017;9(10):e435. doi:10.1038/am.2017.171

155. Porta G Della, Nguyen BNB, Campardelli R, Reverchon E, Fisher JP. Synergistic effect of sustained release of growth factors and dynamic culture on osteoblastic differentiation of mesenchymal stem cells. *J Biomed Mater Res - Part A*. 2015;103(6):2161-2171. doi:10.1002/jbm.a.35354

156. Zhao F, Yao D, Guo R, Deng L, Dong A, Zhang J. Composites of Polymer Hydrogels and Nanoparticulate Systems for Biomedical and Pharmaceutical Applications. *Nanomaterials*. 2015;5(4):2054-2130. doi:10.3390/nano5042054

157. Gaharwar AK, Peppas NA, Khademhosseini A. Nanocomposite hydrogels for biomedical applications. *Biotechnol Bioeng*. 2014;111(3):441-453. doi:10.1002/bit.25160

158. Mufamadi MS, Pillay V, Choonara YE, et al. A Review on Composite Liposomal Technologies for Specialized Drug Delivery. *J Drug Deliv*. 2011;2011:1-19. doi:10.1155/2011/939851

159. Jain S, Patel N, Shah MK, Khatri P, Vora N. Recent Advances in Lipid-Based Vesicles and Particulate Carriers for Topical and Transdermal Application. *J Pharm Sci*. 2017;106(2):423-445. doi:10.1016/J.XPHS.2016.10.001

160. Kuo C-Y, Eranki A, Placone JK, et al. Development of a 3D Printed, Bioengineered Placenta Model to Evaluate the Role of Trophoblast Migration in Preeclampsia. *ACS Biomater Sci Eng*. 2016;2(10):1817-1826. doi:10.1021/acsbiomaterials.6b00031

161. Kuo C-Y, Guo T, Cabrera-Luque J, et al. Placental basement membrane proteins are required for effective cytotrophoblast invasion in a three-dimensional bioprinted placenta model. *J Biomed Mater Res Part A*. 2018;106(6):1476-1487. doi:10.1002/jbm.a.36350

162. Bracaglia LG, Messina M, Winston S, Kuo CY, Lerman M, Fisher JP. 3D Printed Pericardium Hydrogels to Promote Wound Healing in Vascular Applications. *Biomacromolecules*. 2017;18(11):3802-3811. doi:10.1021/acs.biomac.7b01165

163. Narenji M, Talaee MR, Moghimi HR. Effect of charge on separation of liposomes upon stagnation. *Iran J Pharm Res*. 2017;16(2):423-431. Accessed December 4, 2018. http://www.ncbi.nlm.nih.gov/pubmed/28979297

164. Baglo Y, Liang BJ, Robey RW, Ambudkar S V., Gottesman MM, Huang HC. Porphyrin-lipid assemblies and nanovesicles overcome ABC transporter-mediated photodynamic therapy resistance in cancer cells. *Cancer Lett*. 2019;457:110-118. doi:10.1016/j.canlet.2019.04.037

165. Inglut CT, Gaitan B, Najafali D, et al. Predictors and Limitations of the Penetration Depth of Photodynamic Effects in the Rodent Brain. *Photochem Photobiol*. Published online October 13, 2019:php.13155. doi:10.1111/php.13155

166. Huang HC, Rizvi I, Liu J, et al. Photodynamic priming mitigates chemotherapeutic selection pressures and improves drug delivery. *Cancer Res*. 2018;78(2):558-571. doi:10.1158/0008-5472.CAN-17-1700

167. Huang HC, Liu J, Baglo Y, et al. Mechanism-informed repurposing of minocycline overcomes resistance to topoisomerase inhibition for peritoneal carcinomatosis. *Mol Cancer Ther*. 2018;17(2):508-520. doi:10.1158/1535-7163.MCT-17-0568

168. Liang BJ, Pigula M, Baglo Y, Najafali D, Hasan T, Huang HC. Breaking the selectivity-uptake trade-off of photoimmunoconjugates with nanoliposomal irinotecan for synergistic multi-tier cancer targeting. *J Nanobiotechnology*. 2020;18(1):1. doi:10.1186/s12951-019-0560-5

169. Ovsianikov A, Deiwick A, Vlierberghe S Van, et al. Laser Fabrication of Three-Dimensional CAD Scaffolds from Photosensitive Gelatin for Applications in Tissue Engineering. *Biomacromolecules*. 2011;12:851-858. doi:10.1021/bm1015305

170. Hansen J, Platten F, Wagner D, Egelhaaf SU. Tuning protein–protein interactions using cosolvents: specific effects of ionic and non-ionic additives on protein phase behavior. *Phys Chem Chem Phys*. 2016;18(15):10270-10280. doi:10.1039/C5CP07285A

171. Venkiteswaran G, Lewellis SW, Wang J, Reynolds E, Nicholson C, Knaut H. Generation and dynamics of an endogenous, self-generated signaling gradient across a migrating tissue. *Cell*. 2013;155(3):674. doi:10.1016/j.cell.2013.09.046

172. Cussler EL. *Diffusion - Mass Transfer in Fluid Systems, Third Edition*. 3rd ed. Cambridge University Press; 2009.

173. Baishya H. Application of Mathematical Models in Drug Release Kinetics of Carbidopa and Levodopa ER Tablets. *J Dev Drugs*. 2017;06(02). doi:10.4172/2329-6631.1000171

174. Costa P, Sousa Lobo JM. Modeling and comparison of dissolution profiles. *Eur J Pharm Sci*. 2001;13(2):123-133. doi:10.1016/S0928-0987(01)00095-1

175. Wickremasinghe NC, Kumar VA, Hartgerink JD. Two-Step Self-Assembly of Liposome-Multidomain Peptide Nanofiber Hydrogel for Time-Controlled Release. *Biomacromolecules*. 2014;15(10):3587-3595.

doi:10.1021/bm500856c

176. Alemdaroğlu C, Degim Z, Celebi N, Şengezer M, Alömeroglu M, Nacar A. Investigation of epidermal growth factor containing liposome formulation effects on burn wound healing. *J Biomed Mater Res Part A*. 2008;85A(1):271-283. doi:10.1002/jbm.a.31588

177. Bader AR, Li T, Wang W, Kohane DS, Loscalzo J, Zhang Y-Y. Preparation and Characterization of SDF-1a-Chitosan-Dextran Sulfate Nanoparticles. *J Vis Exp*. 2015;(95):448869. doi:10.3791/52323

178. Dhoot NO, Wheatley MA. Microencapsulated liposomes in controlled drug delivery: Strategies to modulate drug release and eliminate the burst effect. *J Pharm Sci*. 2003;92(3):679-689. doi:10.1002/jps.19104

179. Yue K, Trujillo-de Santiago G, Alvarez MM, Tamayol A, Annabi N, Khademhosseini A. Synthesis, properties, and biomedical applications of gelatin methacryloyl (GelMA) hydrogels. *Biomaterials*. 2015;73:254-271. doi:10.1016/j.biomaterials.2015.08.045

180. Gao W, Vecchio D, Li J, et al. Hydrogel Containing Nanoparticle-Stabilized Liposomes for Topical Antimicrobial Delivery. *ACS Nano*. 2014;8(3):2900-2907. doi:10.1021/nn500110a

181. Young S, Wong M, Tabata Y, Mikos AG. Gelatin as a delivery vehicle for the controlled release of bioactive molecules. *J Control Release*. 2005;109(1-3):256-274. doi:10.1016/J.JCONREL.2005.09.023

182. Dealwis C, Fernandez EJ, Thompson DA, Simon RJ, Siani MA, Lolis E. Crystal structure of chemically synthesized [N33A] stromal cell-derived factor 1alpha, a potent ligand for the HIV-1 "fusin" coreceptor. *Proc Natl Acad Sci U S A*. 1998;95(12):6941-6946. doi:10.1073/pnas.95.12.6941

183. Kolambkar YM, Dupont KM, Boerckel JD, et al. An alginate-based hybrid system for growth factor delivery in the functional repair of large bone defects. *Biomaterials*. 2011;32(1):65-74. doi:10.1016/j.biomaterials.2010.08.074

184. Ryu CH, Park SA, Kim SM, et al. Migration of human umbilical cord blood mesenchymal stem cells mediated by stromal cell-derived factor-1/CXCR4 axis via Akt, ERK, and p38 signal transduction pathways. *Biochem Biophys Res Commun*. 2010;398(1):105-110. doi:10.1016/j.bbrc.2010.06.043

185. Cherla RP, Ganju RK. Stromal Cell-Derived Factor 1α-Induced Chemotaxis in T Cells Is Mediated by Nitric Oxide Signaling Pathways. *J Immunol*. 2001;166(5):3067-3074. doi:10.4049/jimmunol.166.5.3067

186. Kucia M, Jankowski K, Reca R, et al. CXCR4–SDF-1 Signalling, Locomotion,

Chemotaxis and Adhesion. *J Mol Histol*. 2003;35(3):233-245. doi:10.1023/B:HIJO.0000032355.66152.b8

187. Mendoza MC, Er EE, Blenis J. The Ras-ERK and PI3K-mTOR pathways: cross-talk and compensation. *Trends Biochem Sci*. 2011;36(6):320-328. doi:10.1016/j.tibs.2011.03.006

188. Xing W, Guo W, Zou CH, et al. Acemannan accelerates cell proliferation and skin wound healing through AKT/mTOR signaling pathway. *J Dermatol Sci*. 2014;79(2):101-109. doi:10.1016/j.jdermsci.2015.03.016

189. Vasandan AB, Jahnavi S, Shashank C, Prasad P, Kumar A, Prasanna SJ. Human Mesenchymal stem cells program macrophage plasticity by altering their metabolic status via a PGE2-dependent mechanism. *Nat Sci Reports*. 2016;6(1):38308. doi:10.1038/srep38308

190. Yentrapalli R, Azimzadeh O, Sriharshan A, et al. The PI3K/Akt/mTOR Pathway Is Implicated in the Premature Senescence of Primary Human Endothelial Cells Exposed to Chronic Radiation. Woloschak GE, ed. *PLoS One*. 2013;8(8):e70024. doi:10.1371/journal.pone.0070024

191. Armstrong D, McCulloch D, de Asla R. Management of Diabetic Foot Ulcers. In: *UpToDate*. ; 2018.

192. Carty F, Mahon BP, English K. The influence of macrophages on mesenchymal stromal cell therapy: Passive or aggressive agents. *Clin Exp Immunol*. 2017;188(1):1. doi:10.1111/cei.12929

193. Yu JR, Janssen M, Liang BJ, Huang H-C, Fisher JP. A liposome/gelatin methacrylate nanocomposite hydrogel system for delivery of stromal cell-derived factor-1α and stimulation of cell migration. *Acta Biomater*. 2020;108:67-76. doi:10.1016/j.actbio.2020.03.015

194. Reiter J, Drummond S, Sammour I, et al. Stromal derived factor-1 mediates the lung regenerative effects of mesenchymal stem cells in a rodent model of bronchopulmonary dysplasia. *Respir Res*. 2017;18(1):137. doi:10.1186/s12931-017-0620-z

195. Amend SR, Valkenburg KC, Pienta KJ. Murine hind limb long bone dissection and bone marrow isolation. *J Vis Exp*. 2016;2016(110):53936. doi:10.3791/53936

196. Dunn L, Prosser HCG, Tan JTM, Vanags LZ, Ng MKC, Bursill CA. Murine Model of Wound Healing. *J Vis Exp*. 2013;2013(75):1-6. doi:10.3791/50265

197. Strudwick XL, Adams DH, Pyne NT, Samuel MS, Murray RZ, Cowin AJ. Systemic Delivery of Anti-Integrin αl Antibodies Reduces Early Macrophage

Recruitment, Inflammation, and Scar Formation in Murine Burn Wounds. *Adv Wound Care*. 2020;9(12):637-648. doi:10.1089/wound.2019.1035

198. Tessaro FHG, Ayala TS, Nolasco EL, Bella LM, Martins JO. Insulin Influences LPS-Induced TNF-α and IL-6 Release Through Distinct Pathways in Mouse Macrophages from Different Compartments. *Cell Physiol Biochem*. 2017;42(5):2093-2104. doi:10.1159/000479904

199. Tanaka A, To J, O'Brien B, Donnelly S, Lund M. Selection of reliable reference genes for the normalisation of gene expression levels following time course LPS stimulation of murine bone marrow derived macrophages. *BMC Immunol*. 2017;18(1):43. doi:10.1186/s12865-017-0223-y

200. Philipp D, Suhr L, Wahlers T, Choi Y-H, Paunel-Görgülü A. Preconditioning of bone marrow-derived mesenchymal stem cells highly strengthens their potential to promote IL-6-dependent M2b polarization. *Stem Cell Res Ther*. 2018;9(1):286. doi:10.1186/s13287-018-1039-2

201. Xu W, Roos A, Schlagwein N, Woltman AM, Daha MR, Van Kooten C. IL-10-producing macrophages preferentially clear early apoptotic cells. *Blood*. 2006;107(12):4930-4937. doi:10.1182/blood-2005-10-4144

202. Zhang X, Edwards JP, Mosser DM. Dynamic and Transient Remodeling of the Macrophage IL-10 Promoter during Transcription. *J Immunol*. 2006;177(2):1282-1288. doi:10.4049/jimmunol.177.2.1282

203. Willemen HLDM, Eijkelkamp N, Garza Carbajal A, et al. Monocytes/macrophages control resolution of transient inflammatory pain. *J Pain*. 2014;15(5):496-506. doi:10.1016/j.jpain.2014.01.491

204. Juban G, Saclier M, Yacoub-Youssef H, et al. AMPK Activation Regulates LTBP4-Dependent TGF-β1 Secretion by Pro-inflammatory Macrophages and Controls Fibrosis in Duchenne Muscular Dystrophy. *Cell Rep*. 2018;25(8):2163-2176.e6. doi:10.1016/j.celrep.2018.10.077

205. Pallai A, Kiss B, Vereb G, et al. Transmembrane TNF-α Reverse Signaling Inhibits Lipopolysaccharide-Induced Proinflammatory Cytokine Formation in Macrophages by Inducing TGF-β: Therapeutic Implications. *J Immunol*. 2016;196(3):1146-1157. doi:10.4049/jimmunol.1501573

206. Nolan A, Kobayashi H, Naveed B, et al. Differential role for CD80 and CD86 in the regulation of the innate immune response in murine polymicrobial sepsis. *PLoS One*. 2009;4(8). doi:10.1371/journal.pone.0006600

207. Balbo P, Silvestri M, Rossi GA, Crimi E, Burastero SE. Differential role of CD80 and CD86 on alveolar macrophages in the presentation of allergen to T lymphocytes in asthma. *Clin Exp Allergy*. 2001;31(4):625-636.

doi:10.1046/j.1365-2222.2001.01068.x

208. Fiorini F, Prasetyanto EA, Taraballi F, et al. Nanocomposite Hydrogels as Platform for Cells Growth, Proliferation, and Chemotaxis. *Small*. 2016;12(35):4881-4893. doi:10.1002/smll.201601017

209. Mantovani A, Biswas SK, Galdiero MR, Sica A, Locati M. Macrophage plasticity and polarization in tissue repair and remodelling. *J Pathol*. 2013;229(2):176-185. doi:10.1002/path.4133

210. Zhu Z, Ding J, Ma Z, Iwashina T, Tredget EE. Systemic depletion of macrophages in the subacute phase of wound healing reduces hypertrophic scar formation. *Wound Repair Regen*. 2016;24(4):644-656. doi:10.1111/wrr.12442

211. Bannon P, Wood S, Restivo T, Campbell L, Hardman MJ, Mace KA. Diabetes induces stable intrinsic changes to myeloid cells that contribute to chronic inflammation during wound healing in mice. *DMM Dis Model Mech*. 2013;6(6):1434-1447. doi:10.1242/dmm.012237

212. Grotenhuis N, Bayon Y, Lange JF, Van Osch GJVM, Bastiaansen-Jenniskens YM. A culture model to analyze the acute biomaterial-dependent reaction of human primary macrophages. *Biochem Biophys Res Commun*. 2013;433(1):115-120. doi:10.1016/j.bbrc.2013.02.054

213. Lin H, Yang Y, Wang Y, et al. Effect of mixed transplantation of autologous and allogeneic microskin grafts on wound healing in a rat model of acute skin defect. *PLoS One*. 2014;9(1). doi:10.1371/journal.pone.0085672

214. Bechtold B, Fletcher P, seamusholden, Gorur-Shandilya S. bastibe/Violinplot-Matlab: A Good Starting Point. Published online February 24, 2021. doi:10.5281/ZENODO.4559847

215. Kumar V. *Robbins Basic Pathology*. 9th e. Saunders; 2012.

216. Badillo AT, Chung S, Zhang L, Zoltick P, Liechty KW. Lentiviral Gene Transfer of SDF-1α to Wounds Improves Diabetic Wound Healing. *J Surg Res*. 2007;143(1):35-42. doi:10.1016/J.JSS.2007.03.051

217. Kottner J, Hillmann K, Fimmel S, Seité S, Blume-Peytavi U. Characterisation of epidermal regeneration in vivo: A 60-day follow-up study. *J Wound Care*. 2013;22(8):395-400. doi:10.12968/jowc.2013.22.8.395

218. Bollag WB, Hill WD. CXCR4 in epidermal keratinocytes: Crosstalk within the skin. *J Invest Dermatol*. 2013;133(11):2505-2508. doi:10.1038/jid.2013.271

219. Unoki N, Murakami T, Nishijima K, Ogino K, van Rooijen N, Yoshimura N. SDF-1/CXCR4 contributes to the activation of tip cells and microglia in retinal angiogenesis. *Investig Ophthalmol Vis Sci*. 2010;51(7):3362-3371.

doi:10.1167/iovs.09-4978

220. Loh SA, Chang EI, Galvez MG, et al. SDF-1α Expression during Wound Healing in the Aged Is HIF Dependent. *Plast Reconstr Surg*. 2009;123(Supplement):65S-75S. doi:10.1097/PRS.0b013e318191bdf4

221. Sadtler K, Allen BW, Estrellas K, Housseau F, Pardoll DM, Elisseeff JH. The Scaffold Immune Microenvironment: Biomaterial-Mediated Immune Polarization in Traumatic and Nontraumatic Applications. *Tissue Eng - Part A*. 2017;23(19-20):1044-1053. doi:10.1089/ten.tea.2016.0304

222. Inglut CT, Sorrin AJ, Kuruppu T, et al. Immunological and toxicological considerations for the design of liposomes. *Nanomaterials*. 2020;10(2). doi:10.3390/nano10020190